Generation and visualization of the flow of a thin layer of viscous liquid over a topography

Houben, A.C.H.

Award date:
1996

Generation and visualisation of the flow of a thin layer of viscous liquid over a topography

A.C.H Houben

14 Aug. 1996

Abstract

At the department of Materials Mechanics and Heat Transfer of the Philips Research Laboratories in Eindhoven coating processes are being studied. In order to improve the understanding of the relevant phenomena, the flow of a thin layer of viscous fluid on an inclined plane is investigated.
In the undisturbed flow a balance between the viscous forces and the gravitational force exists. The presence of a topography however, induces capillary effects. In a theoretical analysis it can be shown that two length scales are of importance. The first is a stagnant length scale, associated to the meniscus of a liquid at a fluid-solid interface. The second length scale is dynamic and occurs when the balance between the viscous forces and gravity is disturbed by a topography. In this latter case surface tension causes a pressure gradient which leads to a disturbance of the fluid profile.
The primary objective of this project was to develop some experimental tools and experience in visualizing the fluid profile on the dynamic length scale. In order to accomplish this the flow had to be theoretically described. This was done by applying the so called lubrication approximation, from which a Green function was derived. This (analytical) theory was verified numerically and thus extended beyond the linear regime.
Before any measurements can take place, the fluid profile has to be made available. Therefore a design has first been made for a setup to generate the required fluid flow. Next, a choice for a suitable measuring technique, for the present and for future research projects, had to be made. It was decided to use a transmission technique, as well as interferometry. These techniques are investigated and a setup is built.
Unfortunately it has proven to be quite cumbersome to generate a stable thin fluid flow, therefore only preliminary measuring results have been obtained. The transmission measurement turned out to be only suitable if a high degree of freedom is available for improving the absorption spectrum of the fluid under investigation. The maximal reachable accuracy will be in the order of microns, which is too low if detailed information of the flow is required. The interferometric technique looks quite promising, a high accuracy can be obtained, but several problems associated with large slopes in the fluid surface arise. Future research into this technique will be performed, but that lies beyond the scope of this traineeship.

Contents

List of symbols

Bold-font represents a three dimensional vector.
Coordinates typeset as subscript represent partial derivatives.
Quantities with a dagger (†) are dimensionless.

Roman

a	amplitude
b	width of the flow
b	length scale
c_1	constant
$c(h)$	wave velocity
d	height of the slit
d	thickness
e_v	evaporation rate
g	acceleration of gravity
h	height (thickness) of the fluid
$\overline{h}$	average thickness of the fluid
h'	fluid profile
k_0	propagation number (vacuum)
n	index of refraction (n_T, n_c, n_f, topography, coating, fluid)
q	fluid flux, of a fluid flowing down an inclined plane
t	time
$\mathbf{u}$	velocity, vector
u	x-component of velocity
v	y-component of velocity
w	z-component of velocity
x	coordinate
y	coordinate
z	coordinate
A	constant (dimensionless)
B	width of the slit
D	diffusivity of vapour in air
D	diameter
D	density
E	Youngs' modulus

$G(x)$	Green function
H	height of a column of fluid
I	moment of inertia
I	irradiance
L	length of the capillary/slit
L_d	capillary length scale (dynamic)
L_s	capillary length scale (stationary)
M	molar weight
N	number of capillaries
P	pressure
P_0	atmospheric pressure
P_{atm}	atmospheric pressure
P_v	vapour pressure
Q	force
R	universal gas constant
R	radius (of capillary)
R_1	radius of curvature
R	reflectance
T	topography height
T_{max}	maximum height of the topography
U	average velocity of a fluid flowing down an inclined plane
Z_{max}	maximum bending of the slit

Greek

α	angle of inclination
β	angle
γ	surface tension
δ	thickness of boundary layer
$\delta(x_0)$	Diracs delta function
ϵ	H/b
ζ	surface parameter
η	height of the capillary effect
θ	contact angle
θ	angle of light ray (θ_i, θ_r, θ_t, incoming, reflected, transmitted)
κ	constant
κ	transmission coefficient
λ	wavelength
μ	viscosity
ν	kinematic viscosity
ρ	density
τ	time scale
ϕ	phase
Δ	phase difference
Δl	lateral displacement of beam

Δx_c	coherence length
$\Delta\phi$	relative phase shift
Γ	optical path length difference

Dimensionless numbers

δ	surface tension and gravity
$e_v^\dagger$	comparison gravity and evaporation
B	Bond number
F	Froude number
Re	Reynolds number
Sh	Sherwood number
Sc	Schmidt number

Chapter 1

Introduction

The present report describes the research on the effect of a line topography on a thin layer of a viscous liquid flowing down an inclined plane. This research is the final project for the study *'Applied Physics'* at the Eindhoven University of Technology. The project was performed at the Philips Research Laboratories Eindhoven. The primary objective of this project (next to being the final learning stage of the study) was to develop some experimental tools and experience in visualizing the fluid profile of a thin layer of liquid. In the next section the interest in this topic will be motivated on the basis of a commercial background.

Motivation

In industrial practice, spin coating has traditionally been a popular means of applying coatings to flat or nearly flat substrates. It can also be used to produce a thin phosphor layer on the inside of a rectangular television screen. The coating process of the screens consists of several stages, the relevant ones are mentioned below:

- Deposition of a phosphor suspension on a slowly rotating inclined screen;
- Sedimentation of the phosphor and complete wetting of the screen by changing the angle of inclination of the screen;
- Spinning at a high rotation rate (typically 200 rpm) of the vertically tilted screen. Excess suspension flows along the rim towards the corners, where it is collected in corner cups;
- Drying of the layer. The screen is still spinning while fresh air is blown towards the screen under infra red irradiation. At this stage it is essential that a uniform layer of phosphor, polymer and a light sensitive agent has formed;
- Illumination by ultraviolet light through the hole of a mask to fix the pattern where the phosphor is wanted;
- Development of the layer by washing away the phosphor were it is unwanted.

In a television screen three colours are needed for the production of apparently white light. This means that the spinning process needs to be performed three times, once for each

colour. Contrary to the first layer, the second and the third have to be deposited on a non-flat surface. It is essential that the same profile of the phosphor layer is obtained for each line or dot. Preferably also the filling of the line or dot should be uniform. This is important in the current design of the television screen for the light output of the phosphor layer under electron bombardment depends on the thickness of the phosphor layer. In practice it is found that the second and the third layer are not uniform. Defects can be observed. The defect under investigation is known as the North-South (NS) line. The properties of the NS-line are that through the centre of rotation in a small line the layer thickness is higher than the ambient, of the order of 10 % and the strength of the defect decreases as the rotation rate is increased.
Numerous experiments have indicated that these defects are caused by the symmetry of the underlying topography [Beerens 95]. On a mini-flow-coater phosphor suspensions were spun onto model substrates, without photo- sensitive agents. The layers were often seen to contain the NS-line, while in the process the separate phases of sedimentation, heating and development were absent. Therefore a simplified model, in which sedimentation (also during spinning phase) is neglected, will be used to try to understand the phenomena. This means that the suspension can be regarded as a Newtonian solution, with the concentration of dissolved material uniform over the layer thickness. Other simplifications are the assumption that the radial liquid velocity can be found by making the lubrication approximation [O'Brien 92], which means that the velocity profile is parabolic in the height. Only the effects of spinning over topography, surface tension and constant evaporation are taken into account.

The report

In order to achieve the objective, as described in the beginning of this section, a theoretical description based on the so called lubrication approximation and a Green function, is presented in Chapter 2. In Chapter 3 this (analytical) theory will validated numerically. In order to verify the theory some experiments can be performed. The starting point for an experimental setup will be the acquirement of a fluid flow of which the profile can be detected. In Chapter 4 such a flow is investigated, after which a design for the generation of a thin layer of water (40 μm) on an inclined plane will be presented in Chapter 6. It is important to study the possible measuring techniques before a choice for a measurement system is made. Several techniques are outlined and a choice for a measuring system is made in Chapter 5. Two techniques, a transmission measurement and an interferometric setup, will be investigated further in Chapter 7. The (preliminary) results of the measurement systems are discussed in Chapter 8. In Chapter 9 conclusions are drawn and recommendations are made.
A typical fluid height associated with the spin coating of the phosphor layer is 40 μm . The physical dimensions of the topography (after development) are a height of 15 μm and a width of 210 μm . The distance between two successive colours is 75 μm . This gives a total length scale of about 500 μm when the third colour has to be spun.

Chapter 2

Theory

In this section the necessary theoretical tools will be derived and presented. The theory which is dealt with will be used to predict a fluid profile. The acquired information will then be used in the subsequent chapters to design an experimental setup.

2.1 A viscous fluid flowing down an inclined plane

In order to get a better understanding of the phenomena which are relevant for spin coating, the flow of a fluid on an inclined plane can be investigated. The driving force on the fluid in the spin coating process is the centrifugal force. On an inclined plane this driving force is gravity. Experiments on an inclined plane are substantially simpler because one can obtain a steady flow (relatively) easily. In this section the effect of a relatively large (line) topography on the flow of a thin layer of a newtonian fluid with a significant surface tension will be examined. In order to accomplish this, the lubrication approximation will be applied. With this approximation a differential equation describing the (stationary) fluid profile is obtained, which will be analytically investigated. The equations governing the spin coating process over topography will be described in Appendix (A), a contribution of J.H. Lammers. But first, the effect of surface tension will be investigated.

2.1.1 Capillarity

A fluid at a curved interface (fluid-air) can be in equilibrium. In this situation the effective pressure due to surface tension is balanced by a difference between the pressures in the fluids on the two sides of the interface. Thus in order to be in equilibrium there must be a jump in the fluid pressure at any point of the interface. This jump has the magnitude:

$$\Delta P = \gamma(\frac{1}{R_1} + \frac{1}{R_2}) \tag{2.1}$$

In this equation R_1, R_2 represent the radii of curvature along two orthogonal directions and γ represents the surface tension. From this point forward the quantities corresponding to the symbols used in the text are listed in the *'List of symbols'*, page vii.

Stagnant fluid

Equation (2.1) gives the balance of a curved interface between a gas, a fluid. The interface separates air, and a liquid of uniform density ρ. If the pressure in air is regarded as constant, the pressure variation with height z in the fluid is given by $P = p_0 - \rho g z$, the formula for an incompressible fluid. The condition for equilibrium at any point of the interface is then

$$\rho g z - \gamma(\frac{1}{R_1} + \frac{1}{R_2}) = \text{const.} \tag{2.2}$$

R_1 and R_2 here being taken as positive when the respective centres of curvature are on the gas side of the interface. The fluid in the experimental design is bound to 'crawl' up the vertical wall (Fig. 2.1).

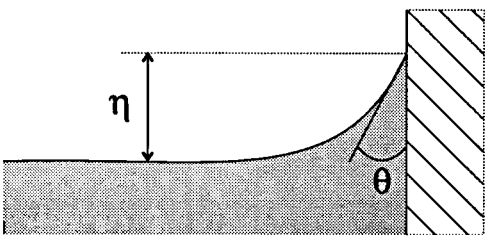

Figure 2.1: A free liquid meeting a vertical plane wall.

Where θ represents the contact angle between the fluid and the solid. In this two-dimensional field, the equation for the liquid-gas interface is $z = \zeta(x)$ and the principal curvatures of the interface are

$$\frac{1}{R_1} = 0, \quad \frac{1}{R_2} = \frac{\zeta''}{(1+\zeta'^2)^{\frac{3}{2}}} \tag{2.3}$$

Equation (2.2) then becomes

$$\frac{\rho g}{\gamma}\zeta - \frac{\zeta''}{(1+\zeta'^2)^{\frac{3}{2}}} = 0 \tag{2.4}$$

The constant on the right-hand side being zero because the interface becomes plane far from the wall, where $\zeta = 0$. After integration the following equation for the height of the capillary effect (η) appears:

$$\eta^2 = 2\frac{\gamma}{\rho g}(1 - \sin\theta) \tag{2.5}$$

In practice this gives $\eta_{H_2O} \approx 1...3$ mm for $\theta = 110°...30°$
Also the width of the effect is of practical importance. After integration (separation of variables) and the usage of the boundary conditions ($x = 0$,for $\zeta = h$) the following equation can be derived [Batchelor 67, p. 60-68]

$$\frac{x}{L_s} = \cosh^{-1}\frac{2L_s}{\zeta} - \cosh^{-1}\frac{2L_s}{\eta} + (4 - \frac{\eta^2}{L_s^2})^{\frac{1}{2}} - (4 - \frac{\zeta^2}{L_s^2})^{\frac{1}{2}} \tag{2.6}$$

where $L_s^2 = \frac{\gamma}{\rho g}$, which is a capillary length scale. This gives (for H_2O) $x_{\zeta=0} \approx 4.3$mm. Note that this is only the case for a stagnant liquid.

2.1.2 Derivation of a differential equation

Consider a broad band of viscous fluid, uniform in depth across a slope released so as to flow down a constant slope. The fluid flow will be described using the coordinate system depicted in figure (2.2). The inclined plane is assumed to be infinite in extent in all directions. The system is described using cartesian coordinates in which the velocity components are denoted by $\mathbf{u} = (u, v, w)$. The flow is assumed translation invariant in the y-direction. This assumption implies: $v = 0$, $\frac{\partial}{\partial y} = 0$, $\frac{\partial^2}{\partial y^2} = 0$. The fluid is assumed to behave Newtonian (which applies for many fluids, for instance H_2O). This assumption is also applicable in case a phosphor coating for television tubes is used [Lammers 94].

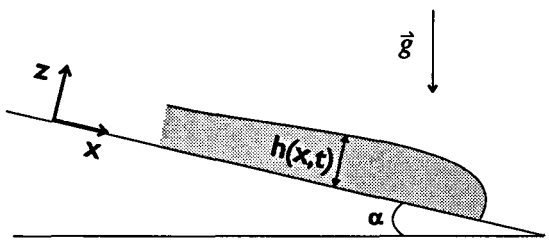

Figure 2.2: A sketch of the flow and the coordinate system.

The most general equations for the flow of a Newtonian viscous incompressible fluid of constant physical properties are the Navier-Stokes equations:

$$\rho \frac{\partial \mathbf{u}}{\partial t} + \rho(\mathbf{u}, \nabla \mathbf{u}) = \rho \mathbf{g} - \nabla P + \mu \nabla^2 \mathbf{u} \tag{2.7}$$

(The quantities which are used are described in the *'List of symbols'*, page vii. The first term on the left hand side represents the unsteady inertia forces, the second the stationary inertia forces. On the right hand side the first term describes the gravitational force, the second term represents a pressure gradient over the fluid and finally the last term represents the influence of viscosity.
If no topography is present, the gravitational force is balanced by the viscous force. It will be shown later that the presence of the topography affects this balance. From this undisturbed balance the mean fluid velocity can be calculated. This calculation is performed in Section (4.2.1), page 26, resulting in: $U = \frac{\rho g \sin \alpha \bar{h}^2}{3\nu}$. With this mean velocity a Reynolds number can be used to determine whether or not the flow is laminar (Section (4.2.1)). For the circumstances which are under investigation, the Reynolds number answers to the requirements for laminar flow (page 26).
The relative importance of the terms of the NS-equations can be determined using dimensionless numbers, which will be discussed below.

- *Stationary inertia forces versus gravity*

  A Froude number can be defined by:

$$F = \frac{|\rho \mathbf{u} \cdot \operatorname{grad} \mathbf{u}|}{|\rho \mathbf{g}|} \tag{2.8}$$

  This number represents the ratio of the stationary inertia forces to the gravitational force.

  Effects of acceleration and deceleration of the fluid caused by the topography occur on the capillary length scale. Therefore the velocity gradient should be scaled with the capillary length scale.

$$F_{L_s} = \frac{U^2}{gL_s} = \frac{U^2}{g\overline{h}} \frac{\overline{h}}{L_s} \tag{2.9}$$

  Because $\frac{h}{L_s} \ll 1$ it is sufficient that F, scaled with $\overline{h}$, (F_h) is small. Again using $U = \frac{\rho g \sin\alpha \overline{h}^2}{3\nu}$, this gives:

$$F_h = \frac{U^2}{g\overline{h}} = \frac{\rho^2 g \sin^2\alpha \overline{h}^3}{9\nu^2} \tag{2.10}$$

  The stationary inertia forces (the velocity squared terms) of the Navier-Stokes equations are negligible if F is much smaller than 1. The maximum thickness of the fluid for which the stationary inertia forces can be neglected is given by:

$$\overline{h} \ll \left(\frac{9\nu^3}{\rho^2 g \sin^2\alpha}\right)^{\frac{1}{3}} \tag{2.11}$$

  For water at 20 °C , and $\alpha = 22°$ this gives $\overline{h} \ll 190\,\mu\text{m}$. Thus the upper limit of the thickness of the film, far from a stationary meniscus, should be of this order of magnitude to neglect the velocity squared terms.

  On the other hand, the lower limit should be approximately 1 μm to disregard long ranged forces, for instance the double-layer forces for an ionic solution like water. [Bordier 91], [Gennes 85].

- *Surface tension versus gravitational force*

  The Bond number is defined by:

$$B = \frac{\rho g}{\operatorname{grad} P} \tag{2.12}$$

  The Bond number represents the ratio of the gravitational force to the surface tension. The surface tension has to be taken into account if the Bond number (B) is small.

The pressure can be replaced by an estimate of the surface tension, $\text{grad}\, P \approx \frac{\gamma}{\overline{L_s}^2}$. In this static case,

$$B = \frac{\rho g \overline{L_s}^2}{\gamma} \tag{2.13}$$

If the surface tension and gravity balance:

$$B_{L_s} = O(1) \rightarrow L_s = \sqrt{\frac{\gamma}{\rho g}} \tag{2.14}$$

Also a dynamical capillary length scale is of importance. The pressure gradient can be estimated to be: $\text{grad}\, P = \frac{\gamma h'}{L_d^3}$. The fluid curvature ($h'$) caused by the topography can roughly be estimated to be of the same order of magnitude as this topography. This topography can be chosen in an experiment to be (roughly) in the same order of magnitude as the average fluid height ($h' \approx T \approx \overline{h}$).

$$\text{grad}\, P = \frac{\gamma \overline{h}}{L_d^3} \tag{2.15}$$

Thus a dynamic capillary length scale can be estimated:

$$B_{L_d} = \frac{\rho g L_d^3}{\gamma \overline{h}} = \frac{\rho g \overline{h}^2}{\gamma} \frac{L_d^3}{\overline{h}} \tag{2.16}$$

$$B_{L_d} = O(1) \rightarrow L_d \simeq \left(\frac{\gamma \overline{h}}{\rho g}\right)^{\frac{1}{3}} \tag{2.17}$$

see Equation (2.44). These two length scales can be compared:

$$L_d^3 \simeq \overline{h} L_s^2 \tag{2.18}$$

Because $\overline{h} \ll L_s$, the dynamical length scale is smaller than the stationary length scale: $L_d \ll L_s$. This implies that in the balance between surface tension and gravity the dynamical forces are more important than the stationary forces.

Thus the surface tension can not be neglected [Lister 92] [Fulford 64] and has to be taken into account when describing the fluid flow.

- *Viscous forces*

  The viscous term is already important in the undisturbed balance and has therefore to be included.

- *Unsteady inertia forces*

  After some period of time, the fluid flow is assumed to be stationary, thus the unsteady inertia forces will be absent.

Using this dimensional analysis the in-stationary inertia forces ($\rho\frac{\partial \mathbf{u}}{\partial t}$) and the stationary inertia forces ($(\mathbf{u}, \nabla\mathbf{u})$) can be neglected, thus the left hand side of Equation (2.7) equals zero. This is the so called lubrication approximation (Huppert, [Huppert 82], presents an analysis without surface tension and O'Brien, [O'Brien 92], presents an analysis for spin coating). This approximation can evidently be used if:

- $h \ll L_d$, in which h represents the film thickness, and L_d the dynamical capillary length scale of the fluid flow.
- Reynolds number is small : $\alpha\rho hu/\mu \ll 1$

This yields for the x-direction:

$$0 = \rho g \sin\alpha - \frac{\partial P}{\partial x} + \mu\left(\frac{\partial^2 u}{\partial z^2}\right) \tag{2.19}$$

in which the horizontal derivatives (x) have been neglected in comparison with the vertical derivatives (z) on the right hand side of (2.19), because the length scale of the flow is very much greater than its thickness.
This equation represents a balance between viscous and gravitational forces while the pressure gradient contains the smoothing effect of surface tension. As shown by the dimensional analysis these terms are not negligible.
Using a different notation, in which the suffices denote the partial derivatives:

$$P_x - \mu u_{zz} = \rho g \sin\alpha \tag{2.20}$$

In order to find an expression for P_x the pressure gradient across the flow will be considered. The balance of momenta in the z-direction can be used to find an expression for P_z:

$$P_z = \rho g \cos\alpha + \mu w_{zz} + \mu w_{xx} \tag{2.21}$$

This equation can be nondimensionalised to estimate the value of the pressure gradient in the vertical direction (P_z). The equation is made dimensionless by using the following reference scales:

$$x = x^\dagger b,\ z = z^\dagger \overline{h},\ u = u^\dagger \frac{\rho g \sin\alpha \overline{h}^2}{\mu},\ w = \frac{\overline{h}}{b} w^\dagger \frac{\rho g \sin\alpha \overline{h}^2}{\mu},\ P = P^\dagger \rho b g \sin\alpha \tag{2.22}$$

in which (from this point forward) daggers (†) are used to identify dimensionless quantities. The velocity due to gravity on an inclined plane without surface tension is used for the scaling. This gives the dimensionless equation (use $\epsilon^\dagger = \frac{\overline{h}}{b}$):

$$P_z^\dagger = \epsilon^\dagger \frac{\cos\alpha}{\sin\alpha} + \epsilon^{\dagger 2} w_{zz}^\dagger + \epsilon^{\dagger 4} w_{xx}^\dagger \tag{2.23}$$

Since $\epsilon^\dagger \approx 0.08 \ll 1$, ($\overline{h} \approx 40\,\mu$m, $b \approx 0.5$ mm, (Section (2.1.1))), this equation indicates that P does not vary with z. This means that the pressure can be assumed uniform over the thickness of the fluid. On the free surface of the liquid the air pressure is constant, nominally zero ($P_{atm} = 0$), and the liquid pressure (capillary pressure, caused by the surface

tension acting upon a curved surface (Section (2.1.1)) can be approximated by the following (dimensional) equation [Gu 95]:

$$P_{z=h} = P = P_{atm} - \gamma \nabla^2 h \tag{2.24}$$

Differentiation with respect to x gives:

$$P_x = -\gamma h_{xxx} \tag{2.25}$$

This result can be put aside to return to Equation (2.20). This equation gives an expression for u_{zz}:

$$u_{zz} = \frac{P_x}{\mu} - \frac{\rho g \sin \alpha}{\mu} \tag{2.26}$$

This equation can be integrated twice with respect to z to yield an equation containing u. The integration constants can be determined using the appropriate boundary conditions:

$$\begin{array}{ll} u_z \mid_{z=h} & = 0 \quad \text{no acceleration} \\ u \mid_{z=T(x)} & = 0 \quad \text{no slip} \end{array} \tag{2.27}$$

After calculation this gives u:

$$u = \left(\frac{P_x}{\mu} - \frac{\rho g \sin \alpha}{\mu} \right) \left(\frac{1}{2} z^2 - hz + Th - \frac{1}{2} T^2 \right) \tag{2.28}$$

The flux (q) of the fluid can be calculated using this equation:

$$q = \int_{T(x)}^{h(x,t)} u \mathrm{d}z = -\frac{1}{3}(h-T)^3 \left(\frac{P_x}{\mu} - \frac{\rho g \sin \alpha}{\mu} \right) \tag{2.29}$$

In order to obtain a differential equation for h the equation of continuity can be applied:

$$\frac{\partial h}{\partial t} + \nabla \cdot q = 0 \tag{2.30}$$

The flux (q) can be inserted in this equation to yield:

$$\frac{\partial h}{\partial t} = -\frac{\rho g \sin \alpha}{3\mu} \frac{\partial}{\partial x}(h-T)^3 + \frac{\partial}{\partial x} \frac{P_x}{3\mu}(h-T)^3 \tag{2.31}$$

Using P_x from Equation (2.25) finally leads to:

$$\frac{\partial h}{\partial t} = -\frac{\rho g \sin \alpha}{3\mu} \frac{\partial}{\partial x}(h-T)^3 - \frac{\gamma}{3\mu} \frac{\partial}{\partial x}(h-T)^3 h_{xxx} \tag{2.32}$$

This equation describes the evolution of a thin layer of viscous fluid flowing laminarly on an inclined plane. The flow is influenced by a topography and governed by surface tension and gravity.

2.1.3 Evaporation

Up to here the evaporation rate was omitted. This evaporation can play an eminent role. It is important in spin coating, for instance it determines the final coating thickness and may induce surface tension gradients. Here, evaporation is desired to be small.
The rate of evaporation of the fluid (e_v, in m/s) can be inserted in Equation (2.32), yielding:

$$\frac{\partial h}{\partial t} = -\frac{\rho g \sin\alpha}{3\mu}\frac{\partial}{\partial x}(h-T)^3 - \frac{\gamma}{3\mu}\frac{\partial}{\partial x}(h-T)^3 h_{xxx} - e_v \tag{2.33}$$

It is quite complicated to calculate the rate of evaporation. An estimate can be obtained using the following equation ([Lammers 94, eq 2.21]):

$$e_v = \frac{M}{\rho_l} Sh(Sc) D \frac{\Delta P_v}{RT}\frac{1}{\delta} \tag{2.34}$$

where M denotes the molar weight of the fluid, Sh (Sherwood number) is the dimensionless mass transfer coefficient, which can be calculated from the dimensionless Schmidt number $Sc = \frac{\nu_a}{D}$. The symbol D denotes the diffusivity of vapour in air. The air has kinematic viscosity $\nu_a = \mu_a/\rho_a$. The vapour pressure is P_v, whereas R denotes the universal gas constant and T the temperature.
The evaporation rate for water can thus be estimated. The Sherwood number can be estimated to be in the order of 1, P_v = 2.3 kPa this gives for 50% relative humidity: ΔP_v = 1.2 kPa, R=8.31 J/(mol K), T = 293 K, D= 2.6 $\cdot 10^{-5}$ m^2/s, M_{H2O}=18 $\cdot 10^{-3}$, ρ_l=998 kg/m^3, $\nu_a = 10^{-5}$m^2/s, $u \approx 0.01$ m/s, $x \approx 0.01$ m. The thickness of the boundary layer is represented by δ (Blasius solution, [Batchelor 67]), $\delta = O((\nu x/u)^{\frac{1}{2}}) \approx 3\cdot 10^{-3}$ m).

$$e_v \approx 8 \cdot 10^{-8} m/s \tag{2.35}$$

The rate of evaporation is assumed to be constant.
It takes a fluid element approximately t_{flow}=0.07 m /0.005 m/s=14 seconds to reach the point of measurement. Thus the decrease in fluid height is :

$$\Delta h_{evaporation} = e_v t_{flow} = 1.1\,\mu\text{m} \tag{2.36}$$

This result is particularly important if the solution is near saturation, because any evaporation will quickly lead to the formation of solid particles.

2.1.4 Non-dimensionalised differential equation

The differential Equation (2.33) of the last section can be made dimensionless. The dimensionless quantities are again denoted by a dagger (†). The reference scales which are used are:

$$h = h^\dagger \bar{h},\ T = T^\dagger \bar{h},\ x = x^\dagger b,\ t = t^\dagger \frac{3\mu b}{g\sin\alpha \rho \bar{h}^2} \tag{2.37}$$

Note that here the typical width b is chosen, rather than the dynamic capillary length L_d. This gives:

$$\frac{\partial h^\dagger}{\partial t^\dagger} = -\frac{\partial}{\partial x^\dagger}(h^\dagger - T^\dagger)^3 - \delta\frac{\partial}{\partial x^\dagger}(h^\dagger - T^\dagger)^3 h^\dagger_{xxx} - e_v^\dagger \tag{2.38}$$

In this equation the following dimensionless numbers are used:

$$\delta = \frac{\gamma\bar{h}}{g\rho b^3 \sin\alpha} \quad e_v^\dagger = \frac{2e_v\mu b}{g\rho\bar{h}^3 \sin\alpha} \tag{2.39}$$

If $e_v^\dagger$ equals 1 the effects of gravity and evaporation are of the same magnitude. Using the result of section (2.1.3), this can be calculated to be: $e_v^\dagger \approx 3.3 \cdot 10^{-4}$ for H_2O, ($\bar{h}$=40 μm, b=500 μm, $e_v = 8 \cdot 10^{-8}$m/s).
If $\delta \approx 1$, the surface tension and gravitational force balance, i.e. the dynamic capillary length is approximately equal to the topography width. The length scale b plays an important role for it determines the size of the dimensionless numbers δ and $e_v^\dagger$.

2.1.5 Capillarity

In Section (2.1.2) is was suggested that two capillary length scales are important. A capillary length scale for a stationary situation is found in Section (2.1.1). In the next section a dynamical length scale will be derived.

Dynamic situation

A capillary length scale for a dynamic situation can be found, using the differential Equation (2.32). In this (dimensional) equation, omitting the rate of evaporation, the surface tension and the viscous force are the dominant factors:

$$\frac{\partial h}{\partial t} = -\frac{\partial}{\partial x}\frac{\rho g \sin(\alpha)(h-T)^3}{3\mu} - \frac{\gamma}{3\mu}\frac{\partial}{\partial x}(h-T)^3\frac{\partial^3(h-T)}{\partial x^3} \tag{2.40}$$

Take $h(x,t)$ to be time independent, a quasi-stationary situation ($h(x)$) and choose the topography $T(x) = 0$ (no topography).

$$0 = -\frac{\rho g \sin\alpha}{\mu}h^2\frac{\partial h}{\partial x} - \frac{\gamma}{3\mu}(3h^2\frac{\partial h}{\partial x}\frac{\partial^3 h}{\partial x^3} + h^3\frac{\partial^4 h}{\partial x^4}) \tag{2.41}$$

The height of the fluid can be written as: $h(x) = \bar{h} + h'(x)$, in which $\bar{h}$ is a constant and h' is a function of the position x. Using the fact that: $|h'(x)| \ll \bar{h}$, equation (2.41) can be linearized. The second term on the right hand side of this equation (2.41) can be neglected in comparison with the third term:

$$\frac{\partial h'}{\partial x} = -\frac{\gamma\bar{h}}{3\rho g \sin\alpha}\frac{\partial^4 h'}{\partial x^4} \tag{2.42}$$

After integration this yields:

$$h' = -\frac{\gamma\bar{h}}{3\rho g \sin\alpha}\frac{\partial^3 h'}{\partial x^3} + \text{constant} \tag{2.43}$$

The constant can be chosen zero (a constant term can always be written as being a part of $\overline{h}$). A length scale can be found to be:

$$L_d = \left(\frac{\gamma \overline{h}}{3\rho g \sin\alpha}\right)^{\frac{1}{3}} \tag{2.44}$$

With $L_s = \sqrt{\frac{\gamma}{\rho g}}$ this can be written as:

$$L_d^3 = L_s^2 \frac{\overline{h}}{3\sin\alpha} \tag{2.45}$$

The dynamic length scale can be related to the dimensionless number δ of the previous section:

$$\delta = 3\left(\frac{L_d}{b}\right)^3 \tag{2.46}$$

In table (2.1) L_d is calculated as a function of $\overline{h}$, γ and α. This length scale can be used to make Equation (2.43) dimensionless.

Table 2.1: Some values of L_d. The flow is predicted to become unstable for a thickness of 120 μm with angles larger than 22 °(Section (4.2.1)).

$\overline{h}$ μm	γ (10^{-3}Nm^{-1})	α (°)	L_d (10^{-4}m)
40	20	45	3.4
40	20	22	4.2
40	73	45	5.1
40	73	22	6.3
100	20	45	4.6
100	20	22	5.7
100	73	45	7.0
100	73	22	8.6
120	20	22	6.0
120	73	22	9.1

2.1.6 A Green function

The dynamical capillary length scale (L_d) can be used to write Equation (2.43) dimensionless. Write $h'^{\dagger} = \frac{h'}{T_{max}}$ and $x^{\dagger} = \frac{x}{L_d}$, where daggers are again used to denote non-dimensional quantities. The equations which will be derived in the remaining of this section will only use non-dimensional quantities. For the sake of clarity the daggers are omitted. The dimensionless equation can be written as:

$$h' = -\frac{\partial^3 h'}{\partial x^3} \tag{2.47}$$

A solution of this equation can be found by using an exponential function as 'ansatz':

$$h' = c\exp(\kappa x) \tag{2.48}$$

which yields after substitution:

$$\kappa^3 = -1$$

Thus a solution of (2.47) is given by:

$$h' = c_1\exp(-x) + c_2\exp((\frac{1}{2} + \frac{1}{2}\sqrt{3}\,i)x) + c_3\exp((\frac{1}{2} - \frac{1}{2}\sqrt{3}\,i)x) \tag{2.49}$$

With the Euler formula this can be written as:

$$h' = h_1\exp(-x) + h_2\exp(\frac{1}{2}x)\cos(\frac{1}{2}\sqrt{3}\,x + \phi) \tag{2.50}$$

For arbitrary topography ($T(x_0)$) the liquid height can be described by a Green function:

$$h'_T(x) = \int_{-\infty}^{\infty} T(x_0)G(x - x_0)\mathrm{d}x_0 \tag{2.51}$$

Take $T(x_0) = \delta(x_0)$, in which δ represents Dirac's delta function. According to the definition of the Green function, the height profile of the fluid (h') is given directly by $G(x)$:

$$h'_{\delta(x)}(x) = G(x) = h_1\exp(-x) + h_2\exp(\frac{1}{2}x)\cos(\frac{1}{2}\sqrt{3}\,x + \phi)$$

This equation is valid for $x > 0$ ($G_+(x)$) and for $x < 0$ ($G_-(x)$) the constants have to be determined for both sides. At $x = 0$, a discontinuity, the delta function, is present, thus the two parts of $G(x)$ must be matched in $x = 0$. This can be done by using the boundary conditions. Six constants have to be determined (using six boundary conditions):

- $$\lim_{x\uparrow\infty} h'_{\delta(x)}(x) = G_+(x) = 0, \text{ which implies } h_{+,1} = 0 \tag{2.52}$$

  $$\lim_{x\downarrow-\infty} h'_{\delta(x)}(x) = G_-(x) = 0, \text{ which implies } h_{-,2} = 0 \tag{2.53}$$

  Because $h_{-,2} = 0$ it is not necessary to determine ϕ_-, which implies that only five boundary conditions have to be used.

- The fluid surface must be continuous:

  $$\lim_{x\uparrow 0} h(x) = \lim_{x\downarrow 0} h(x)$$

- $$\lim_{x\uparrow 0} \frac{\mathrm{d}h(x)}{\mathrm{d}x} = \lim_{x\downarrow 0} \frac{\mathrm{d}h(x)}{\mathrm{d}x}$$

  this boundary condition implies that no nett force in the z-direction is exerted upon the delta function.

$$\frac{\partial h'_{x+\Delta x}}{\partial x} - \frac{\partial h'_{x-\Delta x}}{\partial x} = \int_{x-\Delta x}^{x+\Delta x} \frac{\partial^2 h'}{\partial x^2}\mathrm{d}x = -\frac{1}{\gamma}\int_{x-\Delta x}^{x+\Delta x} P\mathrm{d}x = \frac{1}{\gamma}F$$

Imagine a flat topography, this topography can be described by taking the convolution of this topography and the Green function. No nett force acts upon a flat topography, this implies that no net force can be 'built in' the Green function, therefore the gradient of the Green function must be continuous.

- Suppose a step function at $x = 0$ of magnitude 1. $T(x) = 0\ x < 0$ and $T(x) = 1\ x \geq 0$

$$h'(-\infty) = h'(\infty)$$

The fluid will be conformal at a large distance from the step (at $x = 0$), with equal liquid heights before and after the step.

$$\int_{-\infty}^{\infty} G(x)\mathrm{d}x = 1$$

- The small slope approximation gives that the fluid will be conform: $T = \epsilon x$, $\epsilon \ll 1$, thus $h = \overline{h} + \epsilon x$ for $x \geq 0$.
$T = 0$, thus $h = \overline{h}$ for $x < 0$.
Use this in Equation (2.51).

$$\epsilon x = \int_{-\infty}^{\infty} \epsilon x_0 G(x - x_0)\mathrm{d}x_0$$

In $x = 0$:

$$0 = \int_{-\infty}^{\infty} x_0 G(-x_0)\mathrm{d}x_0$$

$$\int_{-\infty}^{\infty} xG(x)\mathrm{d}x = 0$$

After calculation the constants are determined and h' for $\delta(x - 0)$ (the Green function) is given by the following equation:

$$\begin{array}{ll} h'_+ = \frac{1}{3}e^{(-x)} & x > 0 \\ h'_- = \frac{1}{3\cos\pi/3}e^{(\frac{1}{2}x)}\cos(\frac{1}{2}\sqrt{3}x + \frac{\pi}{3}) & x < 0 \end{array} \tag{2.54}$$

This function (normalized for unit area) is plotted in figure (2.3).
The x-axis represents the mean fluid level. The fluid profile is obtained by multiplying the height $h'(x)$ with the maximum topography height (here the topography is chosen to consist of steps of about 12 μm high). The horizontal scale represents the position, in units equal to the dynamic capillary length (L_d, table (2.1)).
Instead of the delta function, other functions can be used as topography (for example a step function in Figure (2.3)). The fluid surface with that topography can be predicted using the Green function. From the Green function it is clear that for any topography the disturbance before the topography plus the disturbance behind is at least $15L_d$ wide. This has to be taken into account, when designing the topography. The maximum fluid disturbance occurs before the obstacle.

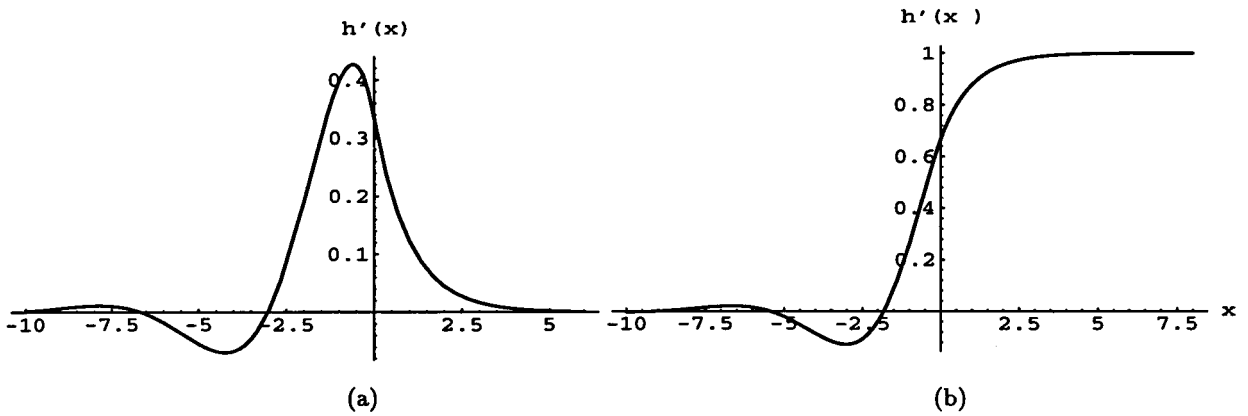

(a) (b)

Figure 2.3: The Green function. In (a) a delta-function is positioned in $x = 0$ and in (b) a step is placed in $x = 0$.

The slopes of the fluid surface

In order to experimentally measure the fluid profile as calculated in Section (2.1.6), the maximum slope of the profile is important. The slope can be calculated by differentiating the Green function ones with respect to the position.

$$\begin{array}{ll} \frac{\mathrm{d}h'_+(x)}{\mathrm{d}x} = -\frac{1}{3}e^{-x} & x > 0 \\ \frac{\mathrm{d}h'_-(x)}{\mathrm{d}x} = \frac{1}{3}e^{\frac{x}{2}}\cos(\frac{\pi}{3} + \frac{1}{2}\sqrt{3}x) - \frac{1}{3}\sqrt{3}e^{\frac{x}{2}}\sin(\frac{\pi}{3} + \frac{1}{2}\sqrt{3}x) & x < 0 \end{array} \tag{2.55}$$

This (normalized) function is plotted in figure (2.4).

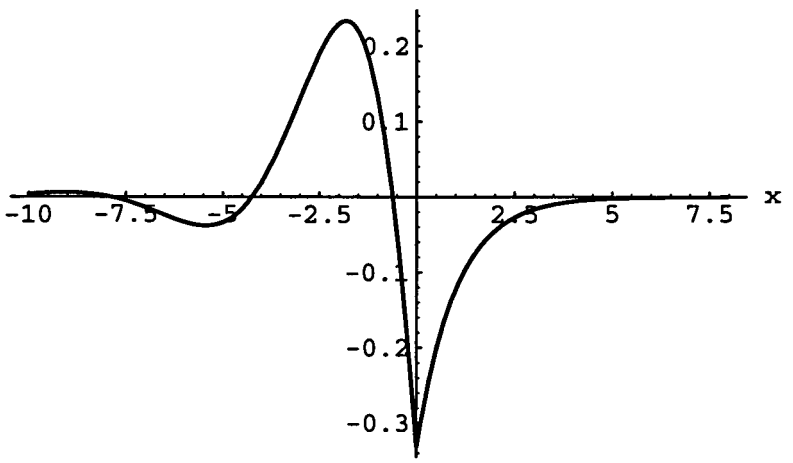

Figure 2.4: The first derivative of the Green function.

The largest slope occurs at the delta function ($x = 0$) and is $-\frac{1}{3}$. Assuming that this maximum slope is the same for all topographies, the largest slope which has to be detected is $-\frac{1}{3}\frac{T_{max}}{L_d}$, its maximum value is $-12\,\mu\mathrm{m/mm}$, this is calculated for the smallest capillary length scale. The maximum slope for the largest capillary length scale is $4\,\mu\mathrm{m/mm}$.

Chapter 3

Numerical calculation

The Green function which was derived in the previous chapter, is based on a linear theory. The predictions of this theory will only be valid for topographies which are relatively small to the fluid thickness. With increasing topography the prediction of the fluid profile will become less accurate. The topography under investigation however is quite large in comparison with the average fluid thickness ($\frac{T}{\bar{h}} = \frac{1}{10}$ up to $\frac{1}{4}$). Therefore a numerical simulation of the fluid profile, which incorporates non-linear effects, is made.

3.1 The program

The solution of the steady flow is calculated as the limit of an unsteady flow for which a numerical program (based on an implicit finite difference scheme) was available. This program performs a numerical calculation of a partial differential equation. The initial condition is taken to be a uniform layer of fluid. The boundary conditions upstream are $h = 1$, and no pressure gradient occurs, thus no curvature of the fluid surface is present (h_{xxx}=0). The boundary conditions downstream are not so important for any disturbance which occurs will only influence the fluid downwards. The first condition is taken to be $h = 1$, and the second is still under investigation.
The equation which will be used for the simulation of the fluid profile is the dimensionless Equation (2.38) derived in Section (2.1.4), in which the rate of evaporation ($e_v^\dagger$) is omitted:

$$\frac{\partial h^\dagger}{\partial t^\dagger} = -\frac{\partial}{\partial x^\dagger}(h^\dagger - T^\dagger)^3 - \delta\frac{\partial}{\partial x^\dagger}(h^\dagger - T^\dagger)^3 h^\dagger_{xxx} \tag{3.1}$$

In this equation δ is a dimensionless number representing the relative importance of the surface tension to gravity (Equation (2.39)): $\delta = \frac{\gamma\bar{h}}{g\rho b^3 \sin\alpha}$.

A relation for the calculation time can be calculated. The flow can be regarded steady if all the initial disturbances have disappeared. A typical wave velocity can be found from Equation (3.1). In case no topography is present the differential equation for a small disturbance $h'^\dagger$ can be approximated as:

$$\frac{\partial h'^\dagger}{\partial t^\dagger} + 3h^{\dagger 2}\frac{\partial h'^\dagger}{\partial x^\dagger} = -\delta h^\dagger \frac{\partial h'^\dagger}{\partial x^4} \tag{3.2}$$

The wave velocity can then be taken to be: $c^\dagger(h^\dagger) = +3h^{\dagger 2}$, while the last term is responsible for damping af the waves, especially for shorter wavelengths. The calculation time can therefore be written as:

$$\Delta t^\dagger \propto \frac{\Delta x^\dagger}{c^\dagger} \tag{3.3}$$

Assuming that $\overline{h}^\dagger = 1$, gives $c^\dagger(\overline{h}^\dagger) = +3$. Indeed a fast convergence of the numerical solution was found once this lead time had elapsed.

3.2 Comparison of the Green function to the numerical calculation

In the derivation of the Green function (Section (2.1.6)) a dynamical length scale (L_d) (Equation (2.44)) was derived. The differential equation leading to the Green function was non-dimensionalised using this length scale. In order to compare the predictions made by the Green function and a numerical calculation, the same δ must be used. This δ can be calculated:

$$\delta = \frac{\gamma \overline{h}}{g\rho L_d^3 \sin\alpha} = 3 \tag{3.4}$$

Therefore in comparative calculations $\delta = 3$ will be used.

3.2.1 Relatively low topographies

For low topographies the numerical calculated profile and the prediction made by the Green function should agree very well. In Figure (3.1) the numerical calculation and the prediction for a topography of height 0.01 $T/\overline{h}$ and width L_d are shown. The predictions displayed in one graph (Figure (3.1(d))) coincide. This suggests that the two graphs match well within the desired precision.

3.2.2 The height of the topography relative to the average fluid thickness

The effect of the topography height relative to the average fluid thickness can be determined by investigating different topography heights. In Figure (3.2) several different topography heights are compared. The rectangular topography of which the height (relative to the topography) is varied is shown in Figure (3.2-(a)). The δ is, again, chosen to be the same as in the calculation of the Green function.
An effect not predicted by the Green theory is a dependence of the value of the maximum disturbance on the relative fluid height. Figure (3.2) shows that the disturbance increases more than is to be expected for a linear analysis for increasing topography height. The maximum fluid disturbance as a function of the relative fluid height according to the Green theory and the numerical calculation is plotted in Figure (3.2.2). The prediction made by the Green theory is linear in height. The numerical calculation clearly is not. A simple curve fit is not possible, though the difference between the maximum fluid height of the numerical calculation and the Green function shows a parabolical profile (Figure (3.2.2)).

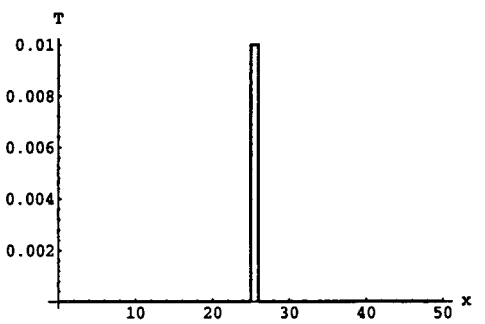

(a) The topography ($T/\overline{h} = 0.01$)

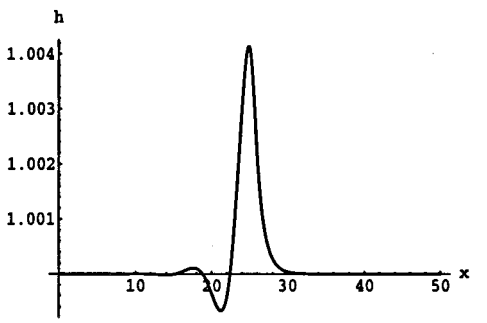

(b) Numerical calculation

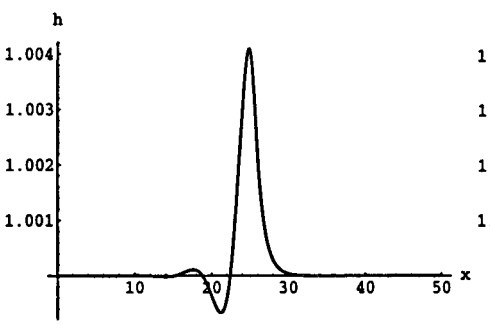

(c) Green function

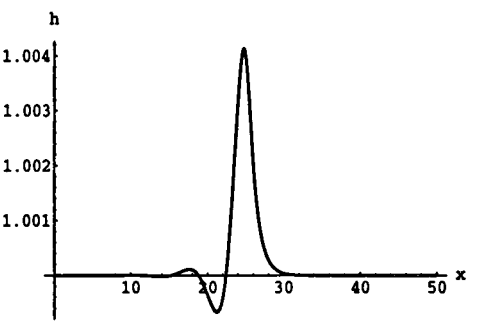

(d) Green + numerical

Figure 3.1: A comparison of the Green function and a numerical calculation ($\delta = 3$). In (a) the used topography is depicted, and in (b) the prediction of the fluid surface by the Green function for this topography. In (c) the prediction by the numerical calculation is shown and in (d) the two plots are placed together in one figure, they coincide.

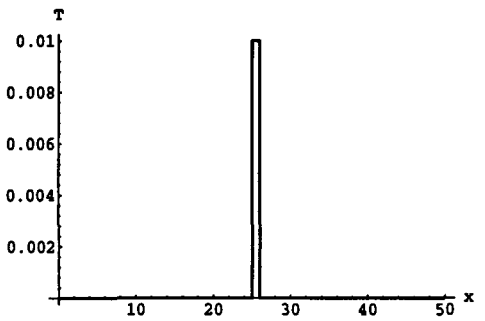

(a) The topography ($T/\overline{h} = 0.01$)

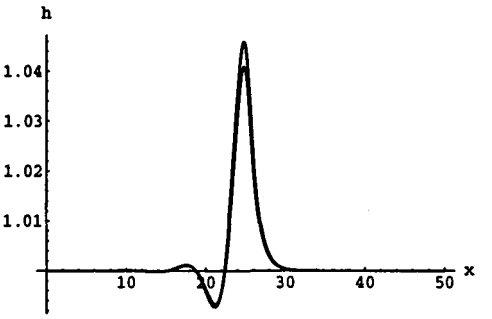

(b) $T/\overline{h} = 0.1$

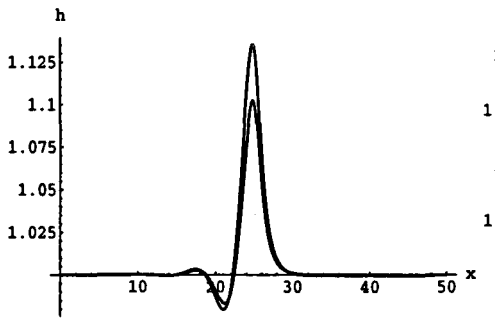

(c) $T/\overline{h} = 0.25$

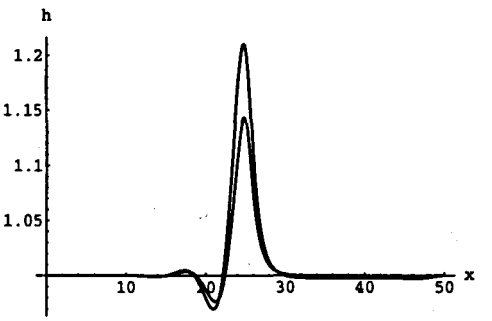

(d) $T/\overline{h} = 0.35$

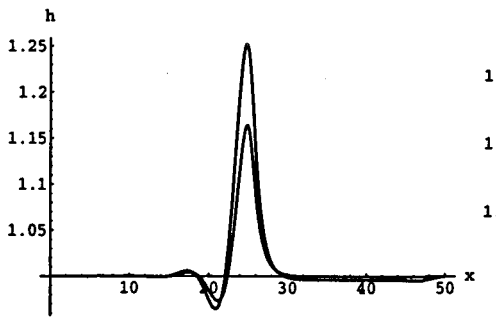

(e) $T/\overline{h} = 0.40$

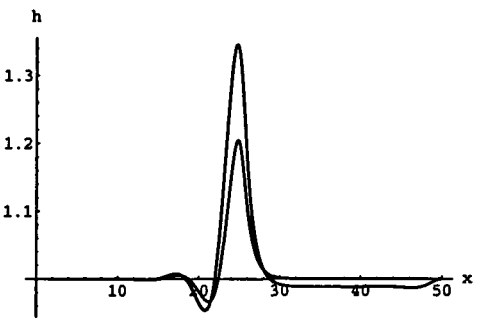

(f) $T/\overline{h} = 0.50$

Figure 3.2: A numerical calculation of the fluid profile ($\delta = 3$). In (a) a used topography is depicted, in (b)-(f) the height of this topography is varied, the Green function as well as the numerical calculations are shown. The topography (of unit width) is placed in the middle of the horizontal axes, e.g. on position (8,25,35,75). The amplitude of the prediction by the Green function is smaller than the amplitude of the prediction by the numerical calculation.

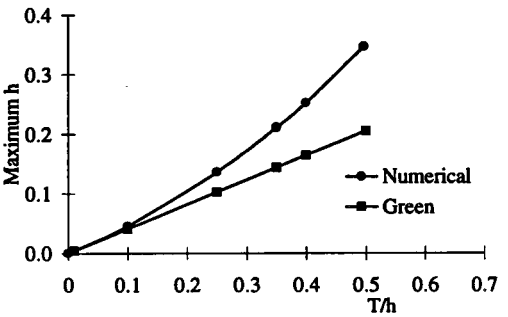

(a) The numerical calculation and the calculation with the Green function.

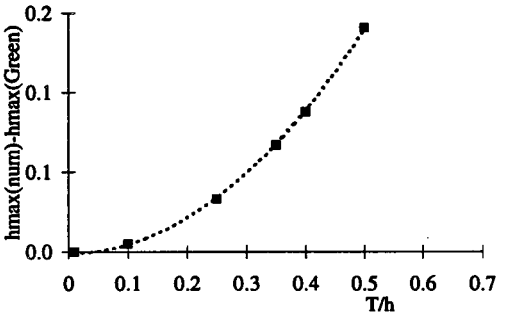

(b) The maximum fluid height according to the numerical calculation minus the maximum fluid height according to the calculation with the Green function. The plotted line is given by: $h = 0.563\left(\frac{T}{h}\right)^2$

Figure 3.3: The maximum fluid surface disturbance as a function of the relative topography height ($\delta = 3$).

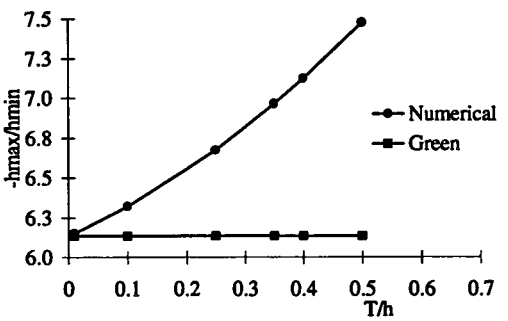

Figure 3.4: The amplitude of the maximum relative to the minimum ($\delta = 3$).

The Green function predicts the ratio of the amplitude of the maximum and the minimum to remain constant. The numerical calculation however shows a different dependence, as can be seen in Figure (3.4).
Another effect which can be observed from Figure (3.2), is a lower fluid profile after the fluid has passed the topography. This clearly is a numerical problem, the discrepancy diminishes as a finer grid is used. It might also be solved by incorporating flux conservation into the program. Of practical importance is the fact that with an increasing topography height the total horizontal extent of the profile remains constant. This was, of course, to be expected, for the differential equation was scaled with this length scale.

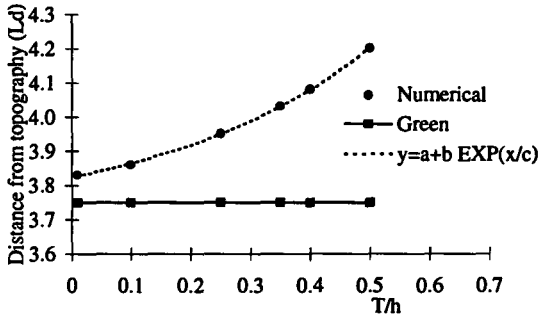

Figure 3.5: The position of the minimum in fluid height, relative to the position of the topography, as a function of the topography height. The constants in the equation describing the line through the numerical data are: $a = 3.70$, $b = 0.126$, $c = 0.361$ ($\delta = 3$).

However, the first maximum and minimum of the liquid profile appear to be (slightly) further upstream located than compared to the linear theory. In Figure (3.5) the horizontal distance (in Ld) of the minimum with respect to the topography is plotted. From this figure it can be seen that the horizontal positions of the minimum fluid height for the two calculations are not the same. In the limit of a very low topography this difference still exists ($\approx 0.08 L_d$). This is remarkable because for low topographies the prediction of the Green function is expected to be in accordance with the numerical calculation. The difference is small, though still larger (ten times) than the chosen calculation unit (grid), which suggests that the inconsistency is not merely an inaccuracy caused by rounding of the position (a too large grid). It is not important from an experimental point of view, for the lateral resolution of the measurement will not be high enough to detect this translation.

3.3 Effect of the dynamic capillary length scale

Another dimensionless parameter, in addition to $T/\overline{h}$, is δ. Varying δ can be accomplished by varying the length scale (b). The effect of changing δ has also been investigated.
Figure (3.6) shows the liquid profiles for several different values of δ.
With increasing δ, the capillary length scale decreases while the width of the topography remains constant. This implies that the topography gets relatively narrower. Thus with increasing δ the numerically calculated fluid profile will tend more to the profile predicted by the Green function for a delta function than a profile for a topography of width L_d. This effect is present in the figure. Another effect which can be noticed is a decreasing profile height with increasing δ. In Figure (3.7) the maximum fluid disturbance as a function of increasing δ is given.

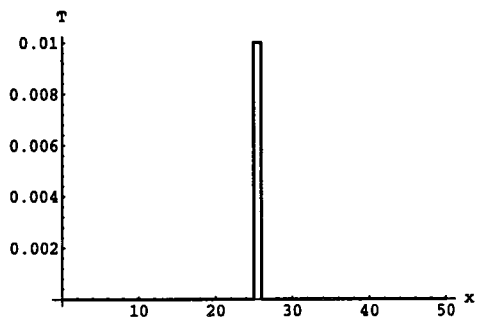

(a) The topography

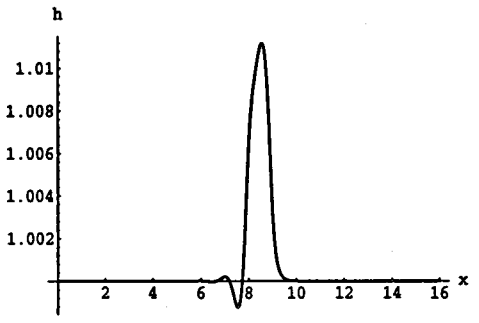

(b) $\delta = 0.01,\ b \approx 7L_d$

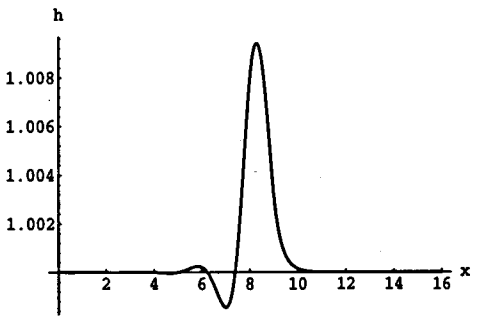

(c) $\delta = 0.1,\ b \approx 3L_d$

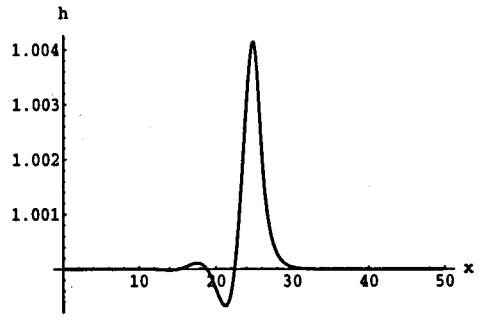

(d) $\delta = 3,\ b = L_d$

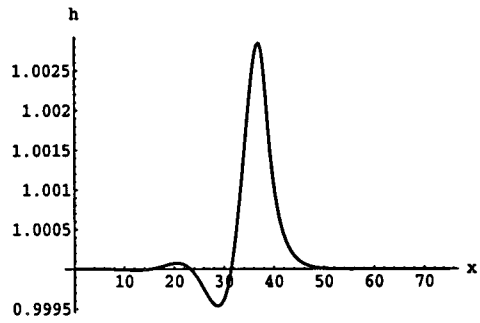

(e) $\delta = 10,\ b \approx 0.7L_d$

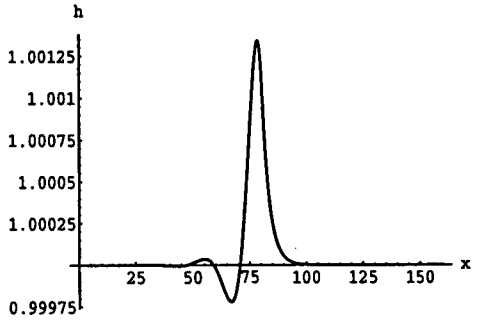

(f) $\delta = 100,\ b \approx 0.3L_d$

Figure 3.6: A numerical calculation of the fluid profile. In (a) the used topography is depicted, in (b)-(f) the dimensionless parameter δ is varied ($T/\overline{h} = 0.01$).

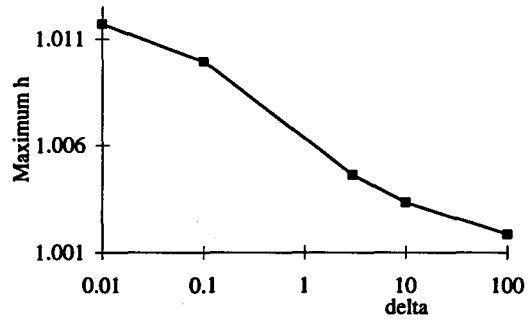

Figure 3.7: The maximum fluid profile height as a function of δ.

3.4 Different topographies

The fluid profile for the different topographies which were designed in Section (6.2.2) can be numerically computed. This will be done for all topographies and a relative topography height of $T/\overline{h} = 0.25$.

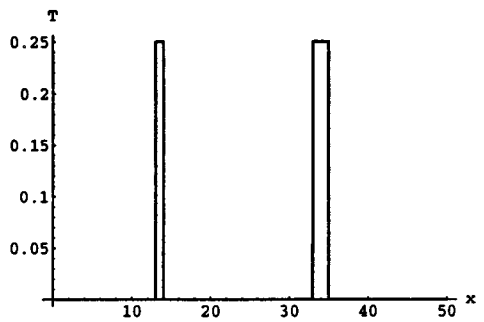

(a) Lines of 500 and 1000 μm

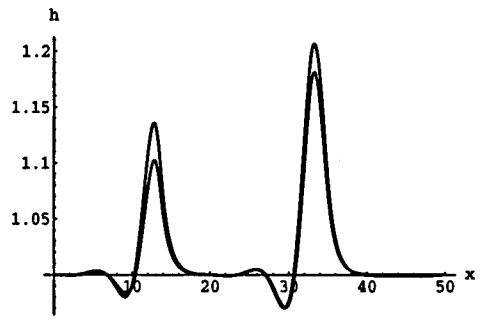

(b) Calculated profile

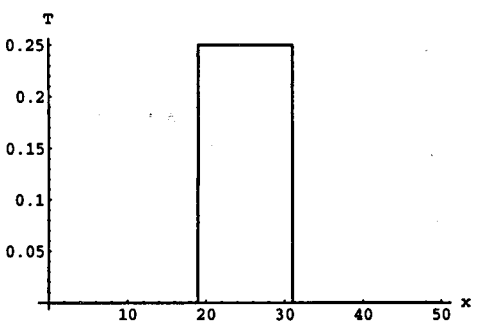

(c) A line of 6000 μm

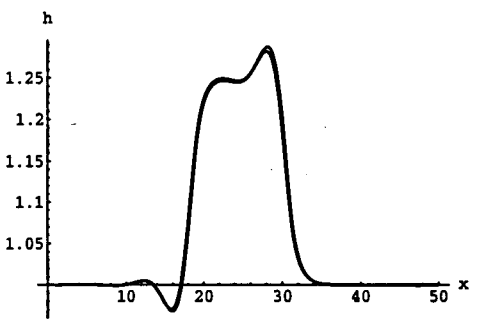

(d) Calculated profile

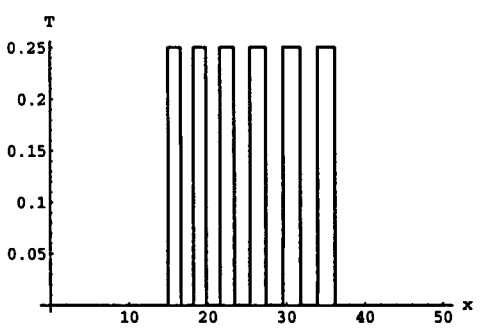

(e) Several lines of increasing width

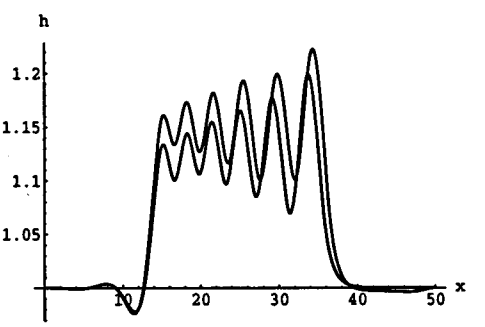

(f) Calculated profile

Figure 3.8: A numerical calculation of the fluid profile of different topographies $T/\overline{h} = 0.25$, ($\delta = 3$).

Chapter 4

The fluid flow

In order to be able to determine the profile of a fluid surface, a fluid flow has to be generated. This flow has to answer to certain requirements, which are needed to validate the theory. For instance, a fluid flow on an inclined plane can become unstable if the flow is too thick, this restricts the scaling possibilities. In this chapter these requirements will be investigated. Furthermore two different methods for generating a fluid flow will be investigated and compared. Finally a choice for a fluid flow assembly is made.

4.1 The requirements of a suitable flow

The most difficult aspect of designing a suitable flow, is the fact that the fluid thickness must be very small ($O(10\,\mu\mathrm{m})$). This causes a number of problems which will not occur for a thicker flow. Some basic requirements which apply to the flow are given below:

- The flow has to be translation invariant (section (2.1.2)) in the direction perpendicular to the flow, e.g.. no fingering or thickness variations in the region of interest may occur.
- The flow has to be fully developed in front of the topography.
- The flow has to be fairly stable with respect to disturbances, e.g. vibrations of the room.
- The flow has to be laminar in front of the topography.
- The flow has to be reproducible.
- The fluid height has to be adjustable.
- Different angles of inclination must be available for experiments.
- A measurement system must be applicable to the setup.
- Several topographies are required.

This list of requirements is an important tool for developing a setup which can be used to generate the flow on an inclined plane. These features are taken into account in the next sections when a suitable setup is designed.

4.2 The generation of a fluid flow

Two options were examined as possible candidates for generating the required flow;
a) generating the flow by using a slit, this option will be described in the next sections. And
b) generating the flow by a number of parallel capillaries. The description of this second assembly is nearly equivalent and will therefore be described in Appendix (C). First some research into the stability of a fluid flow on an inclined plane is conducted, which is applicable for both setup options.

4.2.1 Stability of a fluid flowing down an inclined plane

Under certain conditions a fluid flowing down an inclined plane can become unstable. This (unwanted) effect will be examined in this section. A Reynolds number is given by:

$$Re = \frac{U\bar{h}}{\nu} \tag{4.1}$$

The average velocity (U) can be calculated from Equation (2.28):

$$u = \left(\frac{P_x}{\mu} - \frac{\rho g \sin\alpha}{\mu}\right)\left(\frac{1}{2}z^2 - hz + Th - \frac{1}{2}T^2\right)$$

In this calculation the topography can be omitted ($T = 0$) in order to calculate the average velocity.

$$U = \frac{1}{\bar{h}}\int_0^{\bar{h}} u\mathrm{d}z \tag{4.2}$$

In the unperturbed flow the contribution of the surface tension term to the average velocity is everywhere negligible (except near the contact line [Troian 89]) and viscous and gravitational forces balance.
The result is:

$$U = \frac{g\bar{h}^2 \sin\alpha}{3\nu} \tag{4.3}$$

The Reynolds number (4.1) can now be written as:

$$Re = \frac{g\sin(\alpha)\bar{h}^3}{3\nu^2} \tag{4.4}$$

As shown by [Benney 66], [Yih 63] and [Benjamin 57] the critical Reynolds number for a stable fluid flow on an inclined plane under the influence of gravity and capillarity is given by:

$$Re = \frac{5}{6}\cot\alpha \tag{4.5}$$

With this result the maximum value for the angle of inclination for laminar flow (of water) can be calculated ($\nu = 1 \cdot 10^{-6}$, $h_0 = 40\,\mu$m):

$$\alpha = 76°$$

The maximum fluid thickness for which no surface instabilities occur can also be estimated:

$$\bar{h}^3 < \frac{10\nu^2 \cos\alpha}{4g \sin^2\alpha} \tag{4.6}$$

This gives:

$$h_{max,\, H_2O,\, 45^\circ} = 70\,\mu\text{m}$$

$$h_{max,\, H_2O,\, 22^\circ} = 120\,\mu\text{m}$$

This restricts the thickness of the fluid layer. However, the flow is only convectively unstable so if care is take that no disturbances are introduced upstream, the liquid film will still be smooth.

Scaling of the experiment

In principle it is possible to scale the experiment. This means that other measuring techniques might become available. However, it is sensible to develop some measuring techniques that might (with some adjustment) be applicable to a rotating system or to the spin coating process itself.
After calculation in the previous section it proved not to be possible to generate a stable flow which is more then approximately three times thicker than the coating flow (about $40\,\mu$m). Therefore, the mean fluid thickness will be vary between $30\,\mu$m and $120\,\mu$m .

Fingering and wetting

The size of the contact angle is an important factor in determining whether or not a liquid will wet a solid surface. If a film flowing over a solid is very thin, it is vulnerable to 'spontaneous' rupture. This in turn can lead to the undesired appearance of dry regions over the surface of the solid. A small contact angle promotes rewetting [Silvi 84], [Troian 89]. This implies that in order to improve the wetting (and rewetting) properties of a metal surface, the contact angle must decrease [Gennes 85]. This can be done by raising the surface energy of the metal. As in all natural systems in terms of energy it is advantageous for the metal to lower the surface energy. This causes dust and gases to be attracted and a monolayer will be formed on the surface. Thus the surface energy is lowered and the metal has become less hydrophilic. This in turn decreases the wettability of the surface. If the metal surface is thoroughly cleaned to an extreme level, the wettability will be significantly improved. It is important to maintain it in this state. If the metal is exposed to air, dust will sediment and the wettability will drop. Therefore it is vital to generate the fluid flow as soon as possible after cleaning the surface.
A second problem which might arise is fingering. If a viscous fluid is released on a horizontal surface it spreads in a circular shape [Hocking 83]. This process is stable to small disturbances which are initiated in the front of the spreading. But if the same fluid is released on a sloping surface the resulting shape is far from circular. Often the fluid breaks into rivulets (fingers), an instability [Huppert 82]. This fingering is an inherent phenomenon caused by surface tension and, even with perfect wetting, it ultimately occurs, [Schwartz 89]. While the value of the contact angle seems to play a secondary role in the instability responsible for the appearance of the rivulets, once the rivulets have formed, the contact angle is of prime importance in determining whether or not the surface of the solid

will be completely wetted by the liquid [Silvi 84]. Thus the problem can be minimised by increasing the wettability. If the fluid flux is temporarily increased when these rivulets occur, the fingering instabilities disappear and the surface will be completely wetted. This is experimentally verified (Appendix (J)).
In addition to the wetting properties of metal, the wettability of the substrate is also of importance. The wettability of the substrate has to be well enough to ensure a thin and translation invariant flow. Preferably the wetting properties of the topography and the substrate will be the same. Both of these features are subject to the choice of the substrate and topography and will therefore be dealt with in Section (6.2).

4.2.2 A slit

A thin flow can be generated by a slit: two metal plates with a foil in between, leaving an opening through which the fluid can flow. A cross-section of a slit is shown in Figure (4.2), page 31. It this section some calculations will be performed which are important when a slit is used to generate a thin flow.

Calculation of the slit width

The fluid is assumed incompressible and its viscosity as a constant. If no turbulence is present, the fluid flow inside a slit can be correctly described using a plane Poiseuille flow. The occurrence of turbulence can be estimated by the Reynolds number. After some calculations [Kundu 90] the horizontal velocity for a Poiseuille flow is given by:

$$u = -\frac{1}{2\mu}\frac{\mathrm{d}P}{\mathrm{d}x}y(d-y) \tag{4.7}$$

in which d represents the width of the slit. The flux can be calculated:

$$\phi_{slit} = \int_0^b \mathrm{d}y \int_0^d u\mathrm{d}z = -\frac{1}{12\mu}\frac{\mathrm{d}P}{\mathrm{d}x}bd^3 \tag{4.8}$$

The required flux (ϕ_{plate}) can be calculated using Equation (2.29), which describes the flux of a fluid flowing down an inclined plane:

$$\phi_{plate} = \int_{T(x)}^{h(x,t)} u\mathrm{d}z = \frac{1}{3}(h-T)^3\left(\frac{P_x}{\mu} - \frac{\rho g \sin\alpha}{\mu}\right) \tag{4.9}$$

In this calculation the topography can be omitted ($T = 0$) to calculate the average flux. The pressure gradient caused by capillarity is then negligible in comparison with the gravitational term, therefore:

$$\phi_{plate} = \int_0^B \int_b^h u\mathrm{d}y\mathrm{d}z = \frac{B\rho g \sin\alpha h^3}{3\mu} \tag{4.10}$$

The pressure, needed to force the fluid through the slit, will be applied by a reservoir of fluid with a relative height H to the slit. The pressure gradient can consequently be approximated as:

$$\frac{\mathrm{d}P}{\mathrm{d}x} \approx \frac{\Delta P}{\Delta x} = \frac{-\rho g H}{L} \tag{4.11}$$

For $\alpha = 22°$, $B/b = 6/6 = 1$, $L = 7$ cm, $H = 50$ cm, $h = 40\,\mu$m this gives:

$$d^3 = 4 \sin\alpha \frac{B}{b}\frac{L}{H} h^3 \propto 0.21 h^3 \tag{4.12}$$

$$d \approx 23\,\mu\text{m}$$

From Equation (4.12) the sensitivity to changes in the height of the liquid column can be calculated:

$$\frac{\delta\overline{h}}{\overline{h}} = \sqrt[3]{\frac{\delta H}{H}} \tag{4.13}$$

If the height of the liquid column (H) is known with an accuracy of 1%, the fluid height ($\overline{h}$) will have an accuracy of 0.3%. Note that the liquid height is independent of the viscosity of the fluid.
The deduction of these equations is only valid for certain values of the Reynolds number. The Reynolds number for a flow in a slit [Ward-Smith 80] is given by:

$$\text{Re} = \frac{\rho \overline{u} d}{\mu} \tag{4.14}$$

The length of the slit is represented by b and the height by d, as indicated in Figure (4.2). The average velocity $\overline{u}$ can be calculated:

$$\overline{u} = \frac{\phi_{slit}}{bd} \tag{4.15}$$

$$Re_{H_2O} \approx 0.005 \ll O(10^3) \tag{4.16}$$

This implies that the calculation is justified for this slit (d=26 μm) with H_2O.

Capillary pressure

If the applied pressure is smaller than the capillary pressure caused by a surface curvature at the opening, the fluid flow will stagnate. The required pressure for which the capillary pressure is balanced can be calculated (Figure (4.1)).

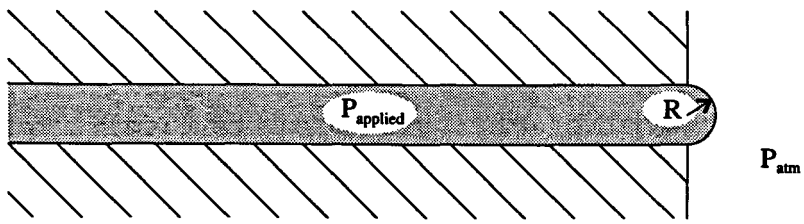

Figure 4.1: Drop forming at the opening of a slit. Drop forming can occur if $P_{capillary} > P_{applied}$.

In a state of equilibrium the capillary force equals the applied force:

$$\gamma\left(\frac{1}{R_1}+\frac{1}{R_2}\right)\pi R^2 = P\pi R^2 \tag{4.17}$$

in which $P = P_{applied} - P_{atm}$. For a slit ($R_1 = \frac{d}{2} \ll R_2$) and this yields for P:

$$P = \frac{2\gamma}{d} \tag{4.18}$$

Thus in order to maintain a steady flow it is required that $P > \frac{2\gamma}{d}$. The applied pressure depends on the slit width and on the required thickness of the fluid flow. In table (4.1) a summary is given. After the construction of the design was completed, it was experimentally verified that the liquid film, once generated, kept flowing and no stagnation was observed.

Table 4.1: Some values of P and P_{cap}. The surface tension of water is taken to be 73 $\cdot 10^{-3}$ Nm^{-1}. The angle of inclination is 22°($L = 0.07$cm). An asterisk (*) indicates that $P > P_{cap}$.

$\overline{h}$ (μm)	d (μm)	H (cm)	P (kPa)	P_{cap} (kPa)
40	15*	197	19	14
40	20*	83	8.1	7.3
40	25	43	4.2	5.8
40	40	10	0.98	3.7
40	60	3.1	0.30	2.4
100	40*	162	16	3.7
100	50*	83	8.1	2.92
100	80*	20	2.0	1.8
100	100	10	0.98	1.4
100	120	6.0	0.59	1.2
chosen	chosen	$\propto \overline{h}^3 d^{-3}$	$\propto \overline{h}^3 d^{-3}$	$\propto d^{-1}$

Deformation of the metal

A force which is exerted to a metal plate will cause the metal to deform. The opening of the slit will have to be in the order of tens of micrometers (Table (4.1)). This implies that deformation (bending) of the metal has to be limited, in order to obtain a smooth fluid surface. The slit will be composed of two sides: a top and a bottom. Each of these can be regarded as a steel plate with length l, width b en height d. The plates are clenched on both ends, some foil in between leaving a slit (figure (4.2)).
Both plates are exposed to a pressure P, which consists of the pressure generated needed to drive the flow. The maximum bending ΔZ_{max} [Creemers 87] occurs in the middle of the plates [Raaijmakers 89] and is given by:

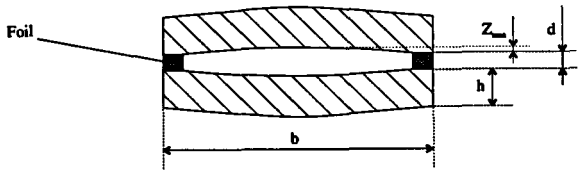

Figure 4.2: A cross-section of a slit.

$$\Delta Z_{max} = \frac{1}{384}\frac{Ql^3}{EI} \approx 1 \cdot 10^{-9}\text{m} \tag{4.19}$$

where E represents Youngs modulus, $I = \frac{1}{12}bh^3$ is the moment of inertia and $Q = Pbl$ is the total, equally distributed force. (l=7 cm, h=1 cm) The maximum deformation is small enough to not cause any problems ($2\Delta Z_{max}/d < 8 \cdot 10^{-4}$). The smallest thickness of one steel plate which is still within the required range ($\Delta Z_{max} < 1\,\mu$m) is:

$$h_{min} > 2.5\text{mm} \tag{4.20}$$

Thus the thickness of the metal plate of which the slit is constructed has to be at least 2.5 mm.

4.2.3 Water-level

If the assembly is not exactly placed water-level, the fluid height can vary over the width (y) of the flow. The fluid surface can be assumed to be flat. In this case the error in placing the setup water-level directly influences the measurement. This can be verified experimentally by measuring the thickness variations in the direction perpendicular to the flow. If the maximum slope is allowed to be 1 μm, then, for a sit width of 90 mm, the slit has to be placed horizontal with an accuracy of 90 μm.

4.3 The selection of a setup

The two designs options, a slit and capillaries, each have their own advantages and disadvantages. Some of these are listed below and summarized in Table (4.2).

1. The setup in which capillaries are used to generate a fluid flow is described in Appendix (C). Some of the advantages and disadvantages are listed here:

   - With a given fluid thickness, the diameter of the capillaries can be larger than the width of the slit. Therefore, the capillary pressure which has to be balanced against the applied pressure will be smaller. Thus less problems in relation to a stagnation of the fluid are expected.
   - The capillaries are less vulnerable with respect to pollution which can obstruct the flow, due to a larger possible diameter.

Some disadvantages of a setup using capillaries are:

- The capillaries must be attached parallel to a base. This can be tiresome, for the outer diameter is smaller than the required space between the capillaries.
- If a single capillary gets obstructed it is difficult to clean it (especially if this should be done during an experiment).
- The cleaning of the capillaries between two experiments can be quite tiresome. Each time another fluid is used, the capillaries have to be rinsed.
- If for any reason the diameter of the capillaries has to be altered, a new setup with different capillaries is needed.
- The absolute accuracy of the diameter of the capillaries is not very high. Probably the deviation between the capillaries is much less (Appendix C).
- The wettability of the surface must be quite good in order to generate and maintain a stable flow. It might be necessary to clean the surface of the base quite thoroughly. The attachment of the capillaries must be able to withstand this cleaning (for instance: organic solubles, UV-Ozone (Appendix (G)).
- The initial fluid profile is not flat but rippled (Appendix (??)).

2. In case an assembly which utilizes a slit is chosen the following advantages apply:

   - The slit can be constructed in such a way that the slit width is adjustable.
   - A demountable slit is a possibility, which makes it fairly easy to clean the parts.
   - The initial fluid profile will be flat in comparison to a system with capillaries. This even valid in case some irregularities are present in the slit, or if the slit is damaged.
   - In case the slit does not function properly, it can be reconstructed into a setup with capillaries, by attaching capillaries to the base of the slit.

   Some disadvantages of a setup using a slit are:

   - The slit width is small, therefore the capillary pressure can cause problems (Table (4.1)).
   - If the slit is demountable, it can be difficult to mount the slit accurately and reproducibly.

If the generated flow is not translation invariant, a groove can be cut after the fluid has left the slit/capillaries. This groove will cause a pressure gradient in the y-direction and will level the fluid surface.
A comparison between a slit and capillaries is given in table (4.2). After consideration of the advantages and disadvantages, it was decided to generate the fluid flow using a slit. The most important considerations in this decision were the facts that an assembly utilizing a slit is much more flexible, the fluid flow initially is more translation invariant and that the cleaning, a necessary evil, is easier.
Some capillaries were obtained as well, they can be used to modify the slit assembly in case this setup does not function properly.

Table 4.2: A summary of the advantages and disadvantages of an assembly utilizing a slit in comparison to an assembly utilizing capillaries. Where: [1] The applied pressure relative to the capillary pressure. [2] Adjustment of the slit width or radius of the capillaries. [3] The means to change the setup. [4] The translation invariance of the fluid profile. [5] The accuracy of the width, or radius.

	Drop forming[1]	Construction	Cleaning	Adjustment[2]
Slit	−	+	+	+
Capillaries	+	−	− −	−
	Backup[3]	**Obstruction**	**Flatness[4]**	**Accuracy[5]**
Slit	+	+	+	+
Capillaries	0	−	−	0

Chapter 5

Measurement systems

In this section a list of applicable measurement techniques is presented. The techniques are compared and a choice for a measurement setup is made.

5.1 Measurement methods

There are many and varied methods for determining the thickness of a fluid layer. They depend on such features as the nature of the layer, whether transparent or absorbing, the thickness range to encompass and whether or not it is required to study thickness changes with time.
In the present case the flow is stationary and thus the thickness will not vary with time. The fluid flow will be very thin, which severely limits the list of possible techniques. The film thickness will be in the order of $40\,\mu$m (Section (4.2.1)). The needed resolution is $1\,\mu$m in the thickness, and the lateral resolution must be close to $250\,\mu$m ($\frac{L_d}{2}$). The technique also has to cause a minimum disturbance to the flow. Although the measurements will be performed on an inclined plane instead of on a rotating disk, it is advisable to choose a technique which can also be used on a rotating disk.
Two main types of methods for fluid thickness measurement exist; (a) direct and (b) indirect methods. The direct methods mainly consist of surface contact devices. The objection to this method is obvious: by touching the surface of the film by a probe, or even worse by introducing the probe into the film, the natural flow of the film is impeded. Therefore, an altered flow is measured and this method does not present accurate information. The indirect method category contains systems using electrical or optical effects and can be divided into systems which measure the properties of the entire fluid or only the surface. Some of the most useful (indirect) techniques are briefly discussed below:

- *Electrical resistance;*
  The change of the electrical resistance due to thickness variations of the liquid film can be utilized as a measuring principle [Miyasaka 74]. This method is temperature dependent and also dependent on the polarization of the fluid and thus on its composition. This can be overcome by using a reference fluid: the same fluid with known thickness. A major drawback is the fact that this method can only measure at discrete points. Another disadvantage is the fact that the measured thickness is actually an average thickness over the area of the electrodes. However, this method is suitable for measurements on a rotating disk.

- *Capacitance;*
  It is possible to measure the thickness of a fluid flow by measuring the capacitance of the fluid and the air above [Black 61] [Fulford 64]. The capacitance sensor directly relates the strength of the electric field to the air gap between the sensor and the fluid [Thomas 91]. The method is dependent on the capacitance of the fluid, and thus a reference measurement has to be obtained. The dielectric constant of the fluid and of the topography can be matched to avoid disturbances by (the discontinuity of) the topography. This implies that the dielectric properties of the coating have to be measured. The dielectric constant should not be too close to that of air. The movement of the sensor might be a practical difficulty. The sensor should remain at the same height with respect to the fluid during scanning. A sensor close to the fluid makes it more difficult to influence the flow if it stagnates.

- *Fluorescent emission;*
  The fluid thickness can also be measured by laser induced fluorescence. To apply this method the fluid has to be coloured with a fluorescent dye. The dye can be excited by the light of a laser beam of appropriate wavelength. When the fluorescein returns to its ground state it emits light of a longer wavelength than the light of the laser. By measuring the intensity of the emitted light the thickness of the fluid layer can be obtained [Schmitt 82], [Driscoll 92]. This optical measurement system is attractive because there is no interference from background light. In order to obtain the absolute thickness a reference measurement must be obtained.

- *Light absorption;*
  As light passes through a non-transparent medium it will be partially absorbed. By detecting the intensity of transmitted light the thickness profile of the fluid can be determined [Charwat 72], [Thomas 91]. This method is fairly easy to implement. The accuracy of the method can be improved by matching the transmission coefficients of the fluid and the topography. The intensity of the transmitted light can be detected by a photocell [Driscoll 92]. The intensity of the transmitted beam can also be determined using a microdensitometer (MDM) [Beerens 95]. If a photograph is taken of the transmitted light, the negative can be scanned by the MDM. A picture can then be taken of the entire flow field at once. This method is difficult to implement on a rotating disk, for it requires a co-rotating camera.

- *Ellipsometry.*
  Ellipsometry is an optical technique which can be used for determining the thickness of a fluid layer. It measures the change in polarization state of a polarized light beam incident on the fluid at an oblique angle. The name originates from the general state of polarization after reflection or transmission which is elliptical. This technique is typically a technique used for very thin layers (up to mono layers) [Snyder 95].

- *Moiré effect;*
  In a Moiré measurement a grating is projected onto the surface. The projected fringes are deformed by the elevation of the liquid depending on the angle of incidence and detection. When this deformed fringe pattern is again imaged onto a grating, aliasing effects can introduce contour lines of the surface. These contour lines can be converted into a height map. This measurement system already is available within the lab

[Harbers 94]. However the maximum precision wich can be obtained is 1 μm [Kheshgi 82].

- *Interferometry;*
  It is possible to measure thickness gradients by using interferometry. The principle of an interferometric measurement consists of the phenomenon that two beams of coherent light show interference. If the two beams have a phase difference of zero, constructive interference occurs, if they are in anti-phase destructive interference occurs. The phase of a beam depends on the distance it has travelled. Interferometric measurements offer high accuracy. It is commonly used, and knowledge is present in the lab. Problems may arise if the thickness gradients are too large. It is possible to match the index of refraction of the fluid and the coating used for the topography. If this is done, the topography will be invisible for the interferometer. With a single beam interferometer no information on the (mean) film thickness is obtained, only surface gradients.

- *Focussing;*
  Complete laser pen systems are already available (for instance in a CD-player). These systems, which utilize a laser beam and a lens, automatically focus on the surface of the sample. As most surface measurement devices this system is not designed for determining a fluid profile. The index of reflection of water is roughly 4%, the laser is designed to work with a reflective coating of 90%. Furthermore these systems are designed for a maximum tilt of the substrate of around 1.6°, which is less than the slope of the fluid profile as calculated in Section (2.1.6). Another problem which might arise is whether the laser pen will focus upon the liquid or the substrate surface. The laser pen has to be scanned over the complete surface to obtain an image. Its low frequency response makes it unsuitable for use in analyzing spin coating over topography.

- *Triangulation;*
  By measuring the lateral movement of an oblique incoming laser beam the fluid profile can be obtained. The maximum resolution that can be obtained with this method lies within in the order of microns. The laser sheet has to be scanned over the surface. The drawbacks are the same as for focussing.

- *A commercial system (profilometer);*
  A commercial profilometer will become available. This system can measure the height of a surface by focussing a laser beam on this surface. The fluid flow has to be placed on a translation table, and therefore may not be too heavy. Due to geometrical constrains it is not possible to directly use the profilometer. The focal length of the used light source is too small to allow the use of mirrors. This method is not applicable on a rotating disk.

These results are summarized in Table (5.1).

Table 5.1: A summary of measuring techniques.

System	Range	Accu-racy	lateral resolution	Data retrieval	Avail-ability	Const-ruction	Height, profile
Resistance	0.3mm→	0.01mm	0.5mm	+	–	–	height
Capacitance	800 μm	80 μm		+	–	– –	height
Fluorescence	0.4 – 4mm	0.01mm	440 μm		–	0	height
Absorption	1 μm →	1 μm	50 μm	0	+	++	profile
Ellipsometry	1 μm	10^{-9} m			-	-	profile
Moiré	1 μm → cm	<1 μm		–	+	+	profile
Interferometry	0.5-100 μm	> 1 μm 100 μm		– –	++	+	profile
Focussing					+	–	height
Triangulation		< 1 μm			–		profile

5.2 Selecting a measurement method

As explained in the last section, each measurement system has its advantages and disadvantages. After evaluation interferometry and the light absorption technique are chosen. The most important consideration for this choice is, besides the fact that the system is suitable for the measuring purpose, that some experience and knowledge is already available within the lab. If some problems might arise during the construction or interpretation of the data, expert users can be consulted. Another consideration is the implementation of the technique for rotating disk measurements. The feasibility of a system for a rotating disk is not represented in table (5.1) for this also depends on a combination of other features as well as the particular design of the assembly.

Chapter 6

A design

6.1 A design of an experimental setup

In Section (4.3) it was decided to generate a fluid flow by using a slit.
The design process of this slit can be divided into a number of items which need attention. Some of these items are already discussed in Section (4.3) and will therefore be omitted.

1. It must be relatively easy to remove any potential air bubbles, and if possible, the design must possess an inherent capability to automatically remove the bubbles.

2. The metal profiles must be as smooth as possible to prevent turbulence from occurring. (Instead of sharp edges, rounded ones can be used.)

3. The properties and limits of the available construction techniques must be taken into account when designing the setup. It must be easy (and thus inexpensive) enough to fabricate.

4. The slit has to be connected to a fluid reservoir. Filters may be necessary to prevent particles from polluting the slit and blocking the flow.

5. The fluid which is used needs to be collected after usage and if possible should be recycled.

6. The flow must be fully developed and stable at the spot where the measurement occurs.

7. The design should allow for the changing of a topography to be simple and fast.

These considerations were taken into account when a design was made. In order to counteract the stagnating effects surface tension, a hydrophobic layer was applied to the front of the design (Appendix (K)). A photograph of the setup is presented in Figure (6.1). The drawing and the construction instructions are presented in Appendix (K).

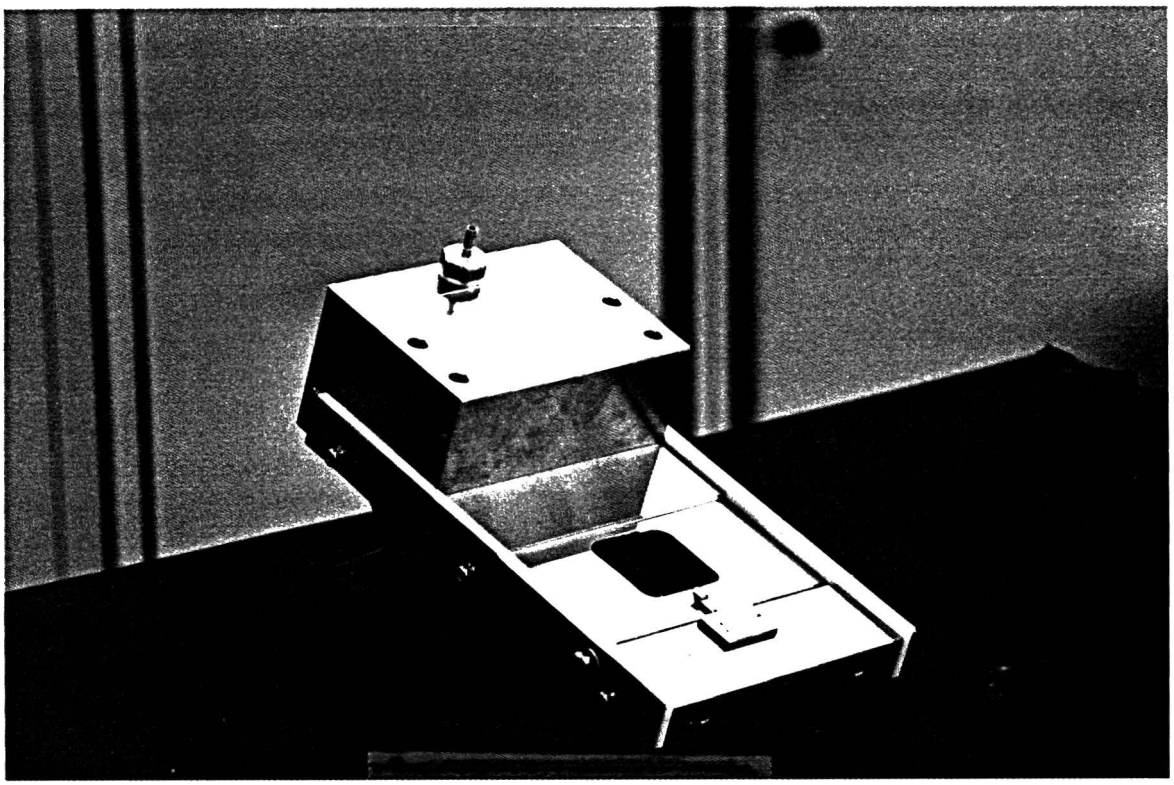

Figure 6.1: A photograph of the construction. The supply pipe can be connected to the bolt on top of the construction. The used fluid can be collected or re-used by means of the two connection holes on the (low) front side. A sample can be clenched in the middle of the construction by a clamp which, by means of a spring, presses the sample to the metal edge.

6.2 The topography

In the experiment the effect of a relatively large topography on a fluid flow on a inclined plane is to be examined. In this section the production of a topography as well as the design will be considered.

6.2.1 The production of the topography

A topography can be produced by a number of different production techniques. In [Beerens 95] Ron Beerens describes a photo lithographical technique. The topography, which was produced using this technique, was used for experiments on spin coating. The physical dimensions are in the same order of magnitude, therefore this method can also be used in the present case (Appendix (D)).

6.2.2 The design of the topography

In order to verify the validity of the theory of the Green function in principle only one topography is needed: a delta function. In practice it is sensible to design several different topographies in order to make a comparison and to vary the measuring range. It can be seen from Figure (2.3) that the distance of the disturbance caused by a delta function is 15 times the dynamical length scale. Thus the minimal distance necessary to remove any possible disturbances is 15 times this length. Using this information 4 topographies are designed on 3 substrates. In Figure (3.8), page (24) the topography as well as the predicted surface profiles are shown. In Figures (3.8(a)) and (3.8(b)) two topographies are placed: a line with a width of 500 μm and a line of 1000 μm, they are positioned 1000 μm apart. The predicted fluid profile caused by one line resembles the Green function for a delta topography. In Figure (3.8(c)) a step function is simulated by using a line of 6000 μm wide. The last topography is shown in Figure (3.8(e)). In this figure a number of lines are used, in order to use the full range of surface heights and slopes.

6.3 Selecting the liquid

Not every fluid can be used to perform the experiment. First of all the fluid has to be non-toxic, chemically stable and non-aggressive towards the coating, the density and viscosity should be in a practical range. Secondly, the fluid should be non-volatile, available in reasonable quantities (liters) and if possible the surface tension should be 'adjustable'. The measurement system further limits the choice of a fluid: the fluid should be optical clear, the index of refraction should be tunable, and the absorption spectrum should be adaptable. A suitable liquid which can be used is water. It meets all the above requirements. The surface tension of water is relatively high. By adding surfactants it is possible to lower this. Thus quite a large range of surface tensions
($73 \cdot 10^{-3}$ up to $20 \cdot 10^{-3}$ Nm^{-1}) can be investigated (Table 6.1).

If the liquid will be used for interferometry (Section (5.1)) it might prove necessary to match the index of refraction to the topography ($n = 1.6$), (Section (7.1.3)), [Budwig 94]. A suitable additive for this purpose is ZnI_2, (Section (7.1.3), Appendix (I)). If the liquid will

Table 6.1: Surfactants and surface tension. Where: [1] Critical Micellar Concentration, [2] (wt%)=(10 g/l), supplied material (not active component).

Surfactant	γ (mN/m)	CMC[1] (wt%)[2]	reactivity
Orotan	45	0.5	
Symperonic PE/F38	43,7	0.1	
Marlipal	28.5	0.02-0.2	
Didodecyldimethyl-ammoniumbromide	22	0.05	no reaction with surface or topography might react with colouring agents
Fluorad 3M	16.1	1.0	turns metal hydrophobic reacts with topography in pure form

be used for transmission measurements (Section (5.1)) the transparency has to be diminished. This can be done by adding colouring agents (Appendix (F)).

Chapter 7

An optical approach

In this section two (optical) techniques for measuring a fluid profile are described. The first technique uses interference, whereas the second is based on the absorption of light in a liquid. Some theory will be presented, as well as an experimental setup.

7.1 Interferometry

Two common types of interferometry systems can be distinguished:

1. *Interference by wavefront division;*
   The two interfering beams originate from the same wavefront. This can be achieved most conveniently by using two closely separated pinholes in order to create two sources. Due to wavefront division an interference pattern is obtained. This classical experiment is known as Young's experiment.

2. *Interference by amplitude division.*
   If a light wave is incident on a half-silvered mirror, or on an air-fluid interface, part of the wave is reflected and part is transmitted. Both the transmitted and reflected waves will have lower amplitudes than the original one. If the two beams are brought together in a detector interference will result (as long as the original coherence is still present).

The latter type of interference will be applied in order to measure the fluid profile.

7.1.1 Theory

In the experimental setup, the indecence of the laser beam will be perpendicular to the substrate. Part of the beam will reflect off the air-fluid interface, while part will be transmitted. The transmitted beam will be incident on the fluid-substrate interface (Figures (7.1) and (7.7)). Part of this beam will be reflected. The waves which are reflected from the first and the second interface will interfere. The interference can be constructive, destructive, or something in between, depending on the phase difference between the beams. This phase difference is influenced by the thickness of the fluid layer. Thus by utilizing interference a map of the fluid profile can be constructed.

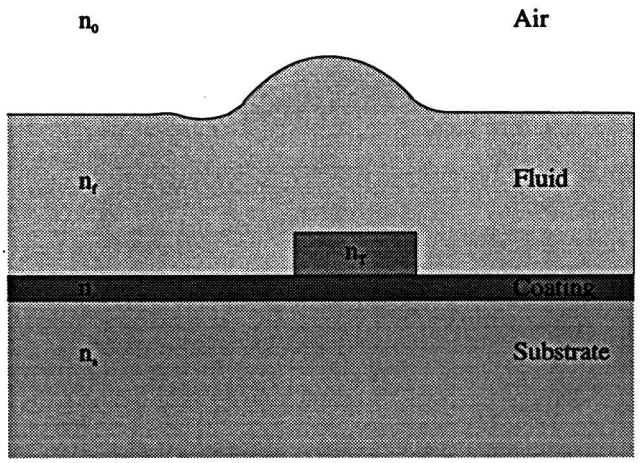

Figure 7.1: Schematic of the substrate and topography. The (line) topography is represented by the block (approximately in the centre), its index of refraction is n_T.

Consider two beams of coherent light. If these beams interfere the total irradiance (I) becomes [Hecht 87, 336]:

$$I = I_1 + I_2 + 2\sqrt{I_1 I_2 \cos\Delta} \tag{7.1}$$

in which I_1, I_2 are the irradiances of the two beams and Δ is the phase difference between the beams. The last term on the right hand side represents the term due to the interference. A maximum in the irradiance is obtained when $\cos\Delta = 1$. The maximum irradiance is then:

$$I_{max} = I_1 + I_2 + 2\sqrt{I_1 I_2} \tag{7.2}$$

A minimum in the irradiance occurs for $\cos\Delta = -1$ and is:

$$I_{min} = I_1 + I_2 - 2\sqrt{I_1 I_2} \tag{7.3}$$

If the irradiance contributions from both sources are equal ($I_1 = I_2 = I_0$) then $I_{min} = 0$ and $I_{max} = 4I_0$, this is the best contrast between the maxima and minima. The chosen fluid is of importance in determining whether or not an extra relative phase shift between the two reflected beams occurs. If a fluid is chosen with $n_f < n_c$ no extra relative phase shift will occur because the reflections on both the interfaces are external reflections [Hecht 87, 100]. The relative phase shift ($\Delta\phi$) between the two beams is:

$$\Delta\phi = k_0\Gamma \tag{7.4}$$

in which Γ is the optical path length difference between the two beams and k_0 is the propagation number in vacuum. The optical path length difference can be calculated to be:

$$\Gamma = 2hn_f \tag{7.5}$$

In reflected light an interference maximum occurs if the phase difference between the two beams equals an even multiple of π:

$$2m\pi = k_0\Gamma \tag{7.6}$$

An equation which describes the thickness of the fluid can now be calculated:

$$d = (2m)\frac{\lambda_0}{4n_f} \tag{7.7}$$

In this calculation $k_0 = \frac{2\pi}{\lambda_0}$ is used. The thickness variation between two successive fringes:

$$d = \frac{\lambda_0}{2n_f} \tag{7.8}$$

In Table (7.1) this thickness variation is presented for air, water and a fluid which mathes the index of refraction of the topography ($n_f = 1.6$). This is an important result, for it can be used to transform the fringes in an interferogram to a height profile of the fluid.

Table 7.1: The thickness variation between two successive fringes for different media.

d_{air}	$3.4 \cdot 10^{-7}$ m
d_{water}	$2.5 \cdot 10^{-7}$ m
d_{match}	$2.1 \cdot 10^{-7}$ m

7.1.2 Experimental setup

In this section the setup of the interferometer is described. A schematic of the setup is shown in Figure (7.2). A solid state laser is positioned in the focal point of a positive lens.

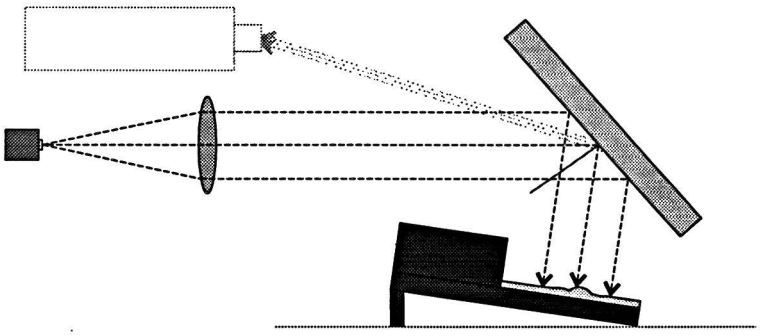

Figure 7.2: Optical setup. The light source is a solid state laser, the detector is a CCD-camera.

After passing the lens the beam is assumed parallel with a diameter of 40 mm. This beam is then diverted by a mirror and is (nearly) perpendicular incident on the substrate. The light which reflects off the first interface (air-fluid) interferes with the light which reflects off the second interface (fluid-substrat/topography). The incidence occurs under a small angle in the y-direction, which causes the beam reflect back under a slightly different angle. This method has the advantage that beam does not return to its point of origin and can be detected by a CCD-camera, without any beam splitters. Thus the image quality is highest. In between the mirror and the detector a lens is placed. This allows the detector to be focussed on the substrate.

7.1.3 Refraction index matching

The index of refraction of the topography is different from the index of refraction of the fluid. This causes a reflection from the fluid-topography interface and in case the entrance is not perpendicular to the topograph an extra refraction of the laser beam. It would be advantageous if a fluid could be used with the same index of refraction as the topography. The index of refraction of the topography for $\lambda = 670$, nm is $n_T = 1.61$ (Appendix (D)). This is a very high index of refraction in comparison with most commonly used liquids. Only a few liquids have an index of refraction which is this high, and these are mostly organic, volatile and toxic (Appendix (I)) . A suitable fluid with such a high index of refraction is a solution of zinc iodide (ZnI_2) in water. In Figure (7.3) the index of refraction as a function of the concentration of a zinc iodide solution is given.

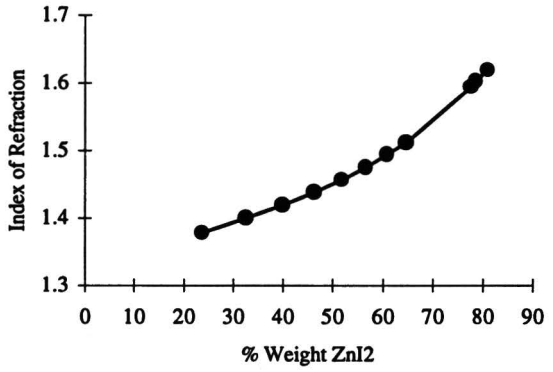

Figure 7.3: The index of refraction of ZnI_2 solutions at 21 °C for light with a wavelength of 633 nm , as a function of concentration [Hendriks 82]

The index of refraction can be matched by increasing or decreasing the concentration of the ZnI_2 solution. The kinematic viscosity is relatively low, which makes this solution even more suitable (Figure (7.4)).

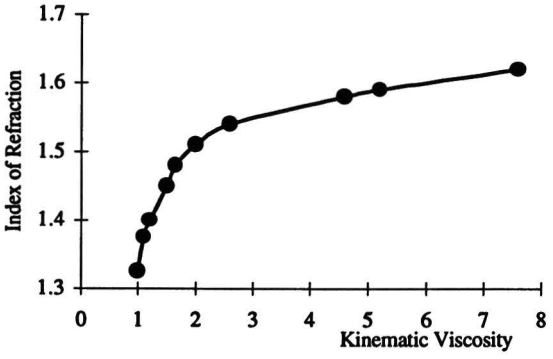

Figure 7.4: The relation between the index of refraction and the kinematic viscosity (in 10^{-6} m/s) for solutions of zinc iodide in water, at 21°C, 633 nm [Hendriks 82].

A requirement for the accuracy of the matching of the index of refraction can be found by stating that the irradiance returning from the fluid-topography interface ($I_{a,f}$) is negligible in comparison with the irradiance retuning from the air-fluid interface ($I_{f,T}$). If $I_{a,f} = 10 I_{f,T}$ then the ratio of the maximum irradiance to the minimum is: $\frac{I_{max}}{I_{min}} \approx 5$. If

$I_{a,f} = 100 I_{f,T}$ then $\frac{I_{max}}{I_{min}} \approx 1.5$. This last ratio can be used as a requirement for the needed accuracy of the matching of the indices of refraction.
The reflectance can be defined as the ratio of the reflected irradiance (I_r) to the incident irradiance (I_i):

$$R = \frac{I_r}{I_i} \tag{7.9}$$

Thus a requirement which states that $I_{a,f} > 100 I_{f,T}$ can be replaced by $R_{a,f} > 100 R_{f,T}$.
The refraction can be calculated using:

$$R = \left(\frac{n_f - n_T}{n_f + n_T} \right)^2 \tag{7.10}$$

The requirement then becomes:

$$R_{f,T} < 0.01 \cdot R_{a,f} \tag{7.11}$$

Thus:

$$n_f - n_T < 0.07 \tag{7.12}$$

7.1.4 Secondary interference

In addition to the required interference between the fluid surface and the (coated) glass surface, interference can also occur between the two surfaces (bottom and top) of the glass substrate. This secondary interference could be subtracted from the measurement by software calculations. It is easier, however, to suppress this interference. This can be done by utilizing the coherence length of the laser. The application of an anti-reflective coating on the back of the glass substrates was omitted.
The coherence length (Δx_c) is the extent in space over which a wave is nicely sinusoidal so that its phase can predicted reliably. Interference can only occur if the two beams are coherent. In order to obtain interference, the coherence length has to be larger than twice the thickness of the fluid layer. If the coherence length is smaller than twice the thickness of the glass plate (d_{glass}), no interference will occur between the beams reflected off the top of the glass and off the bottom. This means that a laser with a suitable coherence length can suppress the secondary interference, while the necessary interference still occurs. In order to achieve this the coherence length of the laser must be in the range:

$$2\overline{h} < x_c < d_{glass} \tag{7.13}$$

In practice this means 0.3 mm $< x_c <$ 2.8 mm. It has proven to be quite difficult to obtain a laser with such a coherence. It is possible, however, to decrease the coherence length of a solid state laser by reducing the power output of the laser. In the lower limit the laser will not produce any coherent light and will be similar to a normal light emitting diode (LED).

7.1.5 Gauge

A problem with constructing an interferometer for measuring a fluid thickness is the fact that a stable fluid flow is needed to perform a measurement. Because numerous problems arose while generating the flow this was quite cumbersome. Therefore a wedge, filled with air was constructed. This wedge, of which a schematic is shown in Figure (7.5), was used for measurements. An interferogram is shown in Figure (7.6).

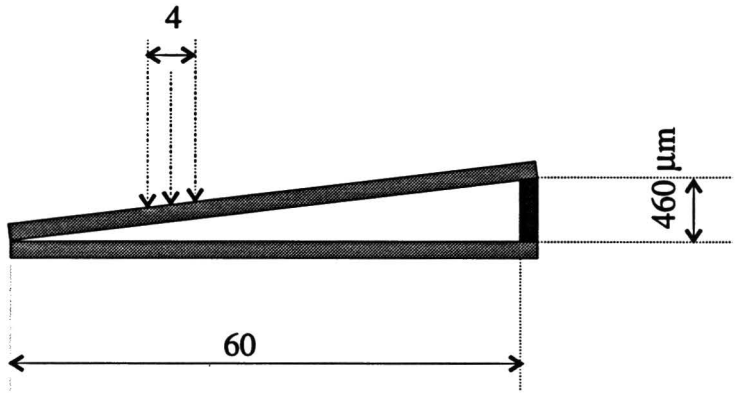

Figure 7.5: A schematic of a wedge, filled with air.

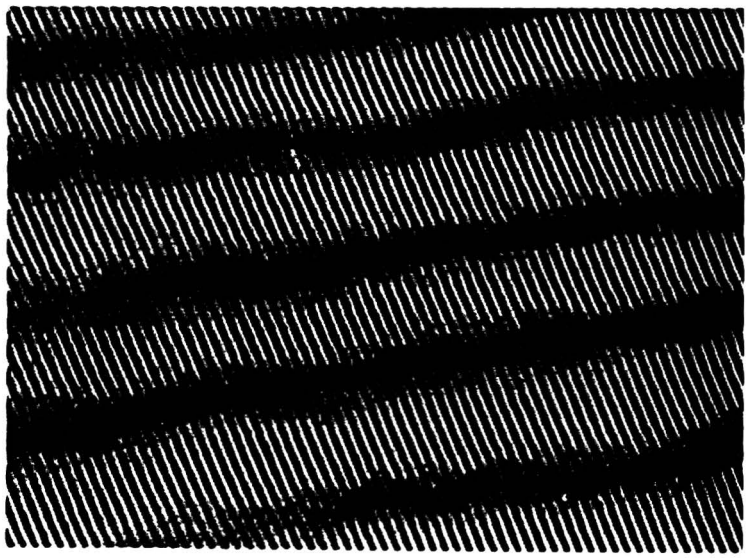

Figure 7.6: Interferogram of the wedge (from Figure (7.5)), filled with air.

In Figure (7.6) it can be seen that the fringes are parallel, and thus only a slope in one direction (the wedge) is present. The slope of the air inside the wedge is 7.7 μm/mm. The area which is visible in the interferogram is 4 mm long. In this area 112 fringes can be counted. If the slope of the wedge increases, the number of fringes increases with the same

factor. This corresponds to a detected slope of 9.4 μm/mm (Equation (7.8)). The horizontal lines also appear if only one of the glass plates of the wedge is used. Note that the index of refraction of air is only 1.0, thus for a liquid more fringes correspond the the same thickness. The picture can be enlarged, though, so that even for an index of refraction of 1.6 the slope can be detected. In Section (2.1.6) it was shown that the largest slope which has to be detected is of the order of 10 μm/mm. Thus by using a wedge is can be shown that the separation of the fringes caused by the predicted fluid surface is not too small to be detected.

7.1.6 Fluid surface curvature

If the fluid surface is curved, the incidence of the beam will not be perpendicular. This will cause refraction of the beam. In Section (2.1.6), the slopes of the fluid surface were calculated to be in the order of 10 μm/mm. In order to calculate the refraction the angle of incidence must be known. A slope of 10 μm/mm corresponds to an angle of the fluid surface relative to the substrate of: $\alpha = 0.57°$ (Figure (7.7)).

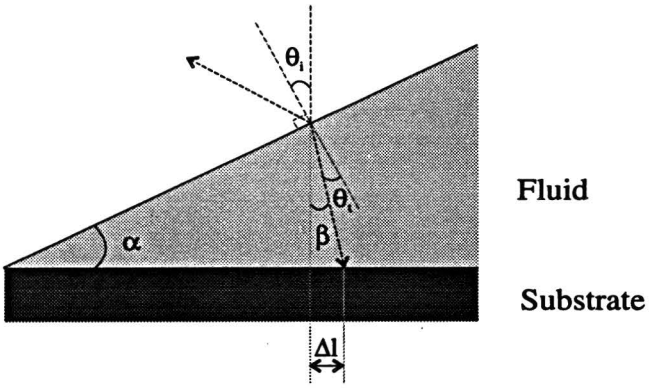

Figure 7.7: Refraction caused by a slope in the fluid surface.

The incoming beam is perpendicular to the substrate, which corresponds to an angle of incidence θ_i to the fluid surface. It can be shown that $\theta_i = \alpha$. The refraction can be calculated using Snell's law:

$$\sin\theta_t = \frac{n_a}{n_f}\sin\theta_i \tag{7.14}$$

For a matching fluid and slopes in the order of 10 μm/mm this yields: $\theta_t \approx 0.35°$.
The refraction caused by the slope of the fluid surface causes the optical path length to increase, thus giving rise to a larger measured thickness than the actual thickness of the fluid. The length the beam has to traverse before reaching the substrate can be calculated to be ($\beta = \theta_i = \theta_t$):

$$h_{slope} = h\cos(\theta_i - \theta_t) \tag{7.15}$$

This beam is reflected at the substrate and travels the same distance before reaching the surface of the fluid again (actually the 'return path' can be longer or shorter due to the slope of the surface, but this is negligible).
The length which will be traversed is therefore: $2 \cdot h_{slope}$. The deviation from the thickness of the fluid is : $(2 \cdot \overline{h}_{slope} - 2\overline{h}) \approx 1.5 \cdot 10^{-3}\ \mu$m) ($n_f = 1.6$). This is negligible in comparison with the differences in fluid height that have to be detected.

The horizontal displacement caused by the refraction is of importance in determining the spatial resolution of the measurement. With some basic geometry, and the assumption that the fluid height at the place of measurement can be approximated by the average fluid thickness, the lateral displacement of the beam can be calculated to be:

$$\Delta l \approx \overline{h} \tan(\theta_i - \theta_t) \tag{7.16}$$

The beam reflects off the substrate and the total lateral displacement will be ($\overline{h} = 100\,\mu$m) $2\Delta l \approx 0.8\,\mu$m, for $\overline{h} = 100\,\mu$m.
After this reflection the beam passes the fluid-air interface again, and will leave the fluid parallel to the incoming beam.
The slope of the fluid profile not only influences the refracted beam, but also the beam which reflects off the air-fluid interface (Figure (7.7)).
The angle of the reflected beam with respect to the incoming beam will be $\theta_r = 2\theta_i$. If the measurement occurs at a distance of 20 cm, the beam will have a lateral displacement of 2.4 mm. A beam of a considerable width will be used which implies that the light ray arriving from the surface of the fluid will interfere width the ray coming from the substrate at a lateral distance of 2.4 mm. Thus the lateral accuracy of the measurement will be strongly influenced by the slopes which have to be detected, and by the distance the light must travel before it reaches the point of measurement. The lateral precision can be increased by using a focussing lens.

7.1.7 Diffraction

Common phenomena in interferograms are a number of concentric circles appearing where it is not expected. These circles are caused by diffraction of the light on a small particle such as dust or a damaged lens. In the present case it is difficult to clean the surface of the samples, therefore diffraction will remain in the interferogram. The samples can be cleaned with water and soap. Another possibility might be a Marangoni drying process. If no lens system is used Fresnel diffraction might occur. In Figure (7.8) two examples of Fresnel diffraction are shown.

7.1.8 Position of the measurement

The positioning in the direction perpendicular to the flow (y-direction) is not of real interest because the flow is assumed translation invariant in this direction. However, the positioning in the direction of the flow is important. The positioning must have an accuracy which is better than the size of the dynamic capillary length scale. This can be achieved by placing a cover with a (square) hole above the flow. Only the light which passes the hole will be detected and thus the position of the measurement can be obtained. A disadvantage of this method is the inaccuracy which is caused by the diffraction at the edge of the hole (Figure (7.8)). It is also possible to mark the glass substrate. This mark will be visible in the interferogram.

7.2 Microdensitometer

A transmission measurement is another method for determining the fluid profile. The intensity of the transmitted light is a gauge for the thickness of the fluid. A very accurate

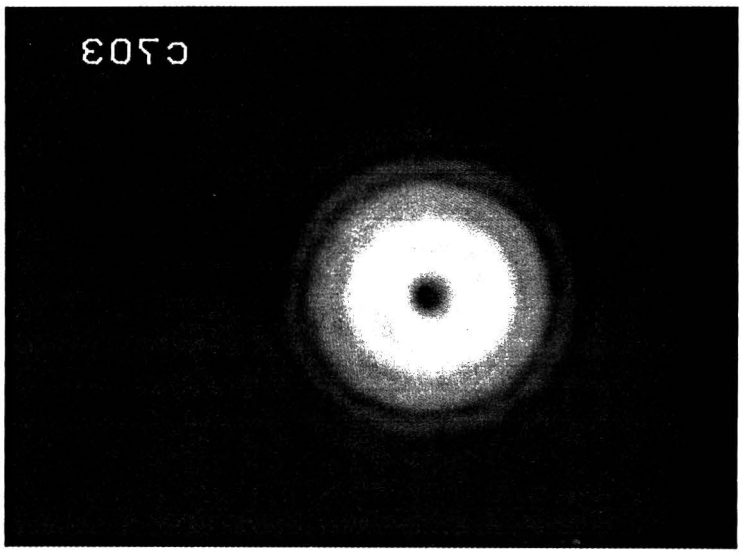

(a) A circular hole with a diameter of 2 mm.

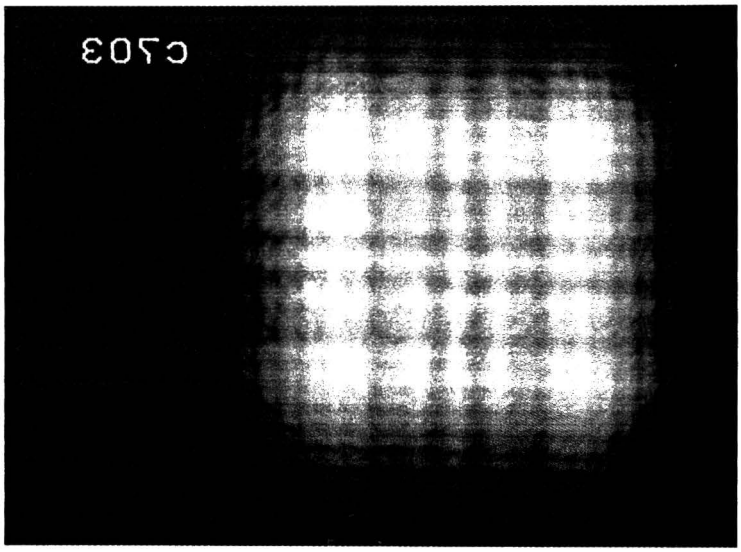

(b) A rectangular hole of 3x3 mm.

Figure 7.8: Fresnel diffraction.

transmission measurement can be obtained by using a microdensitometer (MDM).
The MDM can obtain a very high lateral resolution, as well as a very high density resolution. The MDM is an optical measurement device for transparent objects. It measures the density (blackening) of a sample. The sample must be placed upon a light source while the light beam traverses through the sample. This beam is focused on a light sensitive detector. A diaphragm can be place in the bundle, thereby determining the spot size on the sample. Optical adjustments (such as the focussing, and sensitivity) have to be made on the MDM itself, whereas motion control and measuring have to be performed by a Personal Computer. The microdensitometer does not present absolute data. Only relative densities are accurate.

7.2.1 Transmission measurement

The MDM can not be used on a tilted plane. Therefore it is not possible to determine the transmission of the fluid directly with the MDM. This drawback can be overcome by taking a photograph of the transmission. The negative can then be examined on the MDM. There a two major drawbacks to this detour. First, a measurement will take some time, for the photographs will have to be developed before using the MDM. Second, the blackening of the film is not linearly dependent on the illumination. An advantage is the very short period of time during which the photograph is taken. The flow will not vary during the time the measurement is made. (These variations can occur as disturbances in the flow due to for instance some vibrations of the table.)

The fluid will be illuminated from below by a fluorescent lamp and a diffusor. The negative is exposed to the light which has passed the sample and the fluid. In order to get an accurate measurement the absorption of the light by the fluid has to be increased. This can be done by adding coloring agents.

7.2.2 Theory

As light passes through any non-transparent medium it will be partially absorbed according to the relation:

$$\mathrm{d}I = -I\kappa\mathrm{d}z \tag{7.17}$$

in which I is the intensity (irradiance) of the light, $\mathrm{d}I$ is the differential change in intensity, κ is the absorption coefficient and $\mathrm{d}z$ is the differential path length through the absorbing medium. The intensity of the transmitted light, after the beam has traversed a path length d, is found by integrating Equation (7.17) to obtain:

$$I_t = I_0 e^{-\kappa d} \tag{7.18}$$

This equation is the well known Lambert-Beer law, where I_t is the intensity of the transmitted light and I_0 is the intensity of the incident light in the absorbing medium at the air-fluid interface.
A tradeoff has to be made between sensitivity and the strength of the signal, the best results will be acquired for $\kappa d = 2$.
The signal to noise ratio ($\frac{\Delta d}{d}$) can be calculated:

$$\frac{\Delta I_t}{\Delta d} \approx \frac{\partial I_t}{\partial d} = -I_0 \kappa e^{-kd} \tag{7.19}$$

$$\Delta I_t = -\kappa I_t \Delta d \tag{7.20}$$

$$\frac{\Delta I_t}{I_t} = -\kappa \Delta d = -\kappa d \frac{\Delta d}{d} \tag{7.21}$$

The MDM can reach a relative accuracy of $2.5 \cdot 10^{-4}$. This implies that:

$$\frac{\Delta d}{d} = -\frac{\Delta I_t}{I_t} \frac{1}{\kappa d} \approx 1 \cdot 10^{-4} \tag{7.22}$$

Thus $\Delta d \approx 1 \cdot 10^{-4} 100 \cdot 10^{-6} = 0.01\,\mu\text{m}$ The MDM does not measure the transmission of the fluid but the density of the negative (D). This density can be approximated by stating that the blackening of the negative is proportional to the logarithm of the intensity: $D = c \ln\left(\frac{I_t}{I_{neg}}\right)$. This implies an extra factor in Equation (7.22) of $\ln\left(\frac{I_t}{I_{neg}}\right)$. Unfortunately this relation ship between the blackening of the negative and the intensity of the light is not known. Thus the signal to noise ratio can not be calculated
The transmission coefficient κ is a function of the wavelength. Therefore Lambert-Beer's law is only valid for a small band width. It can also be applied if the coefficient of transmission can be assumed constant for the used wavelengths.

7.2.3 Interface reflection

When light is incident on the boundary between two materials, a portion of the light is reflected, while the remainder is transmitted. The portion which is transmitted depends, (next to the indices of refraction and the state of polarization) on the angle of incidence. Given the polarization state of the incident beam, the Fresnel equations and Snell's law can be used to obtain a transmission coefficient T. It can be shown that the extra reflection on account of the increased angle is negligible.

7.2.4 Gauge

In principle transmission measurements can offer information on the thickness of a fluid layer. The local thickness can be calculated using Lambert-Beer's law. In the present case this is not applicable since the blackening of the negative is not linear with respect to the wavelength and the intensity of the incoming light. It is still possible to acquire some height information by using a wedge filled with the fluid which is used for the experiments. An example of such a wedge is shown in Figure (7.5), page 47. Instead of air, the wedge must be filled with the used fluid.

Chapter 8

Results

In this section the results of the present report are presented. The results are split into two parts. The first describes the results of the design of a fluid flow. The second deals with the measurement of the fluid profile. Results of numerical calculations can be found in chapter (3).

8.1 The design

A comparison of two methods for the generation of a thin layer of fluid on an inclined plane is presented. A setup, based on the flow generation by a slit, was designed and constructed. This design incorporates an adjustable fluid height, easy cleaning, optical access from the bottom and an adjustable angle of inclination. A simple mechanism for inserting a sample has been implemented and three different topographies are fabricated. During the experimental construction some observations were made:

- The metal surface has to be cleaned to a extreme level in order to achieve the necessary wetting properties.
- Flows with a thickness of 40 μm are significantly more difficult to generate and to maintain than flows with a thickness of 100 μm .
- The time during which a stable fluid flow can be generated is strongly dependent upon the surfactant used.
- Air bubbles and obstructions of the slit do not cause problems.
- Only fluids with a low surface tension (< 30 mN/m) can be used due to the properties of the substrates.

8.2 The measurement

Several measurement techniques have been reviewed. It was decided to use two different (supplemental) techniques to determine the fluid profile. These are outlined in the next sections.

8.2.1 Interferometry

A wavefront splitting interferometer, based on a perpendicular incidence of the laser beam, has been constructed. In different regions of interest, different difficulties are encountered. In the first region the fluid elevation remains small, approximately 1 micron. This is valid for the minimum in the disturbance in front of the topography. In the second region the fluid elevation is high and large slopes occur. This is the case just in front, above and behind the topography. In the first region only a few (about 6) fringes can be seen over a distance of 5 L_d. This makes is difficult to determine the fluid surface. The fluid flow must be very stable in order to be able to measure the profile on a submicron scale. In the second region the fluid profile stretches up to 10 μm. The slopes are high (10 μm/mm) and thus a large number of fringes (> 40) are to be expected over a relatively small distance (1 mm). It has proven to be quite difficult to obtain an interferogram of the flow which has to be measured. The required slope can be tested by using a wedge, and this functions properly. In Figure (8.1) an interferogram is shown. The relevant data is presented in the caption. No interference can be seen. This is unexpected, for the measurement with the wedge did present satisfactory results. Some diffraction patterns can be noticed as well as some contamination. The figure also shows a bubble which floats with the flow. It can also be noticed that the topography appears to be slightly damaged.

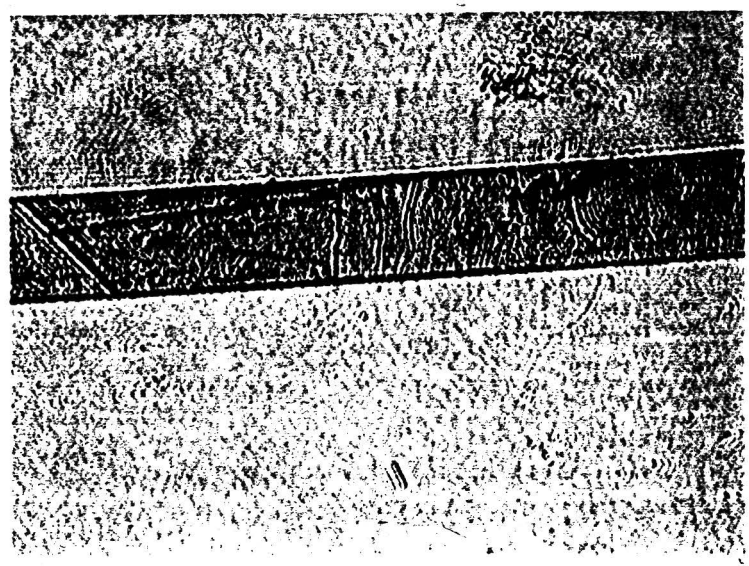

Figure 8.1: An interferometric measurement. The fluid flows from the top to the bottom. The line has a width of 1000 μm, and a hight of 12 μm. The average fluid thickness is calculated to be 133 μm, The fluid used is water with a surfactant (Fluorad), $\gamma = 16.1$ mN/m, $\alpha = 22°$, $n = 1.33$. The dynamic length scale is calculated to be: $L_d = 5.7 \cdot 10^{-4}$ m. The photo is two times enlarged.

If the fluid feed is interrupted, the layer becomes thinner. In Figure (8.2) an interferogram of this thinning flow can be seen. The interference pattern is not very stable and changes with time have been observed. The number of interference fringes seen here in front of the topography (10) indicates a slope of 1.8 μm/mm. This is much less than is expected from

the theoretical prediction for a stationary flow over topography (6.4 μm/mm). The number of rings seen behind the topography varies between 16 and 26, which corresponds to a slope of 1.6 μm/mm and 2.6 μm/mm. According to the theoretical prediction this should be 1.7 μm/mm, but this should occur over only half the distance of the situation in the interferogram.
In Figure (8.3) an interferogram is shown in which on the left hand side some fluid flows, and on the right hand side dry patches appear. On the right hand side a very thin fluid layer remains.

Figure 8.2: An interferogram of a thinning flow. The photo is enlarged two times.

It can be seen from the interferograms that the experimental setup does not reach the required range. A index matching fluid was not used because it is quite laborious to match the index of refraction. It is also convenient that the topography is visible. The topography gives a simple means to calculate the distance over which the fringes can be seen. The contrast of the interferograms will certainly improve if a index matching fluid is used.

8.3 Microdensitometer

In this section a description of the results obtained with a microdensitometer setup is given. After a series of measurements, one is chosen as an example for this section. The flow apparatus was placed on a diffuse light source. A filter (Appendix (F)) was placed in front of the camera, in order to improve the flatness of the transmission spectrum. The fluid is designed to absorb all the relevant frequencies in an equal, large amount, i.e. the fluid appears dark gray. In Appendix (F) the recipe for this 'cocktail' as well as its transmission spectrum is given.
First, a measurement was performed with a dry sample, this can be regarded as a measurement of the background transmission. Any irregularities in this background have to be taken into account when interpreting the data. After this, the fluid flow was started, and

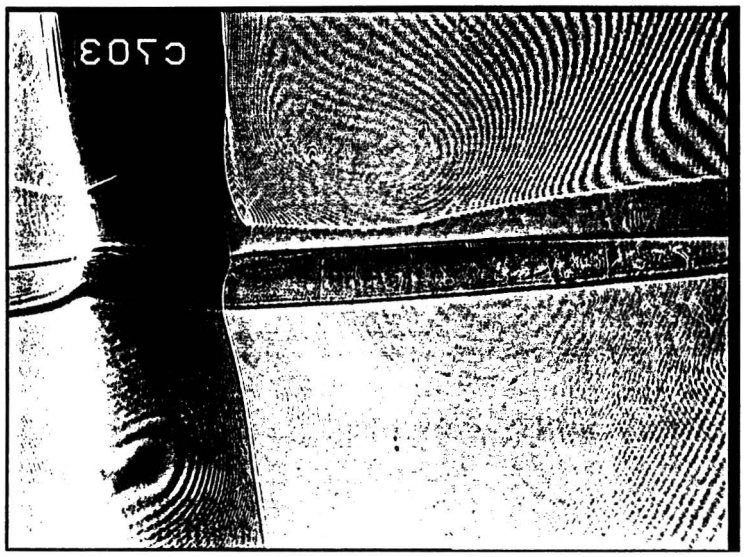

Figure 8.3: An interferogram. On the left hand side the fluid flows, on the right hand side a dry patch has formed. From this picture it can be noticed that the topography underneath the fluid appears translated, this is due to refraction of the light.

some photo's were taken of the substrate plus the fluid flow. The negatives were developed and scanned with a MDM. The results are depicted in Figure (8.4). The necessary data is given in the caption. The total extent of the plot can be related to a physical size of the sample of 30x30 mm^2. The lines are actually measuring points of 25x25 μm^2, a distance of 50 μm apart, on the negative. This is equivalent to an area of 65x65 μm^2 on the sample. Dark colours in the figure represent a low density (bright) on the negative, and is thus related to regions of low transmitted intensity. An exception to this is the colour of the topography, which should be darker than the ambient, this discrepancy is entirely due to a software transformation needed for the printing process. The background plot shows an increased amount of light on the sides. This might be caused by a non-even diffusivity of the light source.

If the two plots are compared it can be noticed that the overall darkness has increased, this is due to the absorption of the fluid layer. In Figure (8.5) two line scans, perpendicular and parallel to the topography, are shown. The scans are averaged as indicated in the figure. In this measurement the amplitude of the noise on a single line is 150 density units. This can be decreased by averaging over, for instance, 100 lines. The noise decreases proportional to one over the square root of the number of lines ($\propto n^{-\frac{1}{2}}$). After averaging the amplitude of the noise will be around 15 units. This is experimentally verified, which suggests that the adjoining measuring points are not correlated. The first decrease in density in Figure (8.5(a)) around $y = 5$ is caused by edge effects of the negative. The second decrease is caused by the topography, which is clearly visible. Only one line (500 μm wide) is shown, the other is omitted due to problems in the MDM software. The decrease in density caused by the topography is about 600 density points. The absorption of the topography is about 50%, (Appendix (F)). Therefore 600 density points can be related to an absorption of 50%. The decrease in density between the background measurement and the measurement with

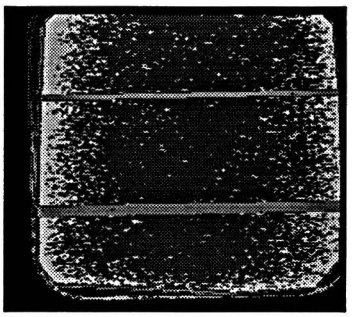

(a) Background measurement, no fluid is present. The picture consists of 243 horizontal lines and 228 vertical.

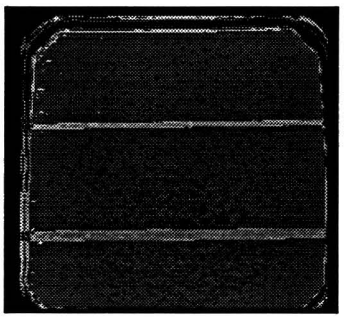

(b) Measurement with a fluid. The fluid flows from the top to the bottom. The picture consist of 236 horizontal lines and 230 vertical.

Figure 8.4: A MDM measurement of a line topography: a line of 500 μm and 1000 μm. The height of the topography is 12 μm, Aperture =(2x2)/80 mm, Step x=50 μm, Step y=50 μm, speed=800 μm/s. The fluid used is water in which a surfactant as well as colouring agents are dissolved. $L_d = 5,5 \cdot 10^{-4}$ m and $\overline{h} = 100\,\mu$m as calculated in Appendix (F).

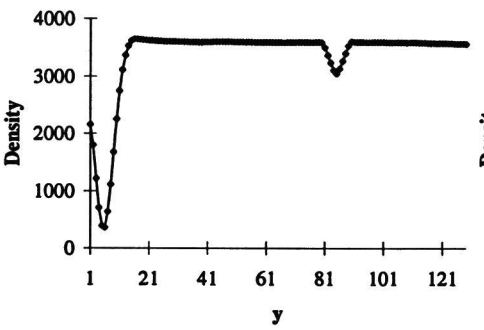

(a) A scan perpendicular to the topography, averaged over: lines 60 to 180. Only the first part of the scan is shown, due to a problem in the MDM-software.

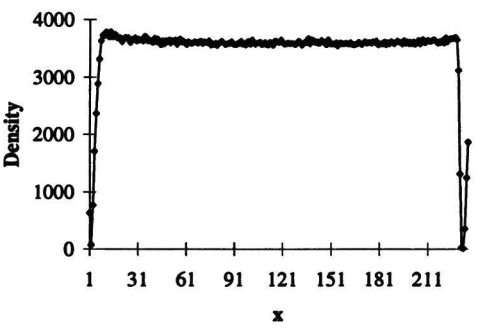

(b) A scan parallel to the topography, averaged over: lines 78 to 82.

Figure 8.5: Line scans from Figure (8.4(b)).

fluid is about 1250 density points. The fluid therefore can be calculated to have a transmission of 23%. The corresponding transmission for 1 μm can be calculated to be 98.5%. This can be related to 13 density points. This analysis shows that the noise level after averaging is of the same order of magnitude as the the required accuracy (1 μm), which can therefore not be reached. The maximum in the fluid elevation (about 6 μm, 80 density points) should become visible. However, this maximum is not observed.
In Figure (8.6) a measurement of a wedge is shown.

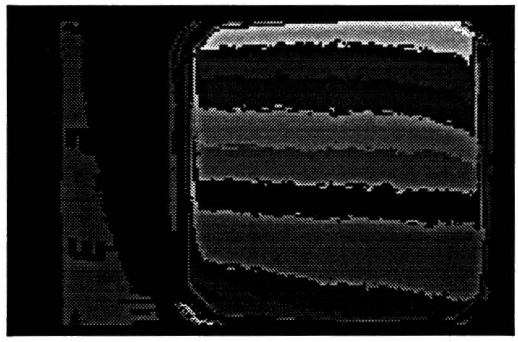

Figure 8.6: A MDM measurement of a wedge. On the top the fluid thickness equals 35 μm and on the bottom fluid thickness is 139 μm. The different colours indicate a different hight, the colour scheme is not correct due a non monotonic colour table in the software. Going from top to bottom, every subsequent colour should be one level lighter. A ruler is shown next to the wedge. The picture consists of 176 horizontal lines and 110 vertical.

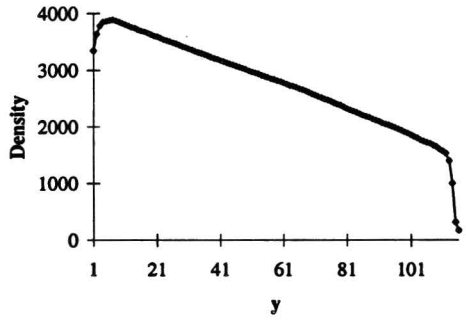

Figure 8.7: A MDM measurement of a wedge. Averaged over lines: 71 to 161. The thickness variation of the fluid is 104 μm.

The average fluid thickness can be determined by using the wedge. The change in intensity due to the fluid can be compared to a change in density of the wedge. The decrease in density points over the wedge is 1430. This can be calculated to be a decrease in intensity of 19%. This decrease of 19% can be related to a thickness variation of 104 μm of the wedge. Using this result the average fluid thickness in the experiment can be calculated: a transmission of 23% relates to a thickness of 92 μm. Thus by using a wedge the average fluid thickness can be calculated to be 92 μm , while the calculated fluid thickness is 100 μm. The noise level is approximately the same as for the measurements with the substrates: 100 density points before averaging.
From Figure (8.7) it can be seen that the measured density as a function of the height is approaching linearity. This is only valid for this photo, with this exposure time and blackening.

The aperture of the MDM can be chosen to be larger, to decrease the noise. The same effect can be reached by a manual integration of the data afterwards. This is experimentally verified. It could be advantageous though, to use an aperture of 2x20 mm^2, resulting in an actual spot size of 25x250 μm^2 on the film. If this aperture is used parallel to the lines, a high spatial resolution perpendicular to the line topography (the direction of interest) can be reached, while the data is inherently integrated in the lateral direction. It can be seen from the example in Figure (8.4) that the lines of the topography are not exactly horizontal. This is caused by the fact that the scanning of the negative has not occurred parallel to the topography. This has implications for the averaging, because the averaging should ideally occur in a direction parallel to the topography. This can be achieved by placing some (very dark) markers (for instance 4, one in each corner) on the samples. Then the negative can be (manually) placed parallel on the MDM, or a software rotation can be performed. Of course the markers should be placed on the bottom side, in order not to influence the flow.
The resolution of the present experimental setup is not high enough to distinguish any information about the fluid profile. It might be possible however to increase the sensitivity by using another fluid. It is also of importance to decrease the noise. This might be done by using a better light source.

Chapter 9

Conclusions and recommendations

In this report the flow of a thin layer of viscous fluid over topography on an inclined plane is investigated. The fluid profile was theoretically predicted. In order to provide a suitable flow, a design for a flow apparatus was made. Furthermore two methods for measuring the fluid profile were investigated.

9.1 Conclusions

9.1.1 The fluid profile

The fluid profile can be predicted by applying the lubrication approximation. The solution of the obtained differential equation can be described with a Green function. This Green function has been compared to numerical calculations. For low topographies the predictions of both calculations are equivalent. With increasing (relative) topography height, however, the difference of the two predictions increases. For high topographies the amplitude of the numerical calculation increases more than predicted by the Green theory. For high topographies the distance between the maximum elevation and the minimum as calculated by the numerical calculation is slightly larger. This has, however, no experimental relevance.

9.1.2 The design

A setup for the generation of a thin layer of fluid on an inclined plane was designed and constructed. It has proven to be quite cumbersome as well as time consuming to generate a stable thin layer of liquid. Nevertheless the flow of a thin layer of fluid on an inclined plane has been established. Furthermore different topographies have been designed and produced. The condition of the metal surface over which the fluid has to be generated is of importance. In order to increase the wettability the surface has to be cleaned very thoroughly. This can be successfully done by applying a UV-Ozone reactor. The wettability of the substrates is also of importance. In this research the wettability of the topography produced, was a limiting factor to the range of applicable surface tensions.

9.1.3 Interferometry

Interferometry can provide the means to detect the predicted fluid profile. The setup which was constructed did not (yet) provide the required results. The preliminary results indicate

that the method can and has to be improved. A wedge, filled with air was measured and the results were as expected. Therefore the maximum slopes, which are predicted by the theory can be detected. Some results were also obtained for very thin layers. A fluid with an index of refraction which matches the topography of the samples has been found. However, this interferometer has not yet been tested with this improved fluid.

9.1.4 Microdensitometer

Another method which can be used for determining the fluid profile is densitometry. This method can possibly achieve a height resolution of $1\,\mu$m . However, this has not been reached. The level of the background noise was too large in comparison with the absorption that could be expected from the theory. With this setup the maximum fluid elevation might have been detected, but this was not the case.

9.2 Recommendations

In order to achieve the desired experimental range the following might be considered:

- If new topographies are designed, check whether it is possible to produce the topography without a hydrophobical (HMDS) primer, in order to increase the wettability. Maybe then it will also be possible to entirely cover the substrate with a coating, which ensures the same wetting properties for the substrate as the topography.
- In order to simplify the development of the interferometer, try to find a stable, stagnant liquid film, of which the composition and geometry is known. For instance a drop of oil, or a stable meniscus.
- Use a stagnant fluid with a small (adjustable) thickness, to determine until which thickness the interferometer yields useful data.
- Design a construction which enables a lens to be closer situated to the surface.
- Apply the fluid with a matched index of refraction, in order to make the topography invisible for the interferometer. This will also increase the contrast between the fringes with maximum and minimum intensity.
- The camera in the present setup automatically adjusts the output brightness. It might be advantages to use a manual camera.
- Use a high resolution camera, and monitor.
- For the microdensitometer, try using a fluid, with a higher absorption, in combination of some filters.
- Use a better light source. It will not be easy to find a light source which is more diffuse, and which can be placed under the flow apparatus.
- Use a filter of which the absorption spectrum is similar to the transmission spectrum of the topography. The topography will not be visible in the measurement.

- Place some markers on the (bottom) of the substrate. The enables a better alignment of the negatives on the microdensitometer.
- Try several different photographic films. Experiment with the exposure time, the diaphragm and the method of film development.
- Investigate the possibility of using a digital camera, of which the relation between incoming intensity and the output for different frequencies is known.

We feel that the approach followed so far has been a good one and therefore this approach will be continued. Although the chosen measurement techniques do not yet reach the required range, the prospects for future research look promising. Both techniques have a different, but complementary range, a combination of these techniques will therefore offer a powerful set of experimental measurement tools. If a choice has to be made, interferometry might be more suitable for the present and future research than a transmission measurement, because it reaches the highest accuracy and is most versatile.

Bibliography

[Batchelor 67] G.K. Batchelor,
An Introduction to Fluid Dynamics. Cambridge, University Press (1967)

[Beerens 95] M.N.M. Beerens,
Spin Coating over Topography. Some Experimental Results Relevant to the Flow Coat Process. Nat.Lab. Technical Note NL-TN 139/95 (1995)

[Benjamin 57] T.B. Benjamin,
Wave Formation in Laminar Flow Down an Inclined Plane. J. Fluid. Mech. **2**, 554-574 (1957)

[Benney 66] D.J. Benney,
Long Waves on Liquid Films. J. Maths. & Phys. **45**, 150-155 (1966)

[Black 61] R.H. Black,
Capacitance Method of Measuring Water Film Thickness. Trans. Soc. Civil Engr. **126**, 88 (1963)

[Bordier 91] G. Bordier,
Free Surface Stationary Perturbations of a Thin Liquid Flowing down an Inclined Plane. Eur. J. Mech. B Fluids **10**, 29-49 (1991)

[Budwig 94] R. Budwig,
Refractive Index Matching Methods for Liquid Flow Investigations. Exp. Fluids **17**, 350-355 (1994)

[Camina 72] M. Camina F, D.M. Howell,
The Levelling of Paint Films. J. Oil Colour Chem. Assoc. **55**, 929-939 (1972)

[Charwat 72] A.F. Charwat, R.E. Kelly,
The Flow and Stability of Thin Liquid Films on a Rotating Disk. J. Fluid Mech. **53**, 227-255 (1972)

[Creemers 87] M.R. Creemers (red.), [et al.],
Poly-Technisch Zakboekje. Koninklijke PBNA, Arnhem, The Netherlands, Chapter C2, (1987)

[Driscoll 92] D.I. Driscoll, R.L. Schmitt, W.H. Stevenson,
Thin Flowing Liquid Film Thickness Measurement by Laser Induced Fluorescence. J. Fluids Eng. **114**, 107-112 (1992)

[Emslie 58] Alfred G. Emslie, Francis t. Bonner and Leslie G. Peck, *Flow of a Viscous Liquid on a Rotating Disk,* J. Appl. Phys. **29**, 858-862 (1958)

[Fulford 64] G.D. Fulford, *The Flow of Liquids in Thin Films.* Adv. Chem. Eng. **5**, 151-236 (1964)

[Gennes 85] P.G. de Gennes, *Wetting: Statics and Dynamics.* Rev. Mod. Phys. **57**, 827-863 (1985)

[Green90] F.J. Green, *The Sigma-Aldrich Handbook of Stains, Dyes and Indicators.* Aldrich Chemical Company, Inc. (1990)

[Gu 95] J. Gu, M.D. Bullwinkel, G.A. Campbell, *Spin Coating on a Substrate with Topography.* J. Elec. Chem. Soc. **142**, 907-913 (1995)

[Harbers 94] G. Harbers, P.J. Kunst, *Contactless Topography Measurement.* Nat. Lab. Technical Note 070-94, Philips Research Laboratories, Eindhoven, The Netherlands (1994)

[Hecht 87] E. Hecht, *Optics.* Second edition, Addison-Wesley Publishing Company (1987)

[Hendriks 82] F. Hendriks, A. Aviram, *Use of Zinc Iodide Solutions in Flow Research.* Rev. Sci. Instr.. **53**, 75-78 (1982)

[Higuera 95] F.J. Higuera, *Steady Creeping Flow down a Slope.* Phys. Fluids **7**, 2918-2920 (1995)

[Hocking 83] L. M. Hocking, *The Spreading of a Thin Drop by Gravity and Capillarity.* J. Mech. Appl. Math. **36**, 55-69 (1983)

[Huppert 82] Herbert. E. Huppert, *Flow and Instability of a Viscous Current down a Slope.* Nature **300**, 427-429 (1982)

[Hwang 89] J.H. Hwang, F. Ma, *On the flow of a thin liquid film over a rough rotating disk.* J. Appl. Phys. **66**, 388-394 (1989)

[Kheshgi 82] H.S. Kheshgi and L.E.Scriven, *Measurement of Liquid Film Profiles by Moiré Topography.* Chem. Eng. Sci. **38**, 525-534 (1983)

[Kundu 90] P. K. Kundu, *Fluid Mechanics.*, Academic Press, (1990)

[Lammers 94] J.H. Lammers,
Effects of Evaporation during the Spin Coating Process. Nat.Lab. Technical Note NL-TN 182/94 (1994)

[Lister 92] J. R. Lister,
Viscous Flow down an Inclined Plane from Point and Line Sources. J. Fluid Mech. **242**, 631-643 (1992)

[Meyerhofer 78] Dietriech Meyerhofer,
Characteristics of Resist Films Produced by Spinning. J. Appl. Phys. **49**, 3993-3997 (1978)

[Miyasaka 74] Yoshiki Miyasaka,
On the Flow of a Viscous Free Boundary Jet on a Rotating Fisk. Bull. JSME, **17**, 1469-1475 (1974)

[O'Brien 92] S.B.G. O'Brien,
Flow of a Newtonian Fluid on an Axisymmetric Rotating Substrate with Localised Defect. Nat. Lab. Technical Note NL-TN 266-92, Philips Research Laboratories, Eindhoven, The Netherlands (1992)

[Orchard 62] S.E. Orchard,
On Surface Levelling on Viscous Liquids and Gels. Appl. Sci. Res. A **11**, 451-465 (1962)

[Overdiep 86] W.S. Overdiep,
The Levelling of Paints. Progr. in Organic Coatings, **14** 159-175 (1986)

[Padday 75] J.F. Padday, A.R. Pitt, R.M. Pashley,
menisci at a Free Liquid Surface: Surface Tension from the Maximum Pull on a Rod. J. Chem. Soc. Faraday Trans. I, **71**, 1919-1931, (1975)

[Pozrikidis 88] C. Pozrikidis,
The flow of a liquid film along a periodic wall. J. Fluid Mech. **188**, 275-300 (1988)

[Pozrikidis 91] C. Pozrikidis, S.T. Thoroddsen,
The deformation of a liquid film flowing down an inclined plane wall over a small particle arrested on the wall. Phys. Fluids A, **3**, 2546-2558, (1991)

[Raaijmakers 89] A.A. Raaijmakers,
Werktuigbouwkunde voor E en N, collegediktaat, 004424-500005, Eindhoven University of Technology, The Netherlands, Chapter 1.8, (1989)

[Schmitt 82] R.L. Schmitt, W.H. Stevenson, H.C. Simmons,
Optical Measurement of Liquid Film Thickness. Laser Inst. of America 33, 31-35 (1982)

[Schwartz 89] L. W. Schwartz,
Viscous Flows down an Inclined Plane: Instability and Finger Formation. Phys. Fluids A **1**, 443-445 (1989)

[Silvi 84] N. Silvi, E.B. Dussan V,
On the Rewetting of an Inclined Surface by a Liquid. Phys. Fluids **28**, 5-7 (1985)

[Smith 72] Peter C. Smith,
A Similarity Solution for Slow Viscous Flow down an Inclined Plane. J. Fluid Mech. **58**, 275-288 (1973)

[Snyder 95] P. Snyder,
Ellipsometry. Handbook of Thin Film Process Technology, IOP Publishing Ltd, D2.3:1, D2.3:6 (1995)

[Thomas 91] S. Thomas, A. Faghri, W. Hankey,
Experimental Analysis and Flow Visualization of a Thin Liquid Film on a Stationary and Rotating Disk. J. Fluids Eng. **113**, 73-80 (1991)

[Troian 89] S.M. Troian, E. Herbolzheimer, S.A. Safran, J.F. Joanny,
Fingering Instabilities of Driven Spreading Films. Europhys. Lett. **10**, 25-30 (1989)

[Ward-Smith 80] A.J. Ward-Smith,
Internal Fluid Flow. The Fluid Dynamics of Flow in Pipes and Ducts. Oxford (1980)

[Yih 63] Chia-Shun Yih,
Stability of Liquid Flow down an Inclined Plane. Phys. Fluids, **6**, 321-334 (1963)

[Weast 86] R.C. Weast (ed.),
Handbook of Chemistry and Physics. CRC Press, Inc. (1986)

[Zavonte] L. Zavonte, R. Chiu,
UV-Ozone Cleaning For Organics Removal on Silicon Wafers. SPIE Optical Microlithography III **470**, 164-176, (1984)

Appendix A

Spin coating

This chapter is a contribution of J.H. Lammers (Philips).

A.1 Spin-coating on a flat substrate.

A short introduction of the spin-coating process on a flat substrate will be given.
The spin-coating process is industrially attractive because, ideally
(1) the coating thickness is independent of the amount of liquid dispensed.
(2) the coating is flat, independent of the precise way the liquid is dispensed.
This holds whether or not evaporation is important. If significant evaporation of any solvent occurs while rotating the substrate a thin dry coating is produced quickly.
(3) the evaporation rate for air flow over a rotating disk is quite high.
(4) the evaporation rate on a rotating disk is uniform.
A lot of requirements have to be fulfilled to obtain the ideal situation, e.g. the substrate has to be round and flat, enough coating liquid should be dispensed and it may be considered newtonian (i.e. the viscosity independent of shear rate), the air and liquid flow are stable, etc. Deviations from any of these requirements will show up as defects in the coating.
For a coating produced on a rough surface, one can imagine two limiting situations, i.e. the coating is conformal, or the coating surface is flat. Practically, one finds in-between situations. However, most annoying is the fact that for equal topography near the centre of rotation the coating profile is markedly different from the profile far away. Only this difference is considered to be a defect.
Descriptions of the spin coating process have been given by Emslie *et al.* (1958) for spin coating of non-volatile coating liquids and Meyerhofer (1978) for spin coating with evaporation.
Spin-coating without evaporation
Emslie *et al.* (1958) show how an initially non-flat liquid profile flattens and give an expression for the decrease in liquid height h for an initially flat layer of height h_0. The solution reads

$$h(t) = \frac{1}{\sqrt{\frac{4\rho_l\omega^2 t}{3\mu_l} + \frac{1}{h_0^2}}}.$$

The flow is driven by the centrifugal force, hence the density ρ_l and the square of the rotation rate ω are of importance. The flow is resisted by the viscosity of the liquid μ_l.

After some time $t \gg \frac{\mu_l}{\rho_l \omega^2 h_0^2}$, or equivalently $h \ll h_0$ one finds that

$$h(t) = \frac{1}{\sqrt{\frac{4\rho_l \omega^2 t}{3\mu_l}}}, \tag{A.1}$$

i.e. the layer thickness has become independent of the initial height h_0. This is also the limiting case for an initially non-flat liquid profile.
The reason why spin-coating works is that the average radial liquid velocity depends strongly on the liquid height and that the centrifugal force F_c is exactly proportional to the radius. (Remember the formula $F_c = mv_\theta^2/r$, with $v_\theta = \omega r$.) For a liquid layer which remains flat, the average radial liquid velocity should be proportional to the radius: The drainage is proportional to the area $Q = \dot{h}\pi r^2$, while the liquid flows through a ring of area $2\pi rh$. Hence the average radial liquid velocity $U_r = Q/A = \dot{h}\pi r^2/(2\pi rh)$ should be proportional to r. Indeed, the centrifugal force makes the radial velocity scale this way. It can also be shown that the decrease in liquid height also very strongly depends on the liquid height. Thus the initial flow is so fast, that the initial liquid height does not matter any more after some time.

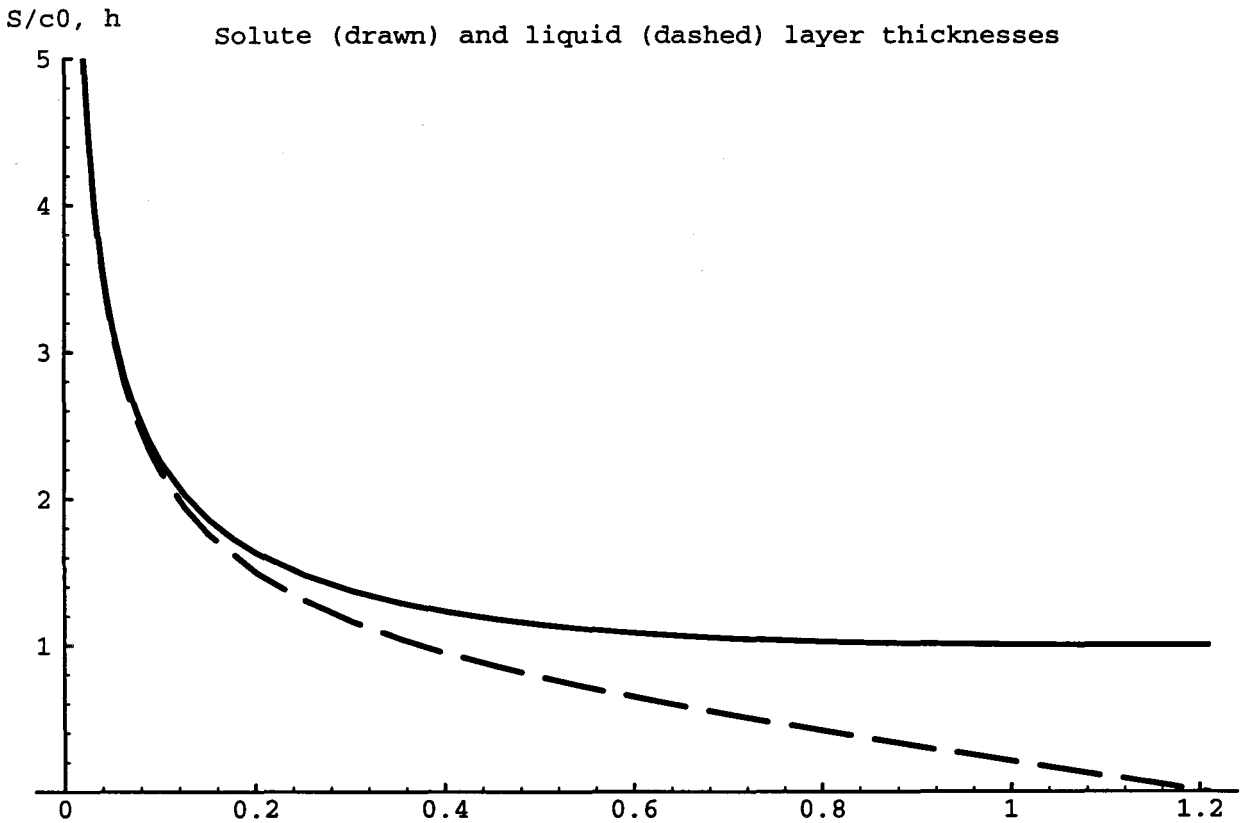

Figure A.1: Dependence of the liquid layer thickness h and solute thickness $S = c \cdot h$ on time t for a dilute coating liquid during spin-coating with evaporation. The height has been non-dimensionalised with $\tilde{h}$, eq.(A.2) the time with $\tilde{h}/e_v$.

Spin-coating with evaporation.
Meyerhofer (1978) has shown that for spin-coating with evaporation the process may conceptually be divided in two phases. The spinning phase, without significant influence of

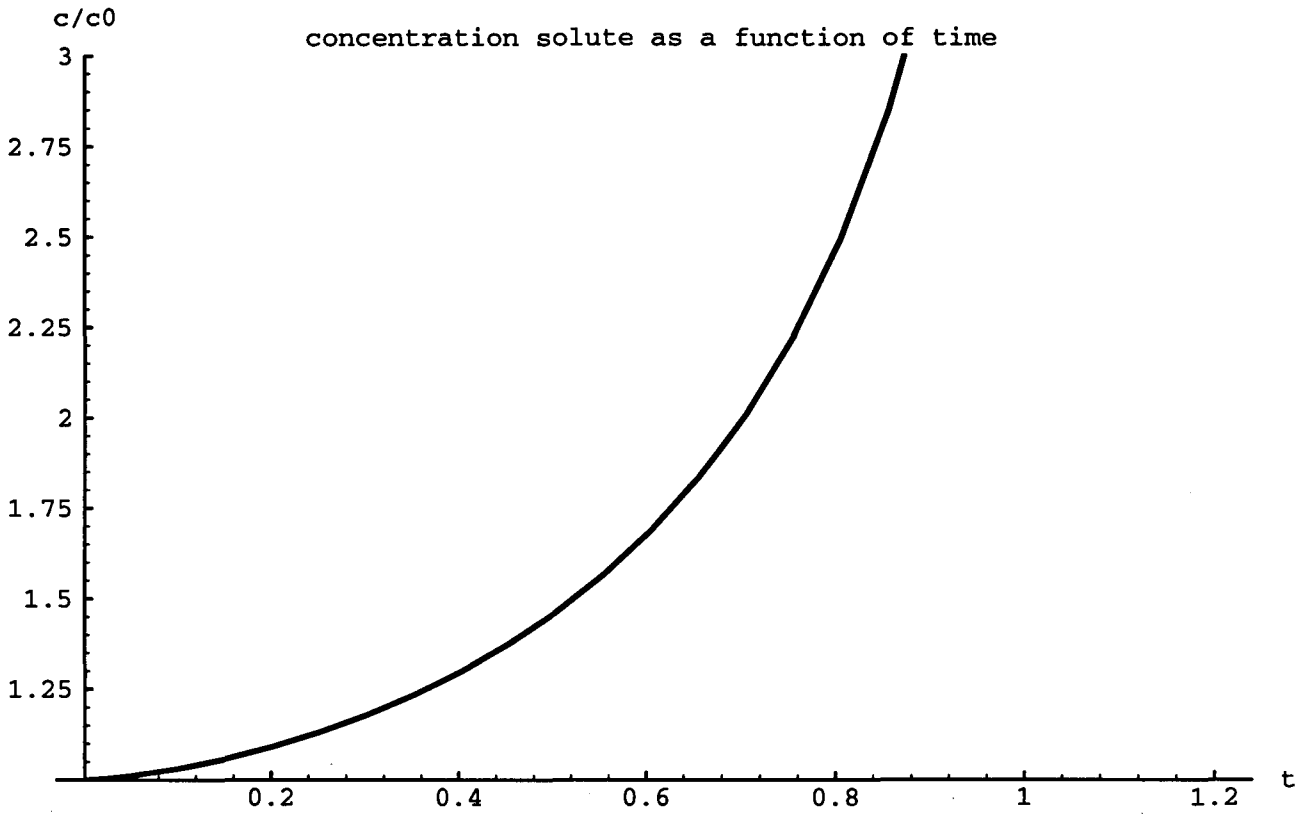

Figure A.2: Dependence of the solute concentration c on time t for a dilute coating liquid during spin-coating with evaporation. The concentration is scaled with its initial value.

evaporation, is as described by Emslie *et al.* (1958), viz. liquid levels and a wet layer results, whose layer thickness has become independent of the initial amount of liquid dispensed. Quite suddenly evaporation becomes dominant, as the decrease in liquid height very strongly depends on the liquid height. During the evaporation phase drainage due to the centrifugal force is negligible, the liquid layer thickness decreases due to evaporation only and the solute concentration of the coating liquid increases. The final coating thickness S_f is determined by the amount of solute present when drainage effectively ceases. This occurs for some typical layer thickness $\tilde{h}$, for which the decreases in liquid layer thickness due to both drainage and evaporation (rate e_v) are equal,

$$\tilde{h} = \left(\frac{3\mu_l e_v}{2\rho_l \omega^2}\right)^{\frac{1}{3}}. \tag{A.2}$$

Hence the final coating thickness is of the order

$$S_f = c_0 \tilde{h},, \tag{A.3}$$

with c_0 denoting the initial solute concentration in the coating liquid. For dilute coating liquids, for which changes in the viscosity and evaporation rate due to the increase in solute concentration are negligible, it can be shown that formula (A.3), obtained by Meyerhofer's crude analysis is the exact result. The exact development of the liquid thickness,

concentration and their product with time for a dilute coating liquid is given in figures (A.1) and (A.2).
Another formula will be useful when the evaporation rate cannot be calculated, but instead the dry-out time t_{dry} measured. It reads

$$\tilde{h} = 1.56 \frac{1}{\sqrt{\frac{4\rho_l \omega^2 t_{dry}}{3\mu_l}}},$$

which closely resembles formula (A.1).

An example.
Typical values for process design are for ethanol, spun at 300 rpm, 18° C, $c_0 = 1$ % :

$$\rho_l = 790 \text{ kg/m}^3,$$

$$\mu_l = 1.15 \text{ mPa.s},$$

$$\omega = 31.4 \text{ rad/s},$$

$$e_v = 0.9 \ \mu\text{m/s},$$

$$\tilde{h} = 13 \ \mu\text{m},$$

$$t_{dry} = 1.21\tilde{h}/e_v = 17 \text{ s}.$$

$$S_f = 130 \text{ nm}.$$

Thus in 17 seconds an optical coating of about quarter lambda thickness can be produced.

Typical values for process design are for a polymer plus water, spun at 120 rpm, 35° C:

$$\rho_l = 1000 \text{ kg/m}^3,$$

$$\mu_l = 10 \text{ mPa.s},$$

$$\omega = 31.4 \text{ rad/s},$$

$$e_v = 0.37 \ \mu\text{m/s},$$

$$\tilde{h} = 33 \ \mu\text{m}.$$

A.2 Spin-coating over topography: The simplest case.

Spin-coating over a step, located far from the centre of rotation, is a situation which lends itself well for both analytical description of the liquid flow and experimental characterization of the resulting coating. The relation with flow over topography on an inclined plane will be given.
Theory

The lubrication approximation yields the following equation for the description of viscous flow in a thin liquid film on a rough disk under the action of a centrifugal field in the presence of surface tension (Hwang & Ma, 1989) :

$$\frac{\partial h}{\partial t} = -\frac{1}{3r}\frac{\rho\omega^2}{\mu}\frac{\partial}{\partial r}\left(r^2(h-T)^3\right) - \frac{\gamma}{3\mu}\nabla\cdot\left((h-T)^3\nabla(\nabla^2 h)\right) - e_v. \tag{A.4}$$

The profile of the topography of the rough disk is given by $T(\boldsymbol{x})$, the surface tension by γ, while the other parameters are familiar from spin coating on a flat disk.
Hwang & Ma (1989) give results of numerical calculations performed for circular symmetric topography $T(r)$, e.g. as present on hard disks for data storage. Upon scaling with the initial liquid height h_0 (vertically) and typical radius R (laterally) they find that only one dimensionless (surface tension) parameter remains, viz.

$$\delta_R = \frac{\gamma h_0}{\rho_l \omega^2 R^4}. \tag{A.5}$$

It is instructive to investigate equation (A.4) in more detail. First of all, for another class of topographies a reduction of equation (A.4) to two dimensions can be found, viz. for a translation independent topography (in cartesian coordinates) $T(x)$ translation invariant solutions $h(x,t)$ exist ! The reason for this is that according to the lubrication approximation, as for Stokes flow, the velocity field responds linearly to the driving force, viz. the centrifugal field. As the centrifugal field is linear in r, so is its y-component, hence also the y-component of the velocity field $U_y = y\hat{U}_y(x,t)$. Note that there is no pressure gradient in the y-direction, since the liquid surface is not curved in that direction. Applying the divergence operator of the continuity equation to this velocity component yields $\partial/\partial y(U_y) = \hat{U}_y(x,t)$, which is independent of y. Likewise, the $x-$component of the centrifugal field, hence the x-component of the liquid velocity, is independent of y.
Upon non-dimensionalisation with the typical radius (shortest distance) R where a step is located, the evaporation rate e_v and with the typical height $\tilde{h}$ the equation becomes

$$\frac{\partial h}{\partial t} = -\frac{1}{2x}\frac{\partial}{\partial x}\left(x^2(h-T)^3\right) - \tilde{\delta}_R\frac{\partial}{\partial x}\left((h-T)^3\frac{\partial^3 h}{\partial x^3}\right) - 1. \tag{A.6}$$

For a flat liquid layer without topography this reduces to

$$\frac{\mathrm{d}h_0}{\mathrm{d}t} = -h_0^3 - 1, \tag{A.7}$$

for which the solution was shown in the previous section.
Next, we will linearize the equation, so the results may be used only for small topography heights $T = \epsilon T_1$, as compared to the typical liquid height. The liquid height is written $h(x,t) = h_0(t) + \epsilon h_1(x,t)$, so for the surface elevation h_1 the equation reads:

$$\frac{\partial h_1}{\partial t} = -3h_0^2(h_1 - T_1) - \frac{3}{2}xh_0^2\frac{\partial}{\partial x}(h_1 - T_1) - \tilde{\delta}_R h_0^3\frac{\partial^4 h_1}{\partial x^4}. \tag{A.8}$$

Note that evaporation does not appear explicitly in this equation.
We will consider the effect of a single disturbance located at $x = 1$. For a small dynamic capillary length (see definition A.10) $L_d \ll 1$ one can apply dominant balance between the

last two terms. This requirement will be met for a disturbance located far away from the centre of location. [1]
The approximation used here amounts to a quasi-steady force balance, assuming $\frac{\partial}{\partial x} \gg 1/x$ and setting x equal to unity near the topography, resulting in

$$0 = -\frac{3}{2}\frac{\partial}{\partial x}(h_1 - T_1) - \tilde{\delta}_R h_0 \frac{\partial^4 h_1}{\partial x^4}. \tag{A.9}$$

The instantaneous dimensionless dynamic capillary length is defined as

$$L_d(t) = \left(\frac{2}{3}\tilde{\delta}_R h_0(t)\right)^{\frac{1}{3}} \tag{A.10}$$

and can be used to rescale equation (A.9) into

$$\frac{\partial h_1}{\partial x} + \frac{\partial^4 h_1}{\partial x^4} = \frac{\partial T_1}{\partial x}, \tag{A.11}$$

One integration is easily performed, for vanishing elevation and topography at infinity,

$$h_1 + \frac{\partial^4 h_1}{\partial x^3} = T_1. \tag{A.12}$$

From this equation, one grasps the idea of the description of the elevation h_1 as a response to the topography T_1 by means of a Green function.
Equation (A.12) also describes the flow on an inclined plane over topography. For a given liquid and equal topography and liquid layer thicknesses the flows on a rotating disk (far from the centre of rotation) and on an inclined plane are similar (Pozrikidis 1988), provided that the driving body forces are comparable, viz. $g \sin\alpha = \omega^2 R$. For flow-coating of a phosphor suspension one typically has $\omega = 120$ rpm $= 13$ rad/s. For R take 3 cm, say the result is $\omega^2 R = 5$ m^2/s, so scaling is possible by choosing $\sin\alpha = 0.5$. But, since no parameters appear in eq.(A.12) one might consider experiments with different liquids, liquid layer thicknesses or even length scales as well.
Experimental verification for spin coating
There are several ways one might verify the description given above for spin coating.
(1) One can dream of visualizing the liquid layer while the average thickness decreases. This is presently not possible.
(2) A stationary flow on a rotating disk can be set up by continuously pouring liquid onto it near the centre of rotation. Visualizing this flow is an option after gaining some experience with visualisation of flow on an inclined plane. Even though the base flows differ somewhat, viz. developing in time or space, one still arrives at the same equation, (A.12).
(3) After suddenly stopping the rotation flow the liquid continues to flow, due to the leveling action of surface tension. One might try to freeze the liquid profile quickly by using a photosensitive coating liquid and suddenly expose the layer to a high dose.

[1] The approximation does not apply near the centre of rotation, where the North-South line in TV screens is formed. In that case another approximation, using strained coordinated, can be made. This is beyond the scope of this research. However, the results of the analysis for the North-South line are easy to interpret, once one knows the phenomena for the simplest case, viz. whether the (local) dynamic capillary length, eq. A.10 is small, large or approximately equal to the wavelength of topography.

(4) As for the case of spin coating on a flat disk, one might be able to invoke Meyerhofer's rough argument that flow effectively ceases as the layer thickness becomes smaller than the typical value $\tilde{h}$. However, this is only true if the dynamic capillary length is not too small compared to the radius, since otherwise just a little flow is sufficient to alter the final coating profile considerably. This has not been analysed thoroughly yet. Numerical calculations can be performed to investigate this further.
Recently, coatings were produced by a colleague, dr. I. Snijkers-Hendrickx by spin coating, until dry, on a substrate on which a piece of cellotape was present. After removing the tape the thickness in front of the tape was measured to obtain the average coating thickness. Usually, a wavy profile as predicted for the liquid profile is observed in the coating as well, see figure (A.3). Since the liquid profile in front of a step is selfsimilar, a similar profile can be expected for the coating profile. Another reason for numerical analysis is obvious here. The deviation of the coating thickness is of the order of the thickness itself. This is because the cellotape thickness is of the order of the typical liquid height. We will proceed with these off-line measurements.

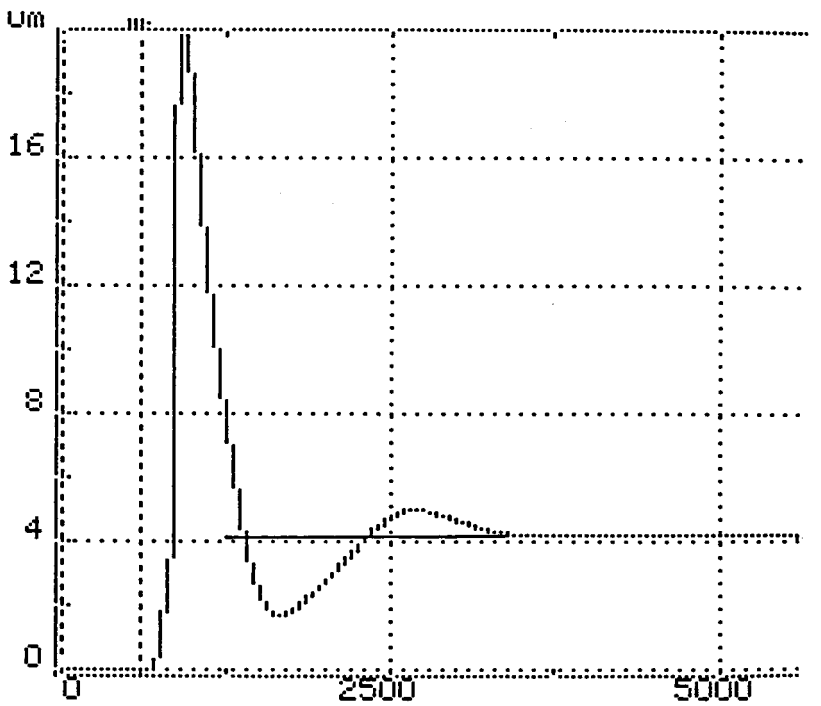

Figure A.3: Coating profile in front of a piece of cellotape, which has been removed. Length scales in microns. Flow was from right to left. Accurate data on the experimental situation are lacking. The lateral scale is clearly small compared to the static capillary length.

Appendix B

Mechanical properties and constants

All properties in this table are given for $T = 293$ K, unless stated otherwise.

ρ_{H_2O}	998 kg m^{-3}
μ_{H_2O}	$1.00 \cdot 10^{-3}$ Pa s
ν_{H_2O}	$1.00 \cdot 10^{-6}$ $m^2 s^{-1}$
γ_{H_2O}	$73 \cdot 10^{-3}$ N m^{-1}
E_{steel}	$0.20 \cdot 10^{12}$ Pa
P_{atm}	0 Pa
ρ_a	1.30 kg m^{-3} *
μ_a	$17.1 \cdot 10^{-6}$ Pa s *
ν_a	$1.32 \cdot 10^{-6}$ $m^2 s^{-1}$ *
M_{H_2O}	$18 \cdot 10^{-3}$
P_v	2.3 kPa
R	8.31 J $mol^{-1} K^{-1}$
g	9.81 m s^{-2}

* $T = 273$ K

Appendix C

Capillaries

A suitable fluid flow can be generated by using a set of capillaries. In this appendix some calculations are performed, and the most suitable set of capillaries is selected.

C.1 Determination of the radius of the capillaries

The fluid is assumed incompressible and it's viscosity as a constant. If no turbulence is present (laminar flow), the fluid flow inside a capillary can be correctly described using a circular Poiseuille flow. The occurrence of turbulence can be estimated by the Reynolds-number. The capillaries are assumed to be placed horizontal. Under these circumstances the Navier-Stokes equations (2.7) apply and the horizontal velocity can be calculated (Poiseuille flow), [Kundu 90], (Section (4.2.2)):

$$u = -\frac{1}{4\mu}\frac{\mathrm{d}P}{\mathrm{d}x}(R^2 - r^2) \tag{C.1}$$

The flux of one capillary is then given by:

$$\phi_{capillary} = \int_0^R u 2\pi r \mathrm{d}r = -\frac{\pi}{8\mu}\frac{\mathrm{d}P}{\mathrm{d}x}R^4 \tag{C.2}$$

The flux needed for a fluid flow of 40 μm (ϕ_{plate}) on an inclined plane is given by Equation (4.10). The two fluxes have to be equal:

$$N\Phi_{capillary} = \Phi_{plate} \tag{C.3}$$

in which N is the number of capillaries used. The pressure will be applied by a reservoir of fluid with a relative height H to the capillaries. Thus the pressure gradient can be approximated as:

$$\frac{\mathrm{d}P}{\mathrm{d}x} \approx \frac{\Delta P}{\Delta x} = \frac{-\rho g H}{L} \tag{C.4}$$

Combining Equations (4.10), (C.2), (C.3) and (C.4) gives an expression for R:

$$R^4 = \frac{8}{3\pi}\frac{Bh^3 \sin\alpha L}{NH} \tag{C.5}$$

With $D = 2R$, the diameter of the capillary the equation becomes:

$$D^4 = \frac{128}{3\pi}\frac{B}{N}L\frac{h^3 \sin\alpha}{H} \tag{C.6}$$

With this equation the required diameter of the capillaries can be calculated. However, the pressure caused by surface tension restricts the choice of diameter. The applied pressure has to be larger than the pressure caused by a surface curvature at the opening of the capillary (Section (4.2.2)). In case a capillary tube is used, $R_1 = R_2$, and the condition for equilibrium (4.18) can be rewritten as:

$$P = \frac{4\gamma}{D} \tag{C.7}$$

in which D is the diameter of the tube. This limits the choice for the diameter of the capillaries. On the one hand the diameter (D) is determined by the applied pressure (via H) and the number of needles per unit width ($\frac{1}{B/N}$), (Equation (C.6)), and on the other hand by the capillary pressure.
In Table (C.1) the capillary pressure is calculated for different diameters.
As stated before, this result is only valid for laminar flows. If the Reynolds number is small the fluid flow can be regarded as laminar [Kundu 90].

$$Re = \frac{\rho U D}{\mu} \tag{C.8}$$

With U the x-component of the average velocity of the fluid this becomes:

$$U = \frac{\phi}{\pi R^2} = \frac{g h^3 \sin\alpha}{\nu \pi R^2}\frac{B}{N}$$

$$Re_{H_2O} \approx 1.8$$

This implies the calculation is justified for the capillaries if water is used.
The absolute accuracy of the diameters of the capillaries is small: 0.02 mm. This implies for D =0.09 mm:

$$\frac{\Delta h}{h} = \frac{4}{3}\frac{\Delta D}{D} = \frac{4 \cdot 0.02}{3 \cdot 0.09} = 0.3 \tag{C.9}$$

The spreading in the diameters within the set of capillaries is probably not as large as the absolute accuracy of the diameters. Therefore this calculated inaccuracy will be smaller.
Capillaries with a diameter of $D = 0.09$ mm and $D = 0.15$ where ordered.

C.2 Entrance length

The velocity profile in a canal is developed into a Poiseuille-profile after a certain length. For a cylindrical tube this length L_e is given by [Ward-Smith 80, p.350-355]:

$$L_e = \frac{D}{4\pi}\frac{UD}{\nu} \approx \frac{DRe}{4\pi} \approx 7 \cdot 10^{-6}\, m \tag{C.10}$$

Thus the usage of the average velocity is justified.

Table C.1: Some values of P and P_{cap}. The surface tension of water is taken to be 73 $\cdot 10^{-3}$ Nm^{-1}. The angle of inclination is 22°(L = 0.07cm).

$\overline{h}$ (μm)	R (mm)	B/N (mm/naald)	H (cm)	P (kPa)	P_{cap} (kPa)
40	0.09	1	35	3.4	3.2
40	0.09	5	174	17	3.2
40	0.15	1	5	0.4	1.9
40	0.15	5	23	2.2	1.9
100	0.09	1	542	53	3.2
100	0.09	5	27	265	3.2
100	0.15	1	70	6.8	1.9
100	0.15	5	352	34	1.9
chosen	chosen	chosen	$\propto \overline{h}^3 d^{-4} B/N$	$\propto \overline{h}^3 d^{-4} B/N$	$\propto d^{-1}$

C.3 Time scale

The fluid surface which leaves the capillaries will not be flat. Under certain conditions the fluid surface will form a flow with uniform height under the influence of surface tension and gravity.
Orchard [Orchard 62] derived an equation for the levelling of a thin layer of fluid. In his theory some assumptions were made:

- Assume the profile of the fluid just after leaving the capillaries to be sinusoidally rippled;
- the average layer thickness is very small compared to the wavelength (λ) of the ripples;
- there are only low flow rates;
- air drag is negligible;
- the surface tension can be regarded as constant;
- the fluid can be regarded as a Newtonian fluid;
- the viscosity is time independent [Overdiep 86].

These requirements are met if the amplitude of the ripples (a) is much smaller than the fluid thickness, thus $a \ll h \ll \lambda$. Orchard's equation can thus be used to estimate the time in which the fluid surface will become flat[Camina 72].

$$\frac{da}{dt} = \frac{-\overline{h}^3}{3}\frac{\gamma}{\mu}\left(\frac{2\pi}{\lambda}\right)^4 a \qquad \text{(C.11)}$$

The wavelength (λ) equals the separation between the capillaries. The solution of this equation can be written as:

$$a = a_0 \exp(-\frac{16\pi^4\gamma\bar{h}^3}{3\mu\lambda^4}t) = a_0 \exp(-\frac{t}{\tau}) \tag{C.12}$$

The characteristic time then becomes:

$$\tau = \frac{3\mu\lambda^4}{16\pi^4\gamma\bar{h}^3} \tag{C.13}$$

This time can be calculated: $\tau_{H_2O} \approx 10^{-3}$ sec, $(B/N = 1\text{mm/capillary})$. The time increases with the wavelength, thus the more capillaries, the faster the surface flattens.

By using the average velocity of the fluid (inside the capillary) a length scale of $l = 10^{-6}$ m can be found.
If one takes one capillary, the broadening of the fluid stream, under influence of gravitation and viscous forces, without surface tension and fluid inertia and for $\alpha \ll 1$ can be approximated as [Higuera 95]

$$y \propto Ax^{\frac{3}{7}} \tag{C.14}$$

in which y is the dimensionless broadening at a (dimensionless) distance x and is calculated by Higuera to be $A \approx 3.8$. The distances are non-dimensionalised with $L = 50\,\mu$m . After calculation this gives:

$$y = 3 \cdot 10^{-3}\text{m}$$

If this is assumed to be half the wavelength the characteristic time becomes: $\tau \approx 1$ sec, and the length scale associated with this period of time: $l \approx 1$mm.
When designing a setup, a sufficient distance should be incorporated for the flow to flatten. This distance can be taken to be in the order of a few centimeters.

Appendix D

The topography

There are a number of steps involved in producing a topography:

- *The substrate;*
  The topography must be applied to quite a flat surface. All un-evennesses of the surface will be detected by the measurement system and will disturb the fluid flow. Therefore optical flats were chosen. They provide the necessary evenness and at the same time allow optical access from the bottom. They consist of $Zkn7$ and are provided by Cor Adema, WZp614, natlab. Nine optical flats are available. All nine are cut to obtain a flat side (Cor Adema). Three of them are not used and kept in reserve.

- *Connection of the substrate;*
  In order to minimize the disturbance to the flow, when flowing from the metal to the glass surface, the glass substrates were be cut to obtain a flat side. In Figure (D.1) a top-view of the cutted substrates is given.

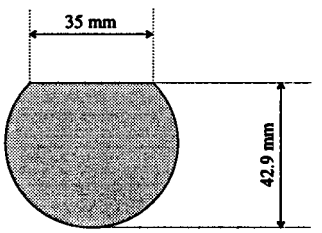

Figure D.1: The substrate.

- *The thickness of the substrates;*
  The transition from metal to glass should be as smooth as possible. Therefore the thickness and the variations in thickness of the several glass substrates must be measured. This was done by M. Breukers, WDp028, natlab. The variation in thickness between the samples is minimal ($1.3941^{+0.001}_{-0.0005}$), which makes it possible to machine a 'hole' in which the substrates can be precisely placed. The thickness of the substrates was measured before an optical coating was applied, in order not to damage the coating. The thickness of the coating is approximately 85 nm, this is much less than the desired accuracy, and is therefore negligible.

- *An optical coating;*
  In order to increase the image quality for an interferometry measurement an optical coating has to be applied. This coating is described in Appendix (E).

- *Applying the desired topography;*
  The topography can be applied using a photo-lithographical process. In this process a lacquer is spun upon the substrates, after which it is exposed to ultra violet light. The lacquer which is not exposed will harden, the rest can be washed away [Beerens 95]. The final topography must have a thickness of approximately ten microns. This limits the choice of lacquer to: AZ-4562 (Aad Engelfriet, CFT), the index of refraction of this lacquer for a wavelength of 670 nm is: $n_{670}^{AZ-4562} = 1.6143$ (Jozef Dekkers, Hoechst, Wiesbaden, Germany).

  The printer which is normally used to produce the mask for the lithographical process is not suitable for this topography. (Its precision is far to high and therefore the prints will be too expensive. A suitable printer can be found at the 'AV-dienst', (Henny Herps).)

  Although explained that the CFT was allowed to apply almost all means to produce the desired topography, as long as the glass was as hydrophilic as possible, no influence on the optical path would occur and the thickness of the substrate would not increase, they decided it was necessary to use a primer. This primer, HMDS (HexaMethylDiSulfide) is strongly hydrophobic. This means that the wetting properties of the glass substrates are very poor, which causes great problems using them. It has proven not to be possible to remove the hydrophobic layer, or to cover it with a hydrophilic layer. The only solution left is to choose a soap with a low surface tension. A measurement of the surface tension of the sample with a HMDS primer (Appendix (H.2)) showed the surface tension to be 31 mN/m. For a stable fluid flow this implies that a fluid with a surface tension smaller than 31 mN/m has to be used. This strongly limits the range over which the surface tension of the fluid can be varied.

Appendix E

Reflection coating

Interferometric measurements are most accurate if the two interfering beams have the same intensity, for then complete constructive or destructive interference can occur. The *reflectance* R can be defined by the ratio of the reflected power (or flux) to the incident power. For perpendicular incidence the reflectance can be approximated [Hecht 87, 102] to be:

$$R = \left(\frac{n_0 - n_1}{n_1 - n_0}\right)^2 \tag{E.1}$$

in which n_0, n_1 represent the index of refraction of the two materials of the interface. With this equation the reflectance for an air-water interface can be calculated to be: $R = 0.017$. The reflectance for a water-glass interface is $R = 0.005$.
In order to achieve complete constructive and destructive interference an optical coating to increase the intensity of the light reflected of the fluid-glass interface can be applied. If the incidence of the laser beam is assumed to be normal to the substrate the reflectance of a thin film can be approximated to be [Hecht 87, 375]:

$$R = \frac{n_c^2(n_0 - n_s)^2 \cos^2 k_0 h_c + (n_0 n_s - n_c^2)^2 \sin^2 k_0 h_c}{n_c^2(n_0 + n_s)^2 \cos^2 k_0 h_c + (n_0 n_s + n_c^2)^2 \sin^2 k_0 h_c} \tag{E.2}$$

in which h_c is the optical thickness of the coating, $k_0 = \frac{2\pi}{\lambda_0}$ is the propagation number and n_0, n_c, n_s are the indices of refraction of air, coating and glass, respectively (Figure (7.1)). If the optical thickness (h_c) of the coating is an odd multiple of $\frac{1}{4}\lambda$, then $k_0 h_c = \frac{1}{2}\pi$ and Equation (E.2) reduces to:

$$R = \frac{(n_0 n_s - n_c^2)^2}{(n_0 n_s + n_c^2)^2} \tag{E.3}$$

This equation is only valid for $h_c = \frac{1}{4}$, and thus the physical thickness of the coating has to be: $d_c = \frac{1}{4}\frac{\lambda_0}{n_c}$. With a wave length of 670 nm this gives $d \approx 84\,\text{nm}$.
The needed index of refraction of the coating can be calculated (using $R = 0.053$ for a matching fluid). The result is $R = 1.96$.
Thus the coating must have an index of refraction of 1.96 and a thickness of 84 nm.
The reflectivity of the coating depends on the fluid which is used. The coating properties calculated above are valid in case a matching fluid is used.
If an index matching fluid is used, the reflectivity at the air-fluid interface is: $R = 0.05$ and at the fluid-coating-glass interface: $R = 0.05$.

The topography however has an index of refraction of $n_T = 1.6$. The reflectance of the reflection coating underneath the topography is therefore: $R = 0.05$. The reflectivity at the topography-water interface is: $R = 0.01$. The reflectivity at the air-water interface is: $R = 0.017$ and for coating-water-glass this becomes: $R = 0.098$.
Interferometry at the topography will give a low resolution with this coating. The coating has to be chosen considering the next steps which are needed to produce the topography. While producing the topography the substrates will be heated to approximately 140 °C. The optical coating also has to be able to withstand lye (4%) and acetone (propanone). The coating is applied by J. Toonen, WZk420, nat-lab.

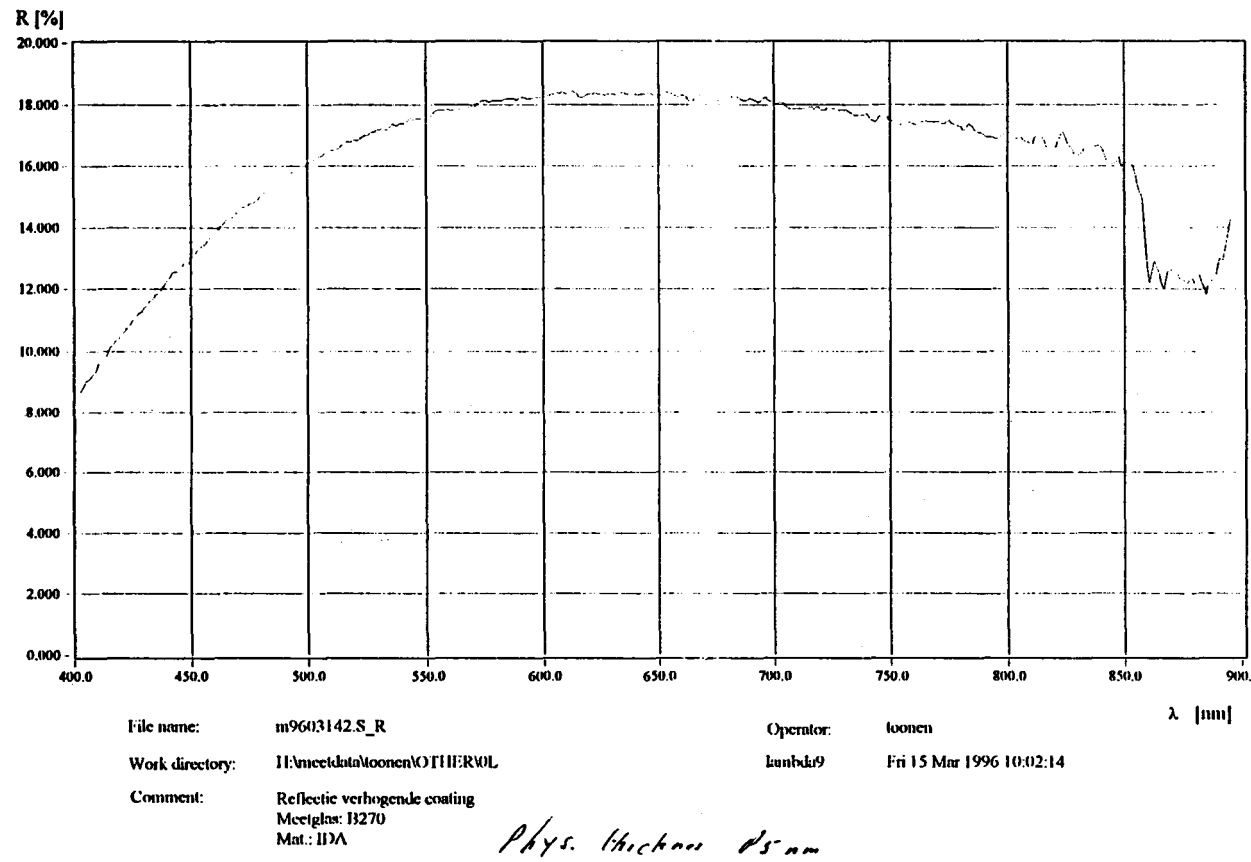

Figure E.1: The reflectance of the optical coating

Appendix F

Microdensitometer

Surfactants

A droplet of pure Fluorad reacts with the topography. After 24 hours a diluted solution (but still above the CMC) has not visibly affected the topography. After using the Fluorad surfactant the metal surface turned hydrophobic. This was not noticed on the glass surface. The active component of Fluorad is a 'potassium-fluoroalkyl-carboxylate'. Once soluted in water the negative part might react with the metal surface. This implies that the metal surface might be positive. Thus a surfactant with a positive active component will not react with the metal. Such a surfactant is found: Didodecyldimethylammoniumbromide. This surfactant does not react with the surface, and a stable fluid flow can be maintained.

Colouring agents

In Figure (F.1), shown below, the transmission spectrum of the fluid used (in the correct concentration) as well as the spectrum of the topography are shown. The diaphragm number was chosen to be 11, and the exposed time was: $\frac{1}{3}$0s.

Liquid

The fluid which is used for the MDM measurement is a cocktail consisting of: 4 gr basantol black x-80, 0.75 gr Fluorad, 760 ml H_2O. The surface tension at 21°C is: $\gamma = 16.1$ mN/m. Quite a large number of colouring agents can be found in [Green90]. Some other experimental data: $H = 0.24$ m, $\alpha = 22°$, $d = 76\,\mu$m , $L = 0.07$ m. The average fluid thickness can be calculated:

$$\overline{h} = \left(\frac{d^3 H}{4L\sin\alpha}\right)^{\frac{1}{3}} \approx 100\,\mu\text{m} \tag{F.1}$$

The dynamic capillary length scale thus becomes (Equation (2.44)):

$$L_d = \left(\frac{\gamma\overline{h}}{3\rho g\sin\alpha}\right)^{\frac{1}{3}} \approx 5.3\cdot 10^{-4}\text{ m} \tag{F.2}$$

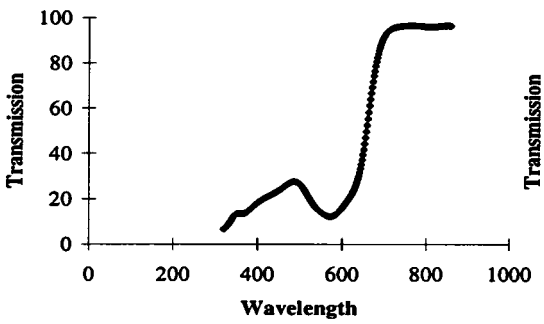

(a) The fluid used, (Basantol solution).

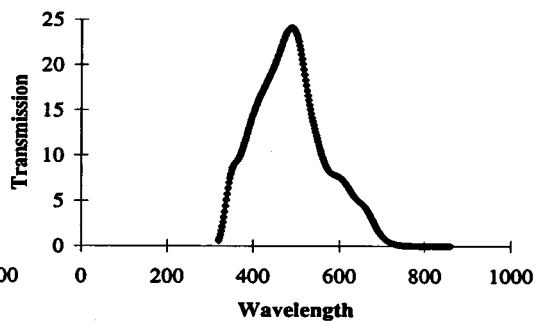

(b) The fluid used, (Basantol solution), an enlargement.

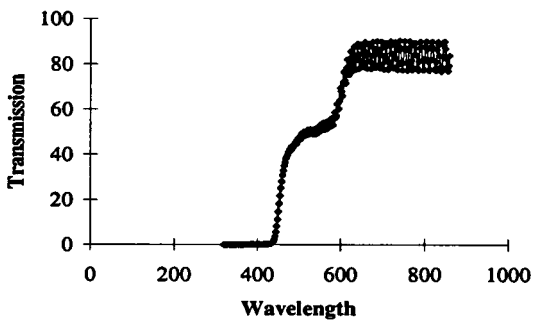

(c) The topography

Figure F.1: The transmission spectra of the fluid used, and the topography

Setup

A photo camera was used: Nikon F801, Micronikkor 105 lens, Kodak Plus-X Black& White film 125 ISO, fluorescent lamp, diffusor (opaque glass), separating-transformer in case some fluid leaks into the fluorescent lamp to prevent the earth-leakage switch from disconnecting the power of the laboratory room.

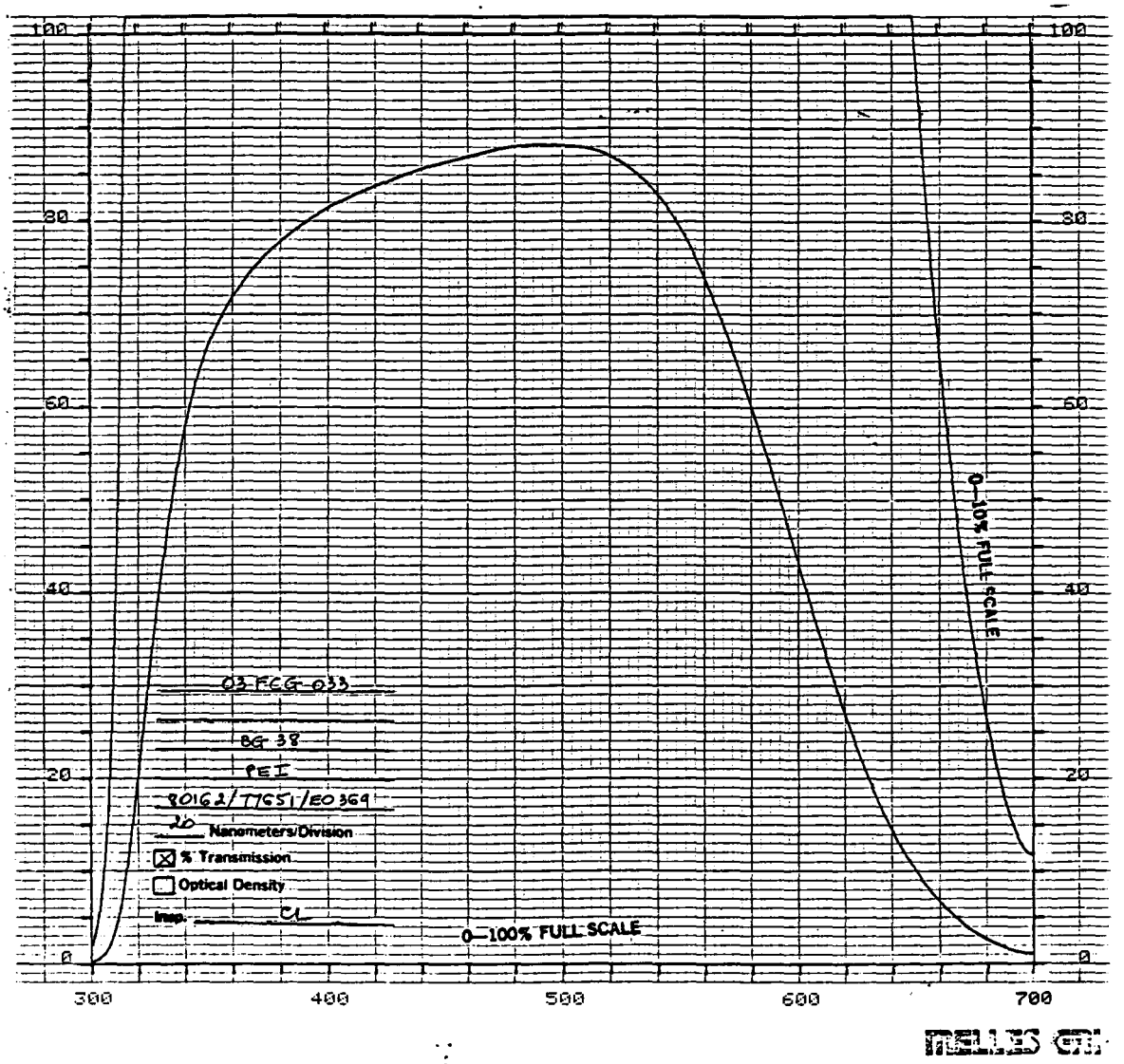

Figure F.2: Transmission spectrum of the filter used.

Appendix G

UV-ozone photo-reactor

The cleaning action of a UV-Ozone photo-reactor depends on the combined action of ultraviolet light from a low pressure mercury lamp (185 nm and 254 nm) and the presence of ozone to produce a chemical cleaning environment that is reactive towards organic chemicals. The primary process for UV-Ozone cleaning involves the photolysis of oxygen (185 nm) and ozone (254 nm) by ultraviolet light. Secondary reactions then take place to oxidize organic contaminations.
Initially, the reaction produces oxygen atoms which create ozone:

$$\begin{array}{ccc} O_2 & \stackrel{185\,\mathrm{nm}}{\longrightarrow} & O(^3P) + O(^3P) \\ O(^3P) + O_2 & \longrightarrow & O_3 \end{array} \tag{G.1}$$

The second wavelength is used to create reactive oxygen:

$$O_3 \stackrel{254\,\mathrm{nm}}{\longrightarrow} O_2 + O(^1D) \tag{G.2}$$

The light source and the surface must be situated close to each other. The reactive oxygen will be formed near to the source and will react instantly. In order to clean the surface, the oxygen must react with the contamination of the metal. If the distance between the light source and the surface is too large (> 1 cm), the oxygen radical will react with an oxygen molecule instead of the contamination. Therefore the cleaning rate drops exponentially with increasing distance from the lamp. The UV-ozone photo-reactor is a product of UVP. Ltd. Science Park, Milton Road Cambridge CB4 4BN, England. Some information on cleaning enhancement as well as the cleaning rate is presented in [Zavonte].

Appendix H

Surface Tension measurement

H.1 Measuring of the force on a rod

The maximum force on a vertical rod supporting a stable meniscus, at equilibrium, formed at the free surface of the liquid, is a characteristic property of the system [Padday 75]. This maximum force depends only on the rod radius, the density of the liquid, the gravitational acceleration and the surface tension. Therefore this can provide a means to measure the surface tension. A graph of the surface tension as a function of the maximum force for different densities (and the same rod radius and gravitational acceleration) can serve as a gauge. This method is used to measure the surface tension of several fluids as well as solutions of surfactants in water. The accuracy of this method is determined to be ± 0.1 mN/m, which is in agreement with [Padday 75]. In Figure (H.1) a photograph of such a measurement is shown.
The method does not involve detachment of the rod from the surface, as can be seen in Figure (H.1). It is a equilibrium method and the maximum force may be approached from both directions. In Figure (H.2) the critical micellar concentration of a surfactant (from Aldrich Chemical Company, Inc.) is determined by measuring the surface tension as described above.

H.2 Markers

The surface tension of a solid surface can be determined with special markers. On the surface a line must be painted with a marker. If after two seconds the line is still visible without contraction of the contours, the surface tension of the material is equal to or larger than the surface tension of the ink of marker. These markers are very simple in usage, but the processes which occur are very complicated. The surface tension of the hydrophobic primer on the substrates was measured to be 31 mN/m. The markers are a product of 'Arcotec Oberflächentechnik', Germany.

Figure H.1: Determination of the surface tension of a fluid, by means of measuring the force on a cylinder. In the picture the situation of the maximal force is shown. The fluid which is used is water with a surfactant and coloring agents and is described in Appendix (F). The maximal exerted force is equivalent to 0.058 mg, which corresponds to a surface tension of: $\gamma = 13.4$ mN/m.

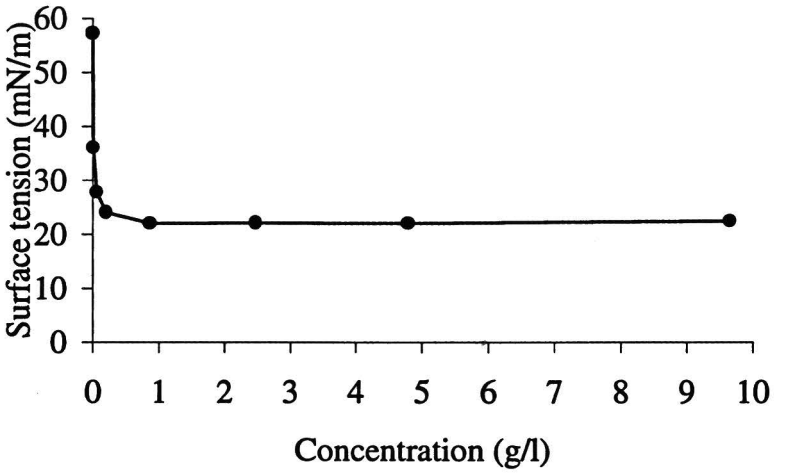

Figure H.2: The surface tension as a function of the concentration, for Didodecyldimethylammoniumbromide, 98%

Appendix I

Matching the index of refraction

There are a number of fluids with an high index of refraction. A lot of fluids can be found in [Weast 86]. A table with some fluids which might be applicable can also be found in [Budwig 94], however the fluids listed there all have an index of refraction of about 1.5.

Appendix J

A preliminary experiment on wettability and fingering

In both design options (capillaries and slit) the fluid flow will be generated on a steel plate. On certain surfaces a thin fluid flow will contract under the influence of surface tension. In order to get an idea of the scale of this effect a few simple experiments were performed on a steel plate. In all experiments demineralised water was used. To generate a thin fluid flow a similar set up as the slit-design was used: a base plate on which the fluid was allowed to flow, on top of this the head (a flat piece of metal) was placed. In between the base and the head two thin ($\pm$ 140 μm) colourless foils of unknown composition were placed to create a slit with a width of 5 cm. Behind the head a simple fluid reservoir was constructed. The entire setup was tilted (45°) and placed in a reservoir. Three different materials were used, all of them were cleaned with acetone before usage:

1. A steel base and a steel head;
   In this experiment the fluid did not flow at all. It remained 'stuck' between the plates. The plates were smooth, and not damaged. Single drops quickly flowed downwards under the influence of gravity.

2. A steel base and an aluminium head;
   The same as experiment 1 applies for experiment 2.

3. An aluminium base and an aluminium head;
   The aluminium base and head were at some spots clearly damaged. The fluid only flowed on a maximum of four 'canals'. If the slit was wetted, the fluid flow became equally divided across the width of the slit. It is important to notice that at some spots sometimes dry regions appeared They did not disappear by themselves, only after the region was re-wetted manually the spots disappeared. On the sides the flow showed a tendency to bend to the middle.

It was decided to increase the width of the design, and thus the width of the flow, to overcome these possible side effects.

Appendix K

The production of the flow apparatus

K.1 Hydrophobical layer

In order to counteract the capillary force and thus to stimulate the fluid to flow out of the apparatus, a hydrophobic layer is applied to the front side of the metal. A series of tests is performed to determine which hydrophobic layer is most suitable for the steel block. This proved to be a OTS-ethoxy layer, applied from the gas-phase (100 °C) This layer increased the contact angle to 110 °. After this treatment the metal has to be cut with a dry cutting system, to prevent possible chemical reactions between the layer and the cooling liquid.

K.2 Wettability

In order to increase the wettability of a surface, this surface needs to be thoroughly cleaned. The procedure to make a steel surface hydrophilic can be summarized:

- The surface has to be cleaned with demineralised water and detergent.
- Ethanol (pro analyse) has to be used to remove the grease and silicon.
- The final cleaning can be done using n-heptane (soluble in ethanol but not soluble in water)
- After this cleaning, a thin monolayer is still present at the surface. It is this monolayer which is responsible for the hydrophobical properties of the metal. This monolayer, which mostly consists of organic materials, can be removed using an UV-Ozone apparatus. (Appendix (G))
- The samples have to be wrapped in aluminium foil to prevent it from becoming hydrophobic again.

K.3 Design

In this section an explanation to the drawing is given (in Dutch). This explanation will be sent along with the drawing to the construction site.

Toevoegingen bij de tekening:

- De tekening is een ontwerp om een vloeistofstroming met een dikte van $\pm$ 40 μm op te wekken. Als vloeistof wordt onder andere gedestilleerd water gebruikt. Waarschijnlijk zal roest vrij staal dus het geschiktste materiaal zijn.
- De onderkant van blok 2 moet pas bewerkt worden nadat de voorkant van een hydrofobe laag is voorzien. Dus gelieve dit blok als eerste te bewerken, zodat in de tijd die nodig is om de laag op te brengen de andere 2 blokken gefabriceerd kunnen worden.
- Op de tekening is aangegeven dat de onderkant van blok 2 vlak moet zijn ($\square$ 0.002). Deze vlakte is vooral van belang in de richting die dwars op de vloeistof stroom staat (in de tekening de kant van 70 mm lengte) hier kan misschien met het kiezen van de bewerk-richting rekening mee gehouden worden.
- De gaten en de schroefdraad in de verschillende blokken moeten op elkaar aansluiten. (Gelieve eerst blok 1 met blokken 2 en 3 te verbinden voordat blok 2 en 3 geboord worden.)
- Blokken 2 en 3 moeten verpind worden, zodanig dat de onderkant van blok 2 en de bovenkant van blok 3 evenwijdig zijn ($\parallel \mu$m). De voorkanten van de twee blokken hoeven niet zo nauwkeurig bevestigd te worden. Blok 2 moet ($0.1^{+0.05}$ mm) 'oversteken' ten opzichte van blok 3.
  Het verpinnen is nog niet in de tekening opgenomen.
- In de tekening van het zij-aanzicht van blok 3 is een afronding opgenomen. Deze ronding dient alleen ter voorkoming van een te scherpe overgang (gradiënt). Als het eenvoudiger is om een andere ronding te gebruiken is dit ook geschikt.
- De bouten (inbus) moeten indien mogelijk verzonken worden.

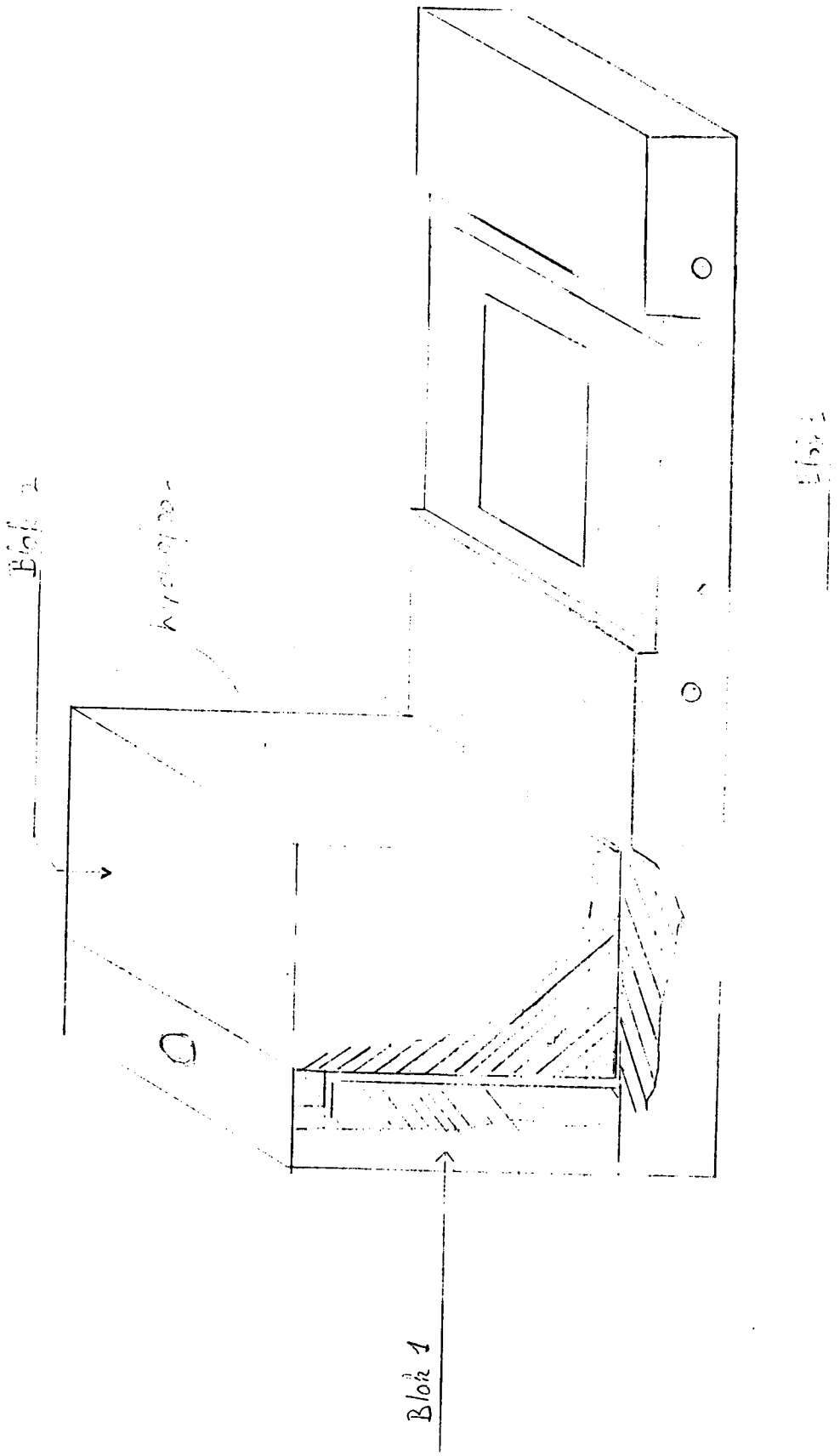
Blok 1

Doorsnede A-A

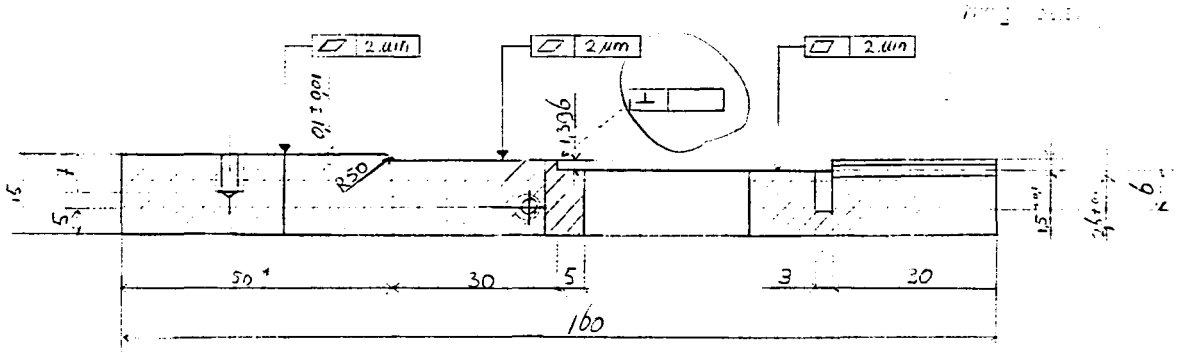

Bovenaanzicht

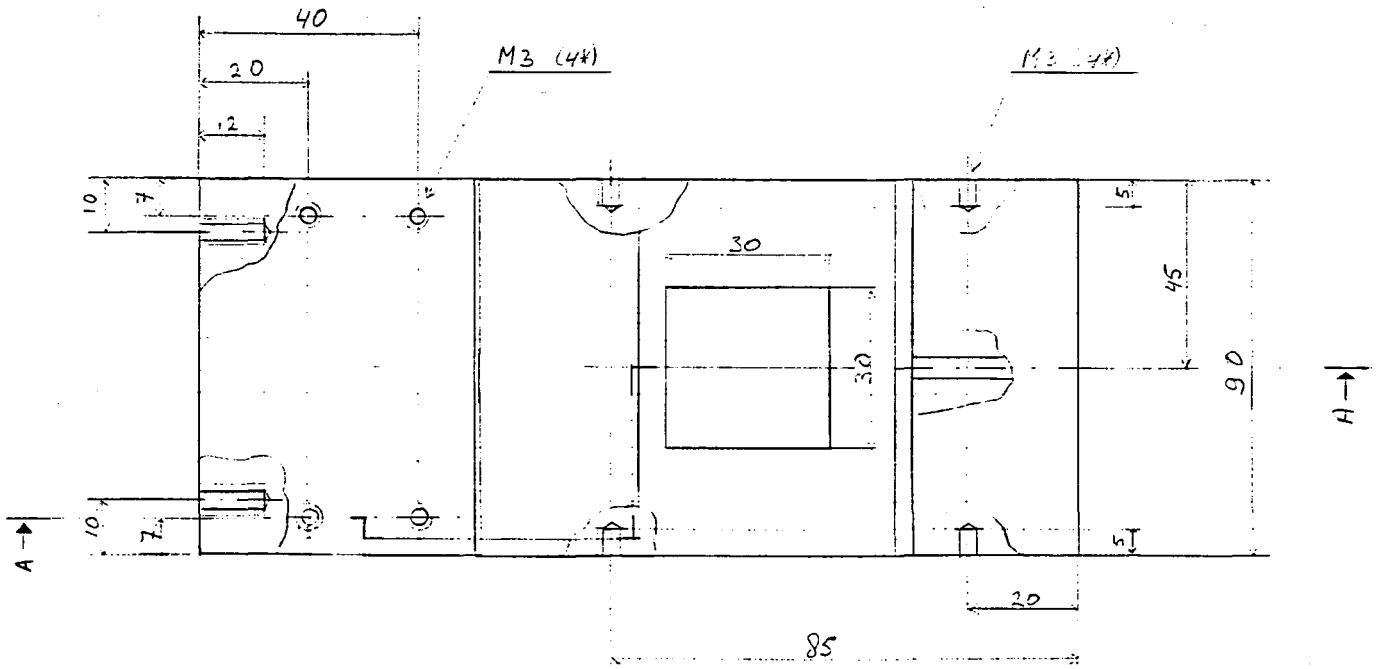

Voorgaand

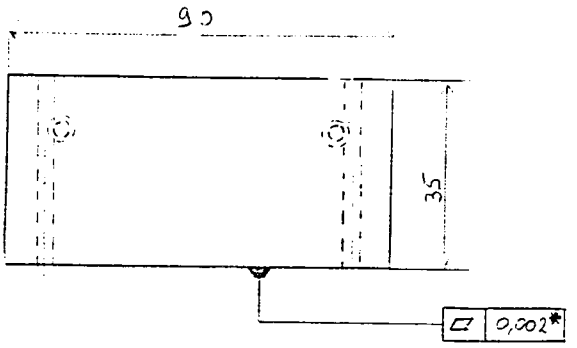

Bovenaanzicht

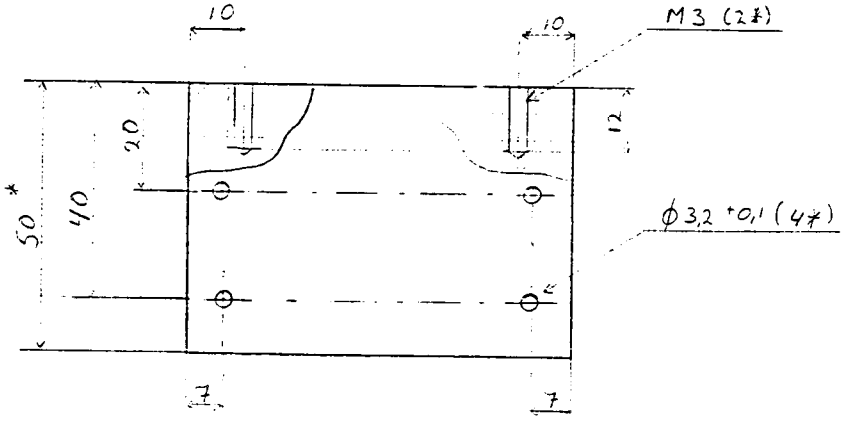

* = zie bijgevoegde

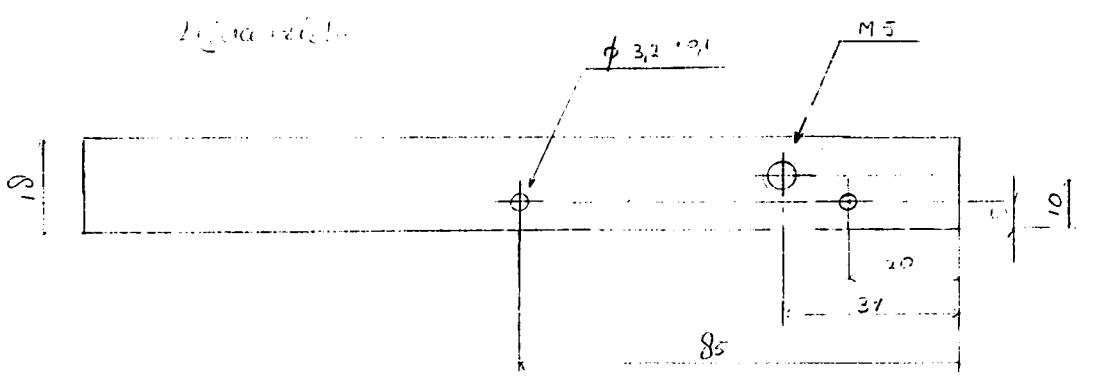
M 5
18
10
20
35
85